International School for Advanced Studies

Spin-Fluctuation Spectra in Magnetic Systems

A Novel Approach Based on TDDFT

Author:
Tommaso Gorni

Supervisor:
Prof. Stefano Baroni

A thesis submitted in fulfillment of the requirements for the degree of Doctor of Philosophy

in

Condensed Matter Theory

CONTENTS

CHAPTER

ONE

INTRODUCTION

Magnetism at the micro- and nano-scale level is a well-established research field, by virtue of its relentless technological impact and astounding variety of structures it can shape in condensed-matter systems. The characterization of most of these structures has become possible in the last fifty years thanks to the development and refinement of magnetic spectroscopies, most notably neutron scattering for bulk magnetism, and electron spectroscopies for surfaces and thin films. A fundamental outcome of the most recent experiments is the need to address magnetism in its full non-collinear nature also at the theoretical level, i.e. by treating the magnetization density as a true vector field, allowed to vary its direction at each point in space. This paves the way to the study of chiral topological magnetic structures such as skyrmions, or of the effect of Spin-Orbit Coupling (SOC) on the ground-state configuration and on the excited-state dynamics. Handling non-collinearity however, a far-from-trivial task on its own, proves to be particularly demanding in ab-initio calculations, where, at present, it is far from being a standard tool in the study of excited states. In this thesis we shall focus on the development of a method to study the dynamical spin-fluctuations of magnetic systems in a fully non-collinear framework, within Time-Dependent Density Function Theory (TDDFT). The outline of the thesis follows. In Ch. 1 the technological framework and the main experimental findings which have inspired our work are presented; a link between the experiments and the relevant physical quantities, namely the magnetic susceptibility, will also be shown. In Ch. 2 and 3 the theoretical framework in which we move will be introduced, namely Time-Dependent Density Functional Theory (TDDFT) and linear response. In Ch. 4 and Ch. 5 original work is presented: in the former, we devise a computational approach for the study of magnetic excitations via TDDFT, in a fully non-collinear framework. In the latter, we discuss the implementation and compute the spin-wave dispersion for BCC Iron. The final chapter is devoted to the conclusions.

1.1 Spin Dynamics

The basic quantity that characterizes the magnetic properties of a system is the microscopic magnetization-density, $\mathbf{m}(\mathbf{r})$. For a system of N electrons in the many-body state Ψ, it is defined by

$$\mathbf{m}(\mathbf{r}) \equiv \langle \Psi, \hat{\boldsymbol{\mathcal{M}}}(\mathbf{r})\, \Psi \rangle \,, \tag{1.1}$$

where

$$\hat{\boldsymbol{\mathcal{M}}}(\mathbf{r}) = \sum_{i=1}^{N} \hat{n}_i(\mathbf{r})\, \hat{\boldsymbol{\mu}}_i \,, \tag{1.2}$$

with $\hat{n}_i(\mathbf{r})$ and $\hat{\boldsymbol{\mu}}_i$ being respectively the density and magnetic-moment operator of the i-th electron. In magnetic materials, the electronic magnetic moments organize in some pattern in the ground state, which results in a non-vanishing $\mathbf{m}(\mathbf{r})$. The low-lying excited states of such systems may feature travelling magnetization waves, also known as spin-waves (a pictorial example is reported in Fig. 1); their dynamics strongly depends on the structure of the *density of excitations* of the system at low energy.

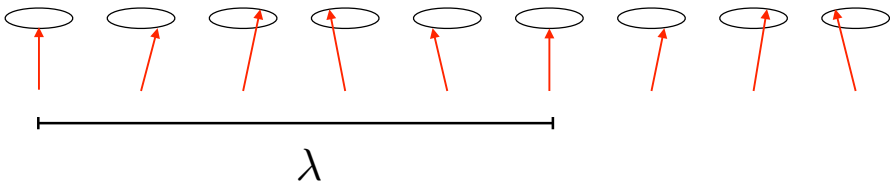

Figure 1. Sketch of a spin wave of wave vector $Q = 2\pi/\lambda$ in a one-dimensional ferromagnetic chain.

1.1.1 Magnonics: Propagation on Ferromagnetic Films

The dynamics of the spin waves has drawn much interest due to their uncommon features: first, the index of refraction of the spin wave in a material can be changed just by altering the magnetization direction of the medium. Secondly, their wave length spans several ordersj of magnitude, from $\sim 10\,\mathrm{mm}$ down to $\sim 1\,\mathrm{nm}$, with frequencies varying from GHz to THz. Lastly, no electrical charge transport is involved during the propagation, and hence no electrical losses or Joule heating occur. These features encouraged the birth of *magnonics*, a branch of spintronics whose aim is to use spin waves as information carriers in circuits made of ferromagnetic guides [1].

The geometry of a spin wave propagating in a ferromagnetic guide, endowed with an in-plane magnetization, is sketched in the left panel of Fig. 2. In the right panel the spin-wave dispersion is reported at two different wave-length scales: the μm-region and nm-region. In the μm-region the dipolar interaction between magnetic domains dominates, and there is a continuum of dispersions according to the angle between the direction of propagation and the magnetization of the guide. Moving

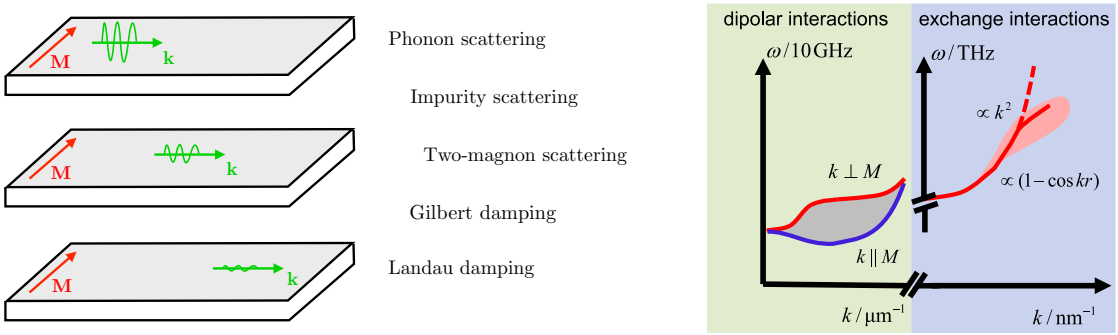

Figure 2. Left: geometry and damping mechanisms in the spin-wave propagation on a ferromagnetic surface. Right: dispersion of spin waves travelling on a ferromagnetic surface, with an in-plane magnetization. The red-shaded area marks the region in which Landau damping becomes active (figure reproduced from [1]).

toward nm-wavelengths and THz-frequencies, the exchange interaction prevails and the dispersion tends to be isotropic. The prototypical material with spin waves in the μm-region is yttrium iron garnet, whose spin waves display a lifetime of $\sim 100\,\text{ns}$ and a mean free path of several millimetres [2]. These materials, however, are not suited for nano-fabrication, because of the long wave length of the carrier, hence one faces the need to study shorter-wavelength spin waves.

Spin-Wave Damping

At the nanometre scale, where standard ferromagnetic materials such as Fe display prononced spin-wave excitations, one incurs the issue of increasing spin-wave damping. In the THz-regime the spin-wave energy becomes comparable to the one of single spin-flips (Stoner excitations), so that it is not possible to excite a single travelling spin-wave, but only a superposition of modes, whose lifetime drops to the order of few tens of fs. Recently, some progress has been made by engineering the density of Stoner excitations by altering the Pd percentage in FePd alloys films, reaching lifetimes of $\sim 100\,\text{fs}$ [3].

The damping due to the superposition of spin waves and Stoner excitations is called *Landau damping*, and it is not the only mechanism which hinders the propagation of a spin wave. Recently, damping related to a strong spin-orbit coupling has been observed experimentally in a two-atomic-layer Fe film on W(110), with an in-plane magnetization $\mathbf{M}$ [4, 5]. When a spin wave propagates perpendicularly to the in-plane magnetization, i.e. $\mathbf{Q} \perp \mathbf{M}$, its lifetime has been measured to be different from the one of another spin wave propagating in the opposite direction, i.e. along $-\mathbf{Q}$. The phenomenon has been attributed to a strong spin-orbit coupling induced by the W substrate, which produces a horizontal shift in the spin-wave dispersion $\omega(\mathbf{Q})$ when inversion symmetry is lacking, such as it happens at an interface. The shift is then related to a different spin-wave lifetime, as showed by the experiements reported in Fig. 3. Tight-binding calculations have confirmed this picture [6], however no calculations with a realistic band structure have been performed so far.

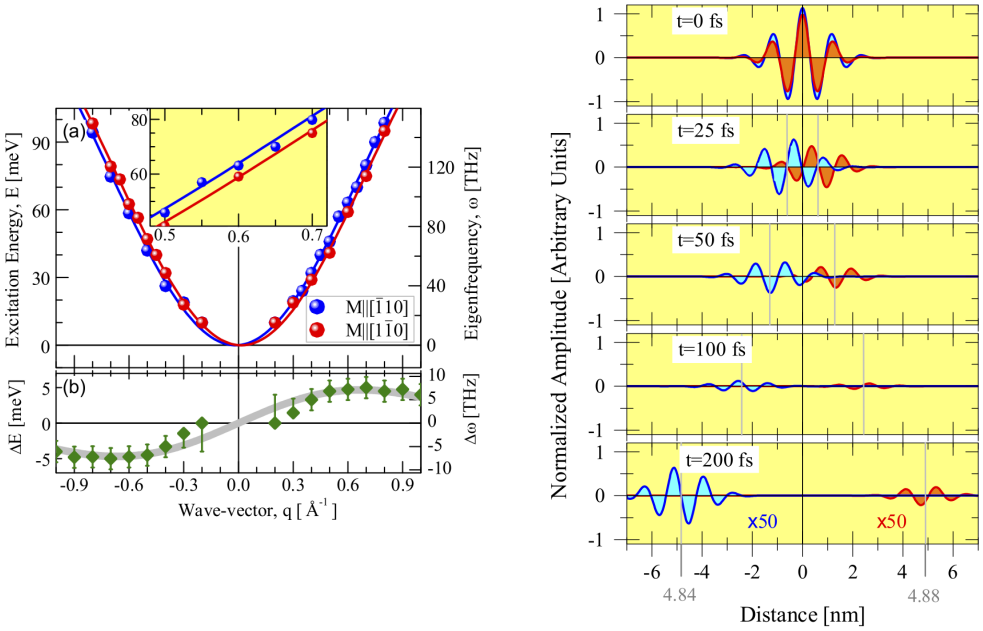

Figure 3. Left: spin-wave dispersion in 2-ML Fe@W(110) at room temperature. The dispersion with **Q** parallel to the magnetization is reported in blue, in red the one with **Q** along the perpendicular direction, where a horizontal shift is observed. This is often called *spin-wave Rashba effect*, due to the parallel with the Rashba splitting of the electronic bands. Right: different damping of two spin waves travelling in opposite direction, perpendicularly to the magnetization. Figures from [5].

Eventually, spin-orbit effects have been related also to the so called *Gilbert damping* [7], which owes its name to the Landau-Lifshitz-Gilbert (LLG) equation [8]

$$\frac{\partial \mathbf{m}(\mathbf{r},t)}{\partial t} = -\gamma\, \mathbf{m}(\mathbf{r},t) \times \mathbf{b}_{\text{eff}}(\mathbf{r},t) - \alpha\, \frac{\mathbf{m}(\mathbf{r},t)}{m(\mathbf{r},t)} \times \frac{\partial \mathbf{m}(\mathbf{r},t)}{\partial t}\,, \tag{1.3}$$

where γ is the electron gyromagnetic ratio, $\mathbf{b}_{\text{eff}}(\mathbf{r},t)$ the effective magnetic field in the medium and α the damping parameter. The LLG equation is of phenomenological origin, and describes the magnetization dynamics in a continuous medium. The first term on the right-hand side of (1.3) is responsible for the precession of the magnetization around the axis perpendicular to the plane defined by $\mathbf{m}$ and $\mathbf{b}_{\text{eff}}$, whereas the second term tends to align $\mathbf{m}$ to $\mathbf{b}_{\text{eff}}$, resulting in a damping of the motion, known as *Gilbert damping*. It is known that SOC induces Gilbert-like terms in the quantum equation of motion, and some attempts to estimate α from linear-response calculations have been made [9, 10].

1.1.2 Chiral Magnetic Structures

We conlude this section by mentioning *chiral magnetic structures*, i.e. magnetization patterns non-symmetric under parity, such as helicoids. The most notable structures of these are *skyrmions*, nanometre-sized chiral spin textures, found as stable or metastable states in different condensed-matter systems (see Fig. 4). Skyrmions have drawn much attention due to their topological origin, which endows them with a long

lifetime and stability under perturbations, so to be considered a strong candidate for the role of spin-carriers in magnetic-transport devices. A first classification of these states [11] is made accordingly to the size of skyrmions: when the skyrmion size is bigger than the lattice constant, its energy density is much smaller than the atomic exchange energy, and the chiral state benefits of topological stability; in other words, the skyrmion lives in a different energy region than the continuum of Stoner excitations. The difference between the standard spin-wave case is that topological states are stable against all the perturbations which have not enough energy to alter their topology (in this case the spin-flip energy). Skyrmions of this type are due to the dipolar ($\sim$ 100 nm–1 μm) and spin-orbit ($\sim$ 5–10 nm) interactions in non-centrosymmetric lattices; in the latter case experimental evidence has come out only recently, with the observation of skyrmions in the non-centrosymmetric bulk magnet MnSi [12], or in 1 ML Fe@Ir(111) [13]. Skyrmions with size of the lattice constant ($\sim$ 1 nm) have been reported in frustated lattices with strong enchange interaction, or systems with a dominant four-spin exchange interaction; their energy is comparable with the one of the Stoner continuum, with the subsequent loss of stability.

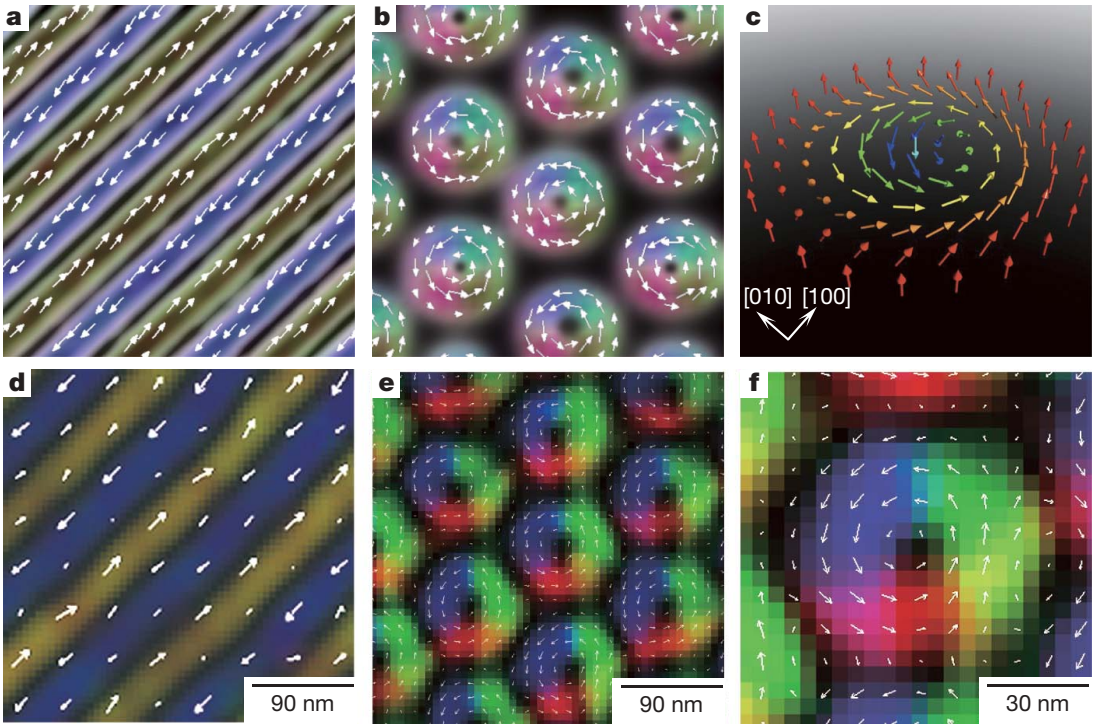

Figure 4. Topological spin textures in a thin film of $Fe_{0.5}Co_{0.5}Si$. In the bottom panels **(d)**, **(e)** and **(f)** Lorentz TEM measurements are reported, the colour map reprensenting the direction of the on-plane magnetization, the arrows put as a reinforce. Panel **d)** show a stripy pattern at zero external field, whereas panel **(e)** displays the transition to a hexagonal skyrmion-lattice configuration for an external field of 50 mT normal to the plane. The top panels **(a)** and **(b)** show the same structures predicted by Monte Carlo simulations and a sketch of a skyrmionic configuration in panel **(c)**. Figure reproduced from [14].

Remarks

From the cases examinated above, a full characterization of the magnetic excitations of a system turns out to be essential in order to predict, and even engineer, the dynamics of quantum non-collinear states. On the experimental side, the two principal spectroscopies which allow such a characterization are Inelastic Neutron Scattering (INS) for bulk and Spin-Polarized Electron Energy Loss Spectroscopy (SPEELS) for surface excitations. In the following the link between these spectroscopies and response functions will be discussed.

1.2 Probing Magnetic Excitations

Historically, neutrons have been the standard probes for magnetic spectroscopies. In fact, due to their neutrality, only two types of interaction are relevant with a condensed-matter system. The first one is the neutron-nucleus short-range interaction, widely used to determine the crystal structure and the phonon excitations of solid-state systems. The second one is the dipolar interaction between the magnetic moment of the neutron $\hat{\boldsymbol{\mu}}_n$ and the one of the electrons $\hat{\boldsymbol{\mu}}_e$,

$$\hat{\boldsymbol{\mu}}_e = \frac{g_e \mu_B}{\hbar} \hat{\mathbf{s}}_e \,, \qquad \hat{\boldsymbol{\mu}}_n = \frac{g_n \mu_n}{\hbar} \hat{\mathbf{s}}_n \,, \tag{1.4}$$

where $g_e \approx 2.002$ and $g_n \approx 3.826$ are the electron and neutron g-factors, $\mu_B = -e\hbar/2m_e < 0$ and $\mu_n = -e\hbar/2m_n$ Bohr and neutron magnetons, $\hat{\mathbf{s}}_e$ and $\hat{\mathbf{s}}_n$ the spin operators acting respectively on the electron and neutron spin degrees of freedom. The dipolar interaction is quadratic in the magnetic moments, therefore the electron-neutron magnetic interaction is roughly 10^3 times stronger that the neutron-nucleus one. When able to separate the crystallographic signal from the magnetic one, Neutron Scattering (NS) immediately returns vital information about the magnetic feautures of electrons in a specimen. Moreover, neutrons display a high mean free path in solids, so that NS is the prototypical bulk spectroscopy. We now focus on Inelastic Neutron Scattering (INS) which sheds lights on the bulk magnetic excitations of a system, to illustrate which physical quantities have to be computed to interpret the experiment.

In a typical INS experiment, a beam of unpolarized neutrons with wavevector $\mathbf{k}_i$ and energy $\varepsilon_i = \hbar^2|\mathbf{k}_i|^2/2m_n$ impinges on a system in the ground state Ψ_i. The intensity I and energy ε_f of the outgoing neutrons are detected at different solid angles, so that also the wave vector $\mathbf{k}_f$ of the outgoing neutrons can be inferred; two examples of recorded $I(\mathbf{q}, \omega)$ signals are reported in Fig. 5. The intensity $I(\mathbf{q}, \omega)$, where $\hbar\omega = \varepsilon_i - \varepsilon_f$ and $\mathbf{Q} = \mathbf{k}_f - \mathbf{k}_i$ are respectively the energy and momentum transfer, displays peaks in correspondence of the $(\mathbf{q}, \omega)$ at which the system is able to exchange energy with the probing particles, i.e. its own excitations. This picture is of course simplified since it considers only single scattering processes, namely assumes the impinging neutrons to undergo only one scattering event while inside the sample; nevertheless, multiple-scattering processes are less likely to occur, appearing as higher-order terms in the transition-probability density, and resulting in a weaker intensity in the $I(\mathbf{Q}, \omega)$ signal.

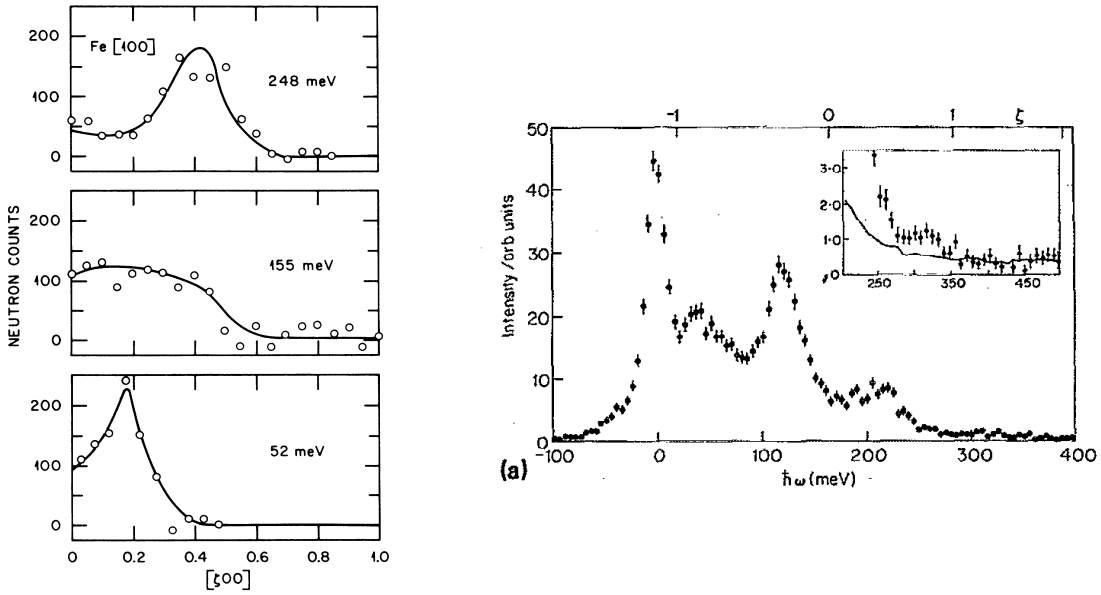

Figure 5. Measurements of the outcoming-neutron intensities $I(\mathbf{Q}, \omega)$ in INS experiments on BCC-Fe, with $\mathbf{Q}$ along the [100]-direction. Left: $I(\mathbf{Q}, \bar{\omega})$ recorded at three fixed neutron energy-losses $\hbar\bar{\omega}$; data coming from the triple-axis neutron spectroscopy measurements of [15]. Right: neutron intensity recorder with the time-of-flight method, which employs a constant scattering angle so that $\mathbf{Q}$ and ω vary together with the scattered neutron time-of-flight; $\mathbf{Q} = (\eta, 0, 0)$ is reported on the x-axis above the figure. Data taken from [16].

1.2.1 Inelastic Neutron Scattering

From a theoretical point of view, considering only single-scattering events corresponds to the Born approximation in the Scattering Theory. We start by defining the cross section as

$$\mathrm{d}\sigma = \frac{1}{J_i} \sum_F \mathrm{d}w_{FI} \,, \tag{1.5}$$

where $J_i = \frac{\hbar k_i}{m}$ is the flux per unit volume of incoming particles and $\mathrm{d}w_{FI}$ is the transition-probability density from the global initial state I (beam+system) to the global final state F per unit of time. The cross section describes the efficiency of a certain scattering process defined by $\mathrm{d}w_{FI}$, which in the Born Approximation is written via first-order time-dependent perturbation theory, namely Fermi's Golden Rule, as [17]

$$\mathrm{d}w_{FI} = \frac{2\pi}{\hbar} \mathrm{Tr} \left[\hat{\rho}_I \hat{\mathcal{V}}^\dagger \hat{\rho}_F \hat{\mathcal{V}} \right] \delta(E_F - E_I) \,, \tag{1.6}$$

where $\hat{\rho}_I$, E_I, $\hat{\rho}_F$, E_F are the density matrices and energies of, respectively, the initial state and final state (beam+system), whereas $\hat{\mathcal{V}}$ the interaction Hamiltonian between the beam and the sample. Eq. (1.6) is the form of the transition probability in terms of the density matrices, which allow to account for non-pure initial states (such, e.g., an unpolarized beam or temperature effects); the density matrix $\hat{\rho}_F$ shall, instead, always represent a pure state.

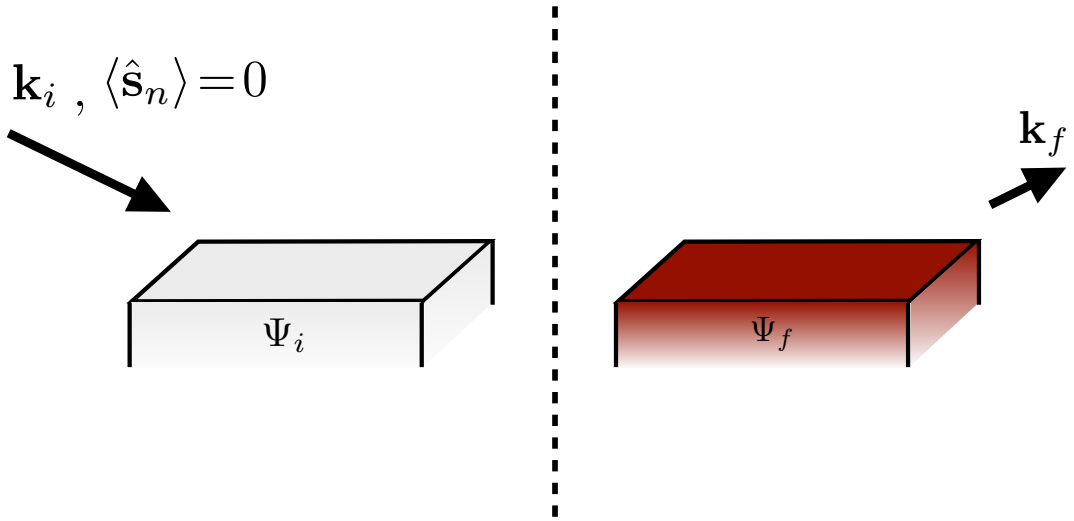

Figure 6. Pictorial view of an INS experiment, a beam of unpolarized neutron with momentum $\mathbf{k}_i$ impinges on a sample in the state Ψ_i. The recording of the momentum of the outgoin neutrons $\mathbf{k}_f$ allows to infer information on the final state of the sample Ψ_f.

As regards the term $\hat{\mathcal{V}}$, the dipolar interaction between a neutron and N electrons reads

$$\begin{aligned} \hat{\mathcal{V}}(\mathbf{r}_n, \mathbf{r}_1, \ldots, \mathbf{r}_N) &= \sum_{i=1}^{N} \hat{V}(\mathbf{r}_{i,n}) \\ &= \sum_{i=1}^{N} \left[\frac{\hat{\boldsymbol{\mu}}_i \cdot \hat{\boldsymbol{\mu}}_n}{r_{i,n}^3} - \frac{3(\hat{\boldsymbol{\mu}}_i \cdot \mathbf{r}_{i,n})(\hat{\boldsymbol{\mu}}_n \cdot \mathbf{r}_{i,n})}{r_{i,n}^5} - \frac{8\pi}{3} \hat{\boldsymbol{\mu}}_i \cdot \hat{\boldsymbol{\mu}}_n \, \delta(\mathbf{r}_{i,n}) \right] . \end{aligned} \tag{1.7}$$

Eq. (1.7) is explicitly written in the coordinates-only representation, not to burden the notation with spin indexes.[1] The letter "i" labels electron quantities, wheres "n" the neutron ones, $\mathbf{r}_{i,n} = \mathbf{r}_i - \mathbf{r}_n$ and $r = |\mathbf{r}|$. We consider as initial state the target system in its ground state Ψ_{GS}, and an unpolarized beam of momentum $\mathbf{k}_i$; as final state the system in a given excited state Ψ_f and a beam of momentum $\mathbf{k}_f$, summed on both the polarizations (which, experimentally, means not to resolve the polarization of the outgoing beam). By substituting (1.7) into (1.6) one obtains the differential cross section for solid angle Ω_f and outgoing neutron energy ε_f

$$\frac{\mathrm{d}^2\sigma}{\mathrm{d}\Omega_f \mathrm{d}\varepsilon_f} = -\frac{1}{\pi} \left(\frac{e g_n}{2\hbar} \right)^2 \frac{k_f}{k_i} \sum_{\alpha\beta} \left(\delta_{\alpha\beta} - \frac{Q^\alpha Q^\beta}{Q^2} \right) L_{\alpha\beta}(\mathbf{Q}, \omega) \, , \tag{1.8}$$

where, we recall, $\hbar\omega = \varepsilon_i - \varepsilon_f$ and $\mathbf{Q} = \mathbf{k}_f - \mathbf{k}_i$. The quantity $L_{\alpha\beta}(\mathbf{Q}, \omega)$, named *loss tensor*, can be shown via linear-response theory (see Ch. 3) to be the anti-hermitian part of $\chi_{\alpha\beta}(\mathbf{Q}, \omega)$, i.e.

$$L_{\alpha\beta}(\mathbf{Q}, \omega) = \frac{1}{2i} \Big[\chi_{\alpha\beta}(\mathbf{Q}, \omega) - \chi^*_{\beta\alpha}(\mathbf{Q}, \omega) \Big] \, , \tag{1.9}$$

[1] Here, the hat refers only to the spin degrees of freedom.

where $\chi_{\alpha\beta}(\mathbf{Q},\omega)$ is the Fourier transform of the magnetic susceptibility, which defines the linear response of a system to a magnetic perturbation. Hence, the solution of a linear-response problem allows to interpret the results of a INS experiment, the peak-structure of the recorder signal $I(\mathbf{Q},\omega)$ should in fact be the same as

$$S(\mathbf{Q},\omega) = -\sum_{\alpha\beta}\left(\delta_{\alpha\beta} - \frac{Q^\alpha Q^\beta}{Q^2}\right) L_{\alpha\beta}(\mathbf{Q},\omega)\,, \tag{1.10}$$

which is nothing but the specialization to the magnetic case of the original study of van Hove about the connection between the cross section in the Born approximation and correlation functions [18].

When the probing species are spin-polarized electrons, such as the case of SPEELS experiments, the dominant scattering mechanism is not due to the dipolar interaction between magnetic moments, but to the Coulomb interaction between charged fermions (i.e. electrons), which endows the total cross section with a magnetic contribution through an exchange process. In spite of that, the final form of the cross section still depends on the loss tensor $L_{\alpha\beta}(\mathbf{Q},\omega)$, which can be used to interpret also surface excitations. For a detailed derivation the reader is referred to [19], for a discussion of the experimental setup to [20].

1.2.2 Polarization Effects

We consider explicitly the polarization of the neutron beam. Before proceeding, it is useful to rewrite Eq. (1.8) by noting that $\left(\delta_{\alpha\beta} - Q^\alpha Q^\beta/Q^2\right)$ is a projector over the plane perpendicular to $\mathbf{Q}$, so that

$$\frac{\mathrm{d}^2\sigma}{\mathrm{d}\Omega_f \mathrm{d}\varepsilon_f} = \left(\frac{e g_n}{2\hbar}\right)^2 \frac{k_f}{k_i} \sum_f \mathbf{m}_\perp^f \cdot \mathbf{m}_\perp^{f*}\, \delta\Big(\hbar\omega - (E_f - E_{\mathrm{GS}})\Big)\,, \tag{1.11}$$

where E_{GS} and E_f are the energy of the target system before and after the scattering process, respectively. We have also used the shorthand

$$m_\perp^{\alpha,f} = \sum_\beta \left(\delta_{\alpha\beta} - \frac{Q^\alpha Q^\beta}{Q^2}\right) \langle \Psi_{\mathrm{GS}}, \hat{\mathcal{M}}^\beta(\mathbf{Q}) \Psi_f \rangle\,. \tag{1.12}$$

Only the fluctuations perpendicular to the $\mathbf{Q}$-direction are meaningful for the cross section: magnetic excitations in the Born approximation are of transverse nature. The polarization of a neutron beam is described by the density matrix in the spin space

$$\hat{\rho}_n^{(i)} = \frac{1}{2}\left(\sigma^\circ + \mathbf{P}_i \cdot \boldsymbol{\sigma}_n\right)\,, \tag{1.13}$$

where $\mathbf{P}_i$ is the polarization vector, related to the expectation value of the spin operator via[2]

$$\langle \hat{\mathbf{s}}_n \rangle_i = \frac{\hbar}{2}\mathbf{P}_i = \mathrm{t}r\Big[\hat{\rho}_n^{(i)} \hat{\mathbf{s}}_n\Big]\,. \tag{1.14}$$

[2]The lower-case tr denotes a trace over the spin degrees of freedom only.

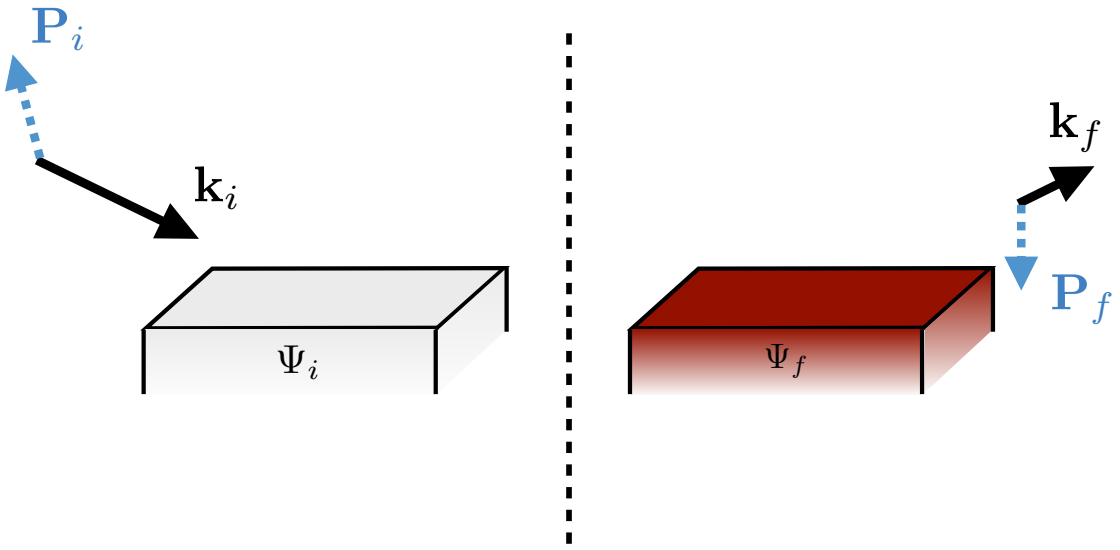

Figure 7. The knowledge of the incoming and outgoing neutron-beam polarization give additional information about the state Ψ_f, such as its chirality.

If one sends a polarized beam (and still records all the outgoing neutrons) the resulting cross section is

$$\frac{\mathrm{d}^2\sigma}{\mathrm{d}\Omega_f \mathrm{d}\varepsilon_f} = \left(\frac{eg_n}{2\hbar}\right)^2 \frac{k_f}{k_i} \sum_f \left[\mathbf{m}_\perp^f \cdot \mathbf{m}_\perp^{f*} + i\,\mathbf{P}_i \cdot \left(\mathbf{m}_\perp^f \times \mathbf{m}_\perp^{f*}\right)\right] \delta\Big(\hbar\omega - (E_f - E_{\mathrm{GS}})\Big)\,, \tag{1.15}$$

where the second term displays an explicit dependence on the direction of the polarization.[3] The origin of the new term can be understood by computing the polarization of the outgoing beam, which is given by [21, 12]

$$\mathbf{P}_f = \left(\frac{eg_n}{2\hbar}\right)^2 \frac{k_f}{k_i} \left(\frac{\mathrm{d}^2\sigma}{\mathrm{d}\Omega_f \mathrm{d}\varepsilon_f}\right)^{-1} \sum_f \Big\{ -\mathbf{P}_i \left(\mathbf{m}_\perp^f \cdot \mathbf{m}_\perp^{f*}\right) + 2\mathrm{Re}\Big[\mathbf{m}_\perp^f \left(\mathbf{P}_i \cdot \mathbf{m}_\perp^{f*}\right)\Big] - i\left(\mathbf{m}_\perp^f \times \mathbf{m}_\perp^{f*}\right)\Big\} \delta\Big(\hbar\omega - (E_f - E_{\mathrm{GS}})\Big)\,. \tag{1.17}$$

The additional term $-i\left(\mathbf{m}_\perp^f \times \mathbf{m}_\perp^{f*}\right)$ gives rise to a polarization in the scattered beam along the $\mathbf{Q}$-direction, even though the impinging beam is unpolarized. Furthermore, it vanishes for simple ferromagnets [21], and therefore is an intrinsic feature of more complex magnetization orderings. We conlcude by noticing that also $-i\left(\mathbf{m}_\perp^f \times \mathbf{m}_\perp^{f*}\right)$ can be obtained by suitable combinations of the loss-tensor elements $L_{\alpha\beta}(\mathbf{Q}, \omega)$, and can therefore be inferred by linear-response theory.

[3] Notice that the new term is real, since, given a complex vector $\mathbf{z} = \mathbf{a} + i\mathbf{b}$, one has

$$(\mathbf{z} \times \mathbf{z}^*) = -2i(\mathbf{a} \times \mathbf{b})\,. \tag{1.16}$$

1.2.3 Summary

In the first part of this chapter we have outlined the phenomenology that has inspired the present work, i.e. the description of damping mechanisms in the propagation of spin-waves, due to a strong spin-orbit interaction. These dampings can be studied by the perspective of the density of magnetic excitations in a system in the $(\mathbf{Q}, \omega)$-space, which is accessible by scattering and energy-loss experiments, as commented in the second part of the chapter. The theoretical tool we need to interpret these experiments is the magnetic susceptibility, which has to be computed in a non-collinear framework in order to account for spin-orbit effects. At the same time, we mentioned that the knowledge of the full magnetic susceptibility of a system can also give information on the structure, in particular on the chirality, of magnetic excitations, and may be used to identify and study the stability of magnetic formations such as skyrmions. We shall pursue this study in the framework of Time-Dependent Density Functional Theory.

CHAPTER

TWO

DENSITY-FUNCTIONAL THEORY

The theoretical study of condensed-matter systems requires to deal with several levels of approximation, due to the impracticability of a brute-force solution of the Schrödinger (or Dirac) equations for a system of interacting electrons and nuclei. A first simplification, known as *Born-Oppenheimer approximation*, is to consider the electron dynamics decoupled from the nuclear one. This has been shown to be a fair good approximation also in some gapless systems, such as ordinary metals, due to the low coupling between electronic excitations and nuclear vibrations in normal conditions [22]. Under this assumption, the problem reduces to a system of interacting electrons subject to the electrostatic potential of the nuclei at rest, which still proves too hard a task and requires further approximations. Density Functional Theory (DFT) is a well-established methodology to tackle such a problem, and will be the theoretical framework of this thesis. The basic equations of DFT, with a focus on its spin-dependent implementation, will be outlined in the first part of this chapter; in the second part, more technical aspects such as pseudopotentials and the Brillouin Zone (BZ) integration will be covered.

2.1 Basic Theory

In the Born-Oppenheimer approximation, the non-relativistic Hamiltonian for a system of N electrons subject to the electrostatic field of M nuclei reads

$$\hat{\mathcal{H}}[\{\mathbf{R}\}] = \sum_{i=1}^{N} \frac{\hat{p}_i^2}{2m} + \frac{1}{2}\sum_{i,j=1}^{N} \frac{e^2}{|\hat{\mathbf{r}}_i - \hat{\mathbf{r}}_j|} - \sum_{i=1}^{N}\sum_{I=1}^{M} \frac{eZ_I}{|\mathbf{R}_I - \hat{\mathbf{r}}_i|} + \frac{1}{2}\sum_{I,J=1}^{M} \frac{Z_I Z_J}{|\mathbf{R}_I - \mathbf{R}_J|}\,, \quad (2.1)$$

where e is the absolute value of the electron charge, m the electron rest mass, Z_I the I-th nuclear charge, $\hat{\mathbf{r}}_i$ and $\mathbf{R}_I$ the electron and nucleus positions. We can rewrite (2.1) as

$$\hat{\mathcal{H}}[\{\mathbf{R}\}] = \sum_{i=1}^{N} \frac{\hat{p}_i^2}{2m} + \frac{1}{2}\sum_{i,j=1}^{N} \frac{e^2}{|\hat{\mathbf{r}}_i - \hat{\mathbf{r}}_j|} + \int_{\mathbb{R}^3} \mathrm{d}^3 r\, \hat{\mathcal{N}}(\mathbf{r})\, v_{\mathrm{ext}}(\mathbf{r}; \{\mathbf{R}\})\,, \quad (2.2)$$

where $\hat{\mathcal{N}}(\mathbf{r}) = \sum_\sigma \hat{\psi}^\dagger_\sigma(\mathbf{r})\hat{\psi}_\sigma(\mathbf{r})$ is the electron density-operator,[1] which couples linearly with the external potential

$$v_{\text{ext}}(\mathbf{r};\{\mathbf{R}\}) = -\sum_{I=1}^{M} \frac{eZ_I}{|\mathbf{R}_I - \mathbf{r}|} + \frac{1}{2}\sum_{I,J=1}^{M} \frac{Z_I Z_J}{|\mathbf{R}_I - \mathbf{R}_J|} \,. \tag{2.3}$$

Eq. (2.2) is the starting point for the application to condensed-matter systems of DFT, where the central role is assigned to the electron charge-density, defined by

$$n(\mathbf{r}) = \left\langle \Psi, \hat{\mathcal{N}}(\mathbf{r})\Psi \right\rangle \,, \tag{2.4}$$

or equivalently, in terms of the many-body wavefunction,

$$n(\mathbf{r}) = N \sum_{\sigma_1,\cdots,\sigma_N} \int_{\mathbb{R}^3} \mathrm{d}^3 r_2 \cdots \int_{\mathbb{R}^3} \mathrm{d}^3 r_N \left|\Psi(\mathbf{r}\,\sigma_1, \mathbf{r}_2\sigma_2, \ldots, \mathbf{r}_N\sigma_N)\right|^2 . \tag{2.5}$$

In the following, it will be shown how the variational principle of quantum mechanics, holding for $\Psi(\mathbf{r}_1\,\sigma_1, \mathbf{r}_2\sigma_2, \ldots, \mathbf{r}_N\sigma_N)$, is recast in terms of the more tractable charge density $n(\mathbf{r})$.

2.1.1 The Energy Functional

Let an N-electron system be described by the Hamiltonian

$$\hat{\mathcal{H}} = \hat{\mathcal{H}}_{\text{sys}} + \hat{\mathcal{V}} \,, \tag{2.6}$$

$$\hat{\mathcal{V}} = \int_{\mathbb{R}^3} \mathrm{d}^3 r\, \hat{\mathcal{N}}(\mathbf{r})\, v_{\text{ext}}(\mathbf{r}) \,; \tag{2.7}$$

in 1965 Hohenberg and Kohn [23] proved that

1. The potential $v_{\text{ext}}(\mathbf{r})$ is (up to a constant) a unique functional of the ground-state density $n(\mathbf{r})$. This implies that the total Hamiltonian $\hat{\mathcal{H}}$, and therefore all the properties of the system, are functionals of the ground-state density.

2. Once fixed the external potential, the energy, viewed as a functional of the density, has a minimum at the ground-state $n(\mathbf{r})$.

Hence one can define the energy functional for a chosen external potential

$$E_{v_{\text{ext}}}[n] = F[n] + \int_{\mathbb{R}^3} \mathrm{d}^3 r\; n(\mathbf{r})\, v_{\text{ext}}(\mathbf{r}) \,, \tag{2.8}$$

$$F[n] \equiv \left\langle \Psi[n], \hat{\mathcal{H}}_{\text{sys}}\Psi[n] \right\rangle \,, \tag{2.9}$$

which has its minimum when $n = n_{\text{GS}}$,and whose stationarity condition reads

$$\frac{\delta F}{\delta n(\mathbf{r})} = -v_{\text{ext}}(\mathbf{r}) \,. \tag{2.10}$$

[1] The Fermi field $\hat{\psi}_\sigma(\mathbf{r})$ annihilates an electron of spin σ in the position $\mathbf{r}$. Fermi fields will be used only to define the density operators in a more compact way and should not be confused with $\psi_i(\mathbf{r})$, which will be used to denote a spinor in the one-particle state i.

2.1.2 The Kohn-Sham Scheme

The most widespread implementation of DFT is due to Kohn and Sham [24], who devised a way to translate the minimization problem with respect to the density into the solution of a set of self-consistent, single-particle equations. They proposed the decomposition

$$F[n] = T_s[n] + E_{\mathrm{H}}[n] + E_{\mathrm{xc}}[n]\,, \tag{2.11}$$

where $T_s[n]$ is the kinetic energy of a system of non-interacting electrons, $E_{\mathrm{H}}[n]$ is the Hartree energy functional

$$E_{\mathrm{H}}[n] = \frac{e^2}{2}\int_{\mathbb{R}^3} \mathrm{d}^3r \int_{\mathbb{R}^3} \mathrm{d}^3r'\, \frac{n(\mathbf{r})n(\mathbf{r}')}{|\mathbf{r}-\mathbf{r}'|}\,, \tag{2.12}$$

and $E_{\mathrm{xc}}[n]$ is the *exchange-correlation functional*, which is actually defined by Eq. (2.11). Within this decomposition, the stationarity condition (2.10) reads

$$\frac{\delta T_s}{\delta n(\mathbf{r})} = -v_{\mathrm{H}}(\mathbf{r}) - v_{\mathrm{xc}}(\mathbf{r}) - v_{\mathrm{ext}}(\mathbf{r})\,, \tag{2.13}$$

with

$$v_{\mathrm{H}}(\mathbf{r}) = e^2\int_{\mathbb{R}^3} \mathrm{d}^3r'\, \frac{n(\mathbf{r}')}{|\mathbf{r}-\mathbf{r}'|}\,, \qquad v_{\mathrm{xc}}(\mathbf{r}) \equiv \frac{\delta E_{\mathrm{xc}}}{\delta n(\mathbf{r})}\,. \tag{2.14}$$

This is exactly the same condition we would find when minimizing the functional

$$E_{\mathrm{KS}}[n] = T_s[n] + \int_{\mathbb{R}^3} \mathrm{d}^3r\; n(\mathbf{r})\, v_{\mathrm{KS}}(\mathbf{r})\,, \tag{2.15}$$

$$v_{\mathrm{KS}}(\mathbf{r}) \equiv v_{\mathrm{H}}(\mathbf{r}) + v_{\mathrm{xc}}(\mathbf{r}) + v_{\mathrm{ext}}(\mathbf{r})\,, \tag{2.16}$$

i.e. the functional of a system of non-interacting electrons under the action of the (fixed) single-particle, local potential $v_{\mathrm{KS}}(\mathbf{r})$. The ground-state wave function of the Kohn-Sham functional (which is not the ground-state wave function of the interacting system, they only share the density) is then a Slater determinant whose orbitals satisfy the so-called *Kohn-Sham equations*:

$$\left[-\frac{\hbar^2}{2m}\nabla^2 + v_{\mathrm{Hxc}}[n](\mathbf{r}) + v_{\mathrm{ext}}(\mathbf{r})\right]\psi_i(\mathbf{r}) = \varepsilon_i\,\psi_i(\mathbf{r})\,, \qquad n(\mathbf{r}) = \sum_i^{\mathrm{occ.}} |\psi_i(\mathbf{r})|^2\,, \tag{2.17}$$

where we grouped the self-consistent terms in $v_{\mathrm{Hxc}} = v_{\mathrm{H}} + v_{\mathrm{xc}}$. Once the density is known from the solution of the Kohn-Sham equations, all the properties of the interacting system are also at hand in virtue of the Hohenberg-Kohn Theorem. Note that, at the minimum, the total energy of the true sytem does not correspond to the sum of the eigenvalues ε_i defined by the Kohn-Sham scheme.

We finally remark that Eqs. (2.17) can also be obtained by minimizing with respect to ψ_i^* the functional

$$E\left[\{\psi\}\right] = \sum_i^{\mathrm{occ.}} \int_{\mathbb{R}^3} \mathrm{d}^3r\; \psi_i^*(\mathbf{r})\left(-\frac{\hbar^2}{2m}\nabla^2\psi_i(\mathbf{r})\right) + E_{\mathrm{Hxc}}\left[n\right] + \int_{\mathbb{R}^3} \mathrm{d}^3r\; n(\mathbf{r})\, v_{\mathrm{ext}}(\mathbf{r})\,, \tag{2.18}$$

under the orthonormality constraint $\langle\psi_i, \psi_j\rangle = \delta_{ij}$.[2] The density has to be considered a function of the orbitals through (2.17).

2.1.3 Spin-Density Functional Theory

Though the total Hamiltonian does not contain any term that couples with the spin degrees of freedom, some systems may exhibit a ground state with non-zero magnetization density due the fermionic statistics of the electrons, i.e.

$$\mathbf{m}(\mathbf{r}) = \frac{\mu_{\mathrm{B}} g_e}{\hbar} \langle \Psi, \hat{\boldsymbol{\mathcal{S}}}(\mathbf{r}) \Psi \rangle \neq 0 \,, \tag{2.19}$$

where $\hat{\boldsymbol{\mathcal{S}}}(\mathbf{r})$ is the spin-density operator

$$\hat{\boldsymbol{\mathcal{S}}}(\mathbf{r}) = \frac{\hbar}{2} \sum_{\sigma\sigma'} \hat{\psi}^\dagger_\sigma(\mathbf{r}) \boldsymbol{\sigma}_{\sigma\sigma'} \hat{\psi}_{\sigma'}(\mathbf{r}) \,, \tag{2.20}$$

and $\boldsymbol{\sigma}$ the vector of Pauli matrices

$$\sigma^x = \begin{pmatrix} 0 & 1 \\ 1 & 0 \end{pmatrix} \qquad \sigma^y = \begin{pmatrix} 0 & -i \\ i & 0 \end{pmatrix} \qquad \sigma^z = \begin{pmatrix} 1 & 0 \\ 0 & -1 \end{pmatrix} \,. \tag{2.21}$$

The theory discussed previously applies also in these cases, but it gives no practical instruction on how to compute the expectation values of the operator of interest, neither a way to distinguish between degenerate ground states.[3] In these cases it is convenient to generalize the theory considering local external potentials $w_{\sigma\sigma'}(\mathbf{r})$ which couple to the spin-resolved density matrix $\hat{\rho}_{\sigma\sigma'}(\mathbf{r}) = \hat{\psi}^\dagger_\sigma(\mathbf{r})\hat{\psi}_{\sigma'}(\mathbf{r})$, i.e. entering the total Hamiltonian as

$$\hat{\mathcal{V}} = \sum_{\sigma\sigma'} \int_{\mathbb{R}^3} \mathrm{d}^3 r \; \hat{\rho}_{\sigma\sigma'}(\mathbf{r}) \, w_{\sigma'\sigma}(\mathbf{r}) \,. \tag{2.22}$$

In this more general case, the spin-resolved density does not determine univocally the external potential $w_{\sigma\sigma'}(\mathbf{r})$; it is nevertheless possible to define an energy-functional $E[\rho]$ which is variational with respect to ground-state ρ [25], and to apply the Kohn-Sham procedure, resulting in[4]

$$\sum_{\sigma'} \left[-\frac{\hbar^2}{2m} \nabla^2 \delta_{\sigma\sigma'} + v^{\sigma\sigma'}_{\mathrm{Hxc}}[\rho](\mathbf{r}) + v_{\mathrm{ext}}(\mathbf{r}) \delta_{\sigma\sigma'} \right] \psi_{i\sigma'}(\mathbf{r}) = \varepsilon_i \, \psi_{i\sigma}(\mathbf{r}) \,, \tag{2.23}$$

[2] The contraint is accounted for via Lagrange multipliers Λ_{ij}. After the minimization, Eqs. (2.17) are recovered performing a unitary rotation of the orbitals ψ_i, so to diagonalize Λ_{ij} into ε_i (the functional E is invariant under unitary rotations of $\{\psi\}$). We also point out that the kinetic-energy term in (2.18) is not the functional $T_s[n]$, but gives the same energy contribution, being the kinetic-energy of a non-interacting system.

[3] Such as in the case of non-relativistic ferromagnetism, where the ground-state energy does not depend on the direction of the magnetization in space.

[4] The generalization is needed just to define the Kohn-Sham functional such as in (2.15), in fact that is the only place in which the (self-consistent) potential couples to the spin. The external potential remains purely scalar.

where

$$v_{\mathrm{Hxc}}^{\sigma\sigma'}(\mathbf{r}) = \delta_{\sigma\sigma'} v_{\mathrm{H}}(\mathbf{r}) + v_{\mathrm{xc}}^{\sigma\sigma'}(\mathbf{r})\,, \tag{2.24}$$

$$v_{\mathrm{xc}}^{\sigma\sigma'}(\mathbf{r}) \equiv \frac{\delta E_{\mathrm{xc}}}{\delta \rho_{\sigma\sigma'}(\mathbf{r})}\,. \tag{2.25}$$

It is usually preferred to work with the charge and magnetization densities

$$n(\mathbf{r}) = \sum_{\sigma} \rho_{\sigma\sigma}(\mathbf{r})\,, \qquad \mathbf{m}(\mathbf{r}) = \mu_{\mathrm{B}} \sum_{\sigma\sigma'} \boldsymbol{\sigma}_{\sigma\sigma'} \rho_{\sigma'\sigma}(\mathbf{r})\,, \tag{2.26}$$

so that we can write

$$v_{\mathrm{xc}}^{\sigma\sigma'}(\mathbf{r}) = \frac{\delta E_{\mathrm{xc}}}{\delta n(\mathbf{r})} \frac{\partial n(\mathbf{r})}{\partial \rho_{\sigma\sigma'}(\mathbf{r})} + \frac{\delta E_{\mathrm{xc}}}{\delta \mathbf{m}(\mathbf{r})} \cdot \frac{\partial \mathbf{m}(\mathbf{r})}{\partial \rho_{\sigma\sigma'}(\mathbf{r})} \tag{2.27}$$

$$= \frac{\delta E_{\mathrm{xc}}}{\delta n(\mathbf{r})} \sigma^{\circ} + \mu_B \frac{\delta E_{\mathrm{xc}}}{\delta \mathbf{m}(\mathbf{r})} \cdot \boldsymbol{\sigma} \tag{2.28}$$

where σ° stands for the 2×2 identity in the spin space. Now we can define

$$v_{\mathrm{xc}}(\mathbf{r}) = \frac{\delta E_{\mathrm{xc}}}{\delta n(\mathbf{r})}\,, \qquad \mathbf{b}_{\mathrm{xc}}(\mathbf{r}) = -\frac{\delta E_{\mathrm{xc}}}{\delta \mathbf{m}(\mathbf{r})}\,, \tag{2.29}$$

so to recast Eq. (2.23) as

$$\left[\left(-\frac{\hbar^2}{2m}\nabla^2 + v_{\mathrm{Hxc}}[n,\mathbf{m}](\mathbf{r}) + v_{\mathrm{ext}}(\mathbf{r})\right)\sigma^{\circ} - \mu_{\mathrm{B}}\,\boldsymbol{\sigma}\cdot\mathbf{b}_{\mathrm{xc}}[n,\mathbf{m}](\mathbf{r})\right]\psi_i(\mathbf{r}) = \varepsilon_i\,\psi_i(\mathbf{r})\,, \tag{2.30}$$

where ψ_i has to be considered a two-component spinor. The charge and magnetization densities of the Kohn-Sham system, which equal by assumption the true ones, read

$$n(\mathbf{r}) = \sum_{i}^{\mathrm{occ.}} \psi_i^{\dagger}(\mathbf{r})\psi_i(\mathbf{r})\,, \qquad \mathbf{m}(\mathbf{r}) = \mu_{\mathrm{B}} \sum_{i}^{\mathrm{occ.}} \psi_i^{\dagger}(\mathbf{r})\boldsymbol{\sigma}\psi_i(\mathbf{r})\,. \tag{2.31}$$

2.1.4 The Exchange-Correlation Functional

The success or failure of DFT depends on the capability of modelling the functional $E_{\mathrm{xc}}[n,\mathbf{m}]$, without which the Kohn-Sham system would reduce to the Hartree equations. In the Local Spin-Density Approximation (LSDA) one uses the form

$$E_{\mathrm{xc}}^{\mathrm{LSDA}}[n,m] = \int_{\mathbb{R}^3} \mathrm{d}^3 r\; n(\mathbf{r})\,\epsilon_{\mathrm{xc}}\big(n(\mathbf{r}),m(\mathbf{r})\big)\,, \tag{2.32}$$

with $m(\mathbf{r}) = |\mathbf{m}(\mathbf{r})|$ and $\epsilon_{\mathrm{xc}}(n,m)$ being the exchange-correlation energy per particle of a homogeneous electron gas, constrained to a collinear spin-polarized state with magnetization m [25]. We have

$$\epsilon_{\mathrm{xc}}(n,m) = \epsilon_{\mathrm{x}}(n,m) + \epsilon_{\mathrm{c}}(n,m)\,, \tag{2.33}$$

where $\epsilon_{\rm x}(n,m)$ is known analitically (see, e.g., Ch. 5 of [26]), and the form of $\epsilon_{\rm c}(n,m)$ has been drawn by fitting Monte Carlo calculations [27].

LSDA is most accurate at slowly-varying densities, since it approximates point-by-point the system with a homogeneous electron gas; to overcome its limitations, functionals depending also on the gradient of the spin-resolved density have been developed throughout the years. The most successful class of these functionals goes by the name of Generalized Gradient Approximation (GGA), which are usually written as

$$E_{\rm xc}^{\rm GGA}[n^\uparrow, n^\downarrow] = \int_{\mathbb{R}^3} {\rm d}^3r \; n(\mathbf{r})\, \epsilon_{\rm x}^{\rm unp.}(n)\, F_{\rm xc}(n^\uparrow, n^\uparrow, \nabla n^\downarrow, \nabla n^\downarrow)\;, \tag{2.34}$$

where $n^\uparrow(\mathbf{r}) = \rho_{\uparrow\uparrow}(\mathbf{r})$, $n^\downarrow(\mathbf{r}) = \rho_{\downarrow\downarrow}(\mathbf{r})$ and $\epsilon_{\rm x}^{\rm unp.}(n) = \epsilon_{\rm x}(n,0)$ is the exchange energy of the unpolarized homogeneous electron gas. The function $F_{\rm xc}$ is a correction factor that restores the LSDA form for when the density gradients vanish.

Nowadays LSDA and GGAs are the most widely used xc-approximations in solid-state DFT computations, and their range of applicability is well enstablished. In the last 20 years, however, several other functional forms have been proposed in order to heal the reknown limits of the local and semilocal (i.e. gradient-based) approximations of the xc-energy, giving birth to orbital-based functionals (such as hybrids), meta-GGA (depending on the Laplacian of the density), or van der Waals functionals. The discussion of the accuracy and limitations of the various functional forms is beyond the scope of this thesis and an active research field. For success and failures of LSDA and GGAs, the reader is referred to standard textbooks, such as Ch. 8 of [26], Ch. 7 of [28], or Sec. 2.5 of [29].

2.1.5 Collinear and Non-Collinear Magnetism

The LSDA and GGA xc-functionals are based on the homogeneous electron gas in a collinear state, in which the magnetization $\mathbf{m}(\mathbf{r})$ is constant in modulus and direction everywhere in space. As a result, the xc-functionals are sensitive only to the modulus of the magnetization, and not to its direction.The xc-magnetic field $\mathbf{b}_{\rm xc}$ generated by this approximations is always locally aligned with the magnetization, in fact

$$\mathbf{b}_{\rm xc}^{\rm LSDA}(\mathbf{r}) = -\frac{\delta E_{\rm xc}^{\rm LSDA}}{\delta \mathbf{m}(\mathbf{r})} = -n(\mathbf{r})\, \frac{\partial \epsilon_{\rm xc}}{\partial m}\, \frac{\mathbf{m}(\mathbf{r})}{m(\mathbf{r})}\,, \tag{2.35}$$

whereas in the GGA case, considering that $n^\uparrow = \frac{1}{2}(n + m/\mu_B)$ and $n^\downarrow = \frac{1}{2}(n - m/\mu_B)$, one has[5]

$$\begin{aligned}
\mathbf{b}_{\rm xc}^{\rm GGA}(\mathbf{r}) &= -\frac{\delta E_{\rm xc}^{\rm GGA}}{\delta \mathbf{m}(\mathbf{r})} \\
&= -\int_{\mathbb{R}^3} {\rm d}^3r' \; \frac{\delta E_{\rm xc}^{\rm GGA}}{\delta m(\mathbf{r}')}\, \frac{\delta m(\mathbf{r}')}{\delta \mathbf{m}(\mathbf{r})} \\
&= -n(\mathbf{r}) \epsilon_{\rm x}(n(\mathbf{r}))\left[\frac{\partial F_{\rm xc}}{\partial m} - \nabla \cdot \frac{\partial F_{\rm xc}}{\partial \nabla m}\right] \frac{\mathbf{m}(\mathbf{r})}{m(\mathbf{r})}\,.
\end{aligned} \tag{2.37}$$

[5]Here we have used the standard differentiation rule

$$F[\rho] = \int {\rm d}^3r \; f(\mathbf{r}, \rho(\mathbf{r}), \nabla\rho(\mathbf{r}))\,, \qquad \frac{\delta F}{\delta \rho} = \frac{\partial f}{\partial \rho} - \nabla \cdot \frac{\partial f}{\partial \nabla \rho}\,. \tag{2.36}$$

This is a general feature of any functional that depends on ∇m, instead of $\nabla \mathbf{m}$. Several efforts to develop xc-functionals yielding a $\mathbf{b}_{\mathrm{xc}}$ field with a component perpendicular to the magnetization have been made, we mention in particular the usage of the electron gas in a spin-spiral wave state (instead of collinear) as a reference to build E_{xc} [30, 31], or orbital functionals [32].

Since LSDA and GGA use the functional dependence of a *collinear* electron gas, their first application has been on collinear magnetic structures, in which the magnetization has the same direction (but may have different magnitude) in all the points in space. This allows to choose a global spin quantization axis along the same direction of $\mathbf{m}$, so that $m^x = m^y = 0$, yielding Kohn-Sham orbitals eigenstates of $\hat{s}^z$, so that

$$\psi_i(\mathbf{r}) = \begin{pmatrix} \varphi_{i\uparrow}(\mathbf{r}) \\ 0 \end{pmatrix} , \qquad i = 1, \ldots, N_\uparrow \tag{2.38}$$

$$\psi_j(\mathbf{r}) = \begin{pmatrix} 0 \\ \varphi_{j\downarrow}(\mathbf{r}) \end{pmatrix} , \qquad j = 1, \ldots, N_\downarrow , \tag{2.39}$$

with $N_\uparrow + N_\downarrow = N$. In this case the Kohn-Sham equations become

$$\begin{aligned} \left[-\frac{\hbar^2}{2m}\nabla^2 + v_{\mathrm{Hxc}}[n^\uparrow, n^\downarrow](\mathbf{r}) + v_{\mathrm{ext}}(\mathbf{r}) - \mu_{\mathrm{B}}\, b^z_{\mathrm{xc}}[n^\uparrow, n^\downarrow](\mathbf{r}) \right] \varphi_{i\uparrow}(\mathbf{r}) &= \varepsilon_{i\uparrow}\, \varphi_{i\uparrow}(\mathbf{r}) , \\ \left[-\frac{\hbar^2}{2m}\nabla^2 + v_{\mathrm{Hxc}}[n^\uparrow, n^\downarrow](\mathbf{r}) + v_{\mathrm{ext}}(\mathbf{r}) + \mu_{\mathrm{B}}\, b^z_{\mathrm{xc}}[n^\uparrow, n^\downarrow](\mathbf{r}) \right] \varphi_{i\downarrow}(\mathbf{r}) &= \varepsilon_{i\downarrow}\, \varphi_{i\downarrow}(\mathbf{r}) , \end{aligned} \tag{2.40}$$

with

$$n^\uparrow(\mathbf{r}) = \sum_{i=1}^{N_\uparrow} |\varphi_{i\uparrow}(\mathbf{r})|^2 , \qquad n^\downarrow(\mathbf{r}) = \sum_{i=1}^{N_\downarrow} |\varphi_{i\downarrow}(\mathbf{r})|^2 . \tag{2.41}$$

Nonetheless, *non-collinear* systems can be described with collinear functionals, considering a local (instead of global) spin-quantization axis: $\mathbf{m}(\mathbf{r})$ is free to vary its direction in space, and at each point the xc-functional is evaluated using only its modulus [33]. In other words, the xc-energy is evaluated as the xc-energy of a collection of infinitesimal boxes of homogeneous electron gases polarized in different directions, in the same spirit of LDA for the density only. In this latter case we have to resort to the general form of the Kohn-Sham equations (2.30) and (2.31), and the Kohn-Sham orbitals have to be considered as two-component spinors. It remains however valid, as showed before, that $\mathbf{b}_{\mathrm{xc}}(\mathbf{r}) \,/\!/\, \mathbf{m}(\mathbf{r})$.

2.1.6 TDDFT

The success of the Kohn-Sham mapping to approximate the solutions of the stationary Shrödinger equation inspired efforts towards the generalization to the dynamical case. The first question to answer is whether the correspondence density and potential still holds in the time-dependent case; if so, the Kohn-Sham Ansatz can be formulated. Affermative answers to this question came by the Runge-Gross Theorem first, and by the van Leeuwen Thereom later, which provides also rigorous foundations to the Kohn-Sham Ansatz.

We consider a time-dependent Hamiltonian of the form of

$$\hat{\mathcal{H}}(t) = \hat{\mathcal{T}} + \hat{\mathcal{H}}_{\text{int}} + \int_{\mathbb{R}^3} \hat{\mathcal{N}}(\mathbf{r})\, v_{\text{ext}}(\mathbf{r}, t)\,, \tag{2.42}$$

where $\hat{\mathcal{T}}$ is the kinetic energy and $\hat{\mathcal{H}}_{\text{int}}$ the particle-particle interaction, the Runge-Gross theorem [34] states:

Runge-Gross Theorem. *The densities $n(\mathbf{r}, t)$ and $n'(\mathbf{r}, t)$ evolving with $\hat{\mathcal{H}}(t)$ from a common initial state Ψ° under the action of two local potentials $v_{\text{ext}}(\mathbf{r}, t)$ and $v'_{\text{ext}}(\mathbf{r}, t)$ that are expandable in Taylor series about the initial time t_0, are necessarily different, provided that*

$$v_{\text{ext}}(\mathbf{r}, t) \neq v'_{\text{ext}}(\mathbf{r}, t) + c(t)\,.$$

Some years later, van Leeuwen proved a generalization of this thereom [35]:

van Leeuwen Theorem. *Consider a Hamiltonian in the form of* (2.42)*, and another Hamiltonian $\hat{\mathcal{H}}'(t)$with a different local potential $v'_{\text{ext}}(\mathbf{r}, t)$ and interacting part $\hat{\mathcal{H}}'_{\text{int}}$. Let $n(\mathbf{r}, t)$ be the density which evolves from the initial state Ψ° under the Hamiltonian $\hat{\mathcal{H}}(t)$, and let $\Psi^{\circ\prime}$ be another initial state with the same density and the same derivative of the density with respect to time $-\nabla \cdot \mathbf{j}(\mathbf{r}, t)$. Then the time-dependent density $n(\mathbf{r}, t)$ uniquely determines, up to a time-dependent constant, the potential $\hat{\mathcal{H}}'_{\text{int}}$ that yields $n(\mathbf{r}, t)$ starting from $\Psi^{\circ\prime}$ and evolving under $\hat{\mathcal{H}}'(t)$.*

Notice that the Runge-Gross theorem is recovered by setting $\Psi^{\circ\prime} = \Psi^\circ$ and $\hat{\mathcal{H}}'_{\text{int}} = \hat{\mathcal{H}}_{\text{int}}$. Most importantly, in the case in which $\hat{\mathcal{H}}'_{\text{int}} = 0$, van Leeuwen's theorem proves the existence of a scalar potential that yields, for a non-interacting system, the same density of the interacting one. This paves the way to the introduction of a time-dependent Kohn-Sham system of equations: we assume our system to be in the ground state, where the density $n(\mathbf{r})$ given by the Kohn-Sham wave function Ψ^{KS} is assumed to be the same as the one given by the true wave function Ψ°, by virtue of DFT. Thanks to van Leeuwen's theorem we know that even the evolution of the Ψ^{KS} will yield the true density $n(\mathbf{r}, t)$, provided with the correct local potential $v_{\text{KS}}(\mathbf{r}, t)$. In principle, by solving the evolution of the non-interacting Kohn-Sham system[6]

$$\begin{aligned} i\hbar \frac{\partial}{\partial t} \psi_i(\mathbf{r}, t) &= \left[-\frac{\hbar^2 \nabla^2}{2m} + v_{\text{KS}}[n](\mathbf{r}, t) \right] \psi_i(\mathbf{r}, t)\,, \\ n(\mathbf{r}, t) &= \sum_i^{\text{occ.}} |\psi_i(\mathbf{r}, t)|^2 \end{aligned} \tag{2.43}$$

we gain access to the evolution of the true density. In practice, we have no recipe on how to build such a potential. Similarly to what has been done in the ground-state case, a time-dependent Hartree term is isolated in the definition of the time-dependent effective potetnial

$$v_{\text{KS}}[n](\mathbf{r}, t) = v_{\text{H}}[n](\mathbf{r}, t) + v_{\text{xc}}[n](\mathbf{r}, t) + v_{\text{ext}}(\mathbf{r}, t)\,, \tag{2.44}$$

[6]Note that the time-dependent Kohn-Sham potential depends self-consistently on the density due to the choice of Ψ^{GS} as a starting state.

where

$$v_{\rm H}[n](\mathbf{r},t) = e^2 \int_{\mathbb{R}^3} \mathrm{d}^3 r' \, \frac{n(\mathbf{r},t)}{|\mathbf{r}-\mathbf{r}'|} \,, \tag{2.45}$$

and $v_{\rm xc}[n](\mathbf{r},t)$ is the time-dependent exchange-correlation potential. In theory, the xc-potential at a time $v_{\rm xc}(\mathbf{r},t)$ should depend on all the past densities $n(\mathbf{r},t')$, with $t' < t$. In practice, it is not clear how to define such a functional and one usually resorts to the *adiabatic local density approximation* (ALDA), where the xc-potential is assumed to be the derivative of the ground-state energy functional evaluated at the instantaneous value of the density:

$$v_{\rm xc}^{\rm ALDA}(\mathbf{r},t) = \frac{\delta E_{\rm xc}^{\rm LDA}}{\delta n(\mathbf{r})}\Big|_{n(\mathbf{r})=n(\mathbf{r},t)} \,. \tag{2.46}$$

This approximation has been extensively tested in linear response calculations, and proved to work fairly well in the computation of optical excitations in finite systems [36], and collective excitations in extended systems [37, 38], whereas is known to fail to reproduce the optical gap in extended systems (see, e.g. Sec. 7.6 of [28]).

TD-SDFT

The generalization of TDDFT to external potentials which couple to the spin degrees of freedom followed the Runge-Gross theorem quite soon [39]. We report here the equations since, though very similar to ones introduced in the last section, they will be the starting point for the derivation of our linear-response working equations in the next chapter.

We consider the time-dependent Hamiltonian

$$\hat{\mathcal{H}}(t) = \hat{\mathcal{H}}^\circ + \int_{\mathbb{R}^3} \left[\hat{\mathcal{N}}(\mathbf{r})\, v_{\rm ext}(\mathbf{r},t) - \hat{\boldsymbol{\mathcal{M}}}(\mathbf{r}) \cdot \mathbf{b}_{\rm ext}(\mathbf{r},t) \right] , \tag{2.47}$$

where the ground state of $\hat{\mathcal{H}}^\circ$ is described by the densities $n(\mathbf{r})$ and $\mathbf{m}(\mathbf{r})$. The time-evolution of the many-body densities can be followed through the auxiliary single-particle system

$$i\hbar \frac{\partial}{\partial t}\psi_i(\mathbf{r},t) = \left[-\frac{\hbar^2\nabla^2}{2m} + v_{\rm KS}[n,\mathbf{m}](\mathbf{r},t) - \mu_{\rm B}\boldsymbol{\sigma}\cdot\mathbf{b}_{\rm KS}[n,\mathbf{m}](\mathbf{r},t) \right] \psi_i(\mathbf{r},t) \,, \tag{2.48}$$

with

$$n(\mathbf{r},t) = \sum_i^{\rm occ.} |\psi_i(\mathbf{r},t)|^2 \,, \qquad \mathbf{m}(\mathbf{r},t) = \mu_{\rm B} \sum_i^{\rm occ.} \psi_i^\dagger(\mathbf{r},t)\boldsymbol{\sigma}\psi_i(\mathbf{r},t) \tag{2.49}$$

and

$$\begin{aligned} v_{\rm KS}[n,\mathbf{m}](\mathbf{r},t) &= v_{\rm H}[n](\mathbf{r},t) + v_{\rm xc}[n,\mathbf{m}](\mathbf{r},t) + v_{\rm ext}(\mathbf{r},t) \\ \mathbf{b}_{\rm KS}[n,\mathbf{m}](\mathbf{r},t) &= \mathbf{b}_{\rm xc}[n,\mathbf{m}](\mathbf{r},t) + \mathbf{b}_{\rm ext}(\mathbf{r},t) \,. \end{aligned} \tag{2.50}$$

As in the unpolarized case, the xc-potential in the adiabatic approximation reads

$$v_{\rm xc}(\mathbf{r},t) = \frac{\delta E_{\rm xc}}{\delta n(\mathbf{r})}\Big|_{\substack{n(\mathbf{r})=n(\mathbf{r},t) \\ \mathbf{m}(\mathbf{r})=\mathbf{m}(\mathbf{r},t)}} \,, \qquad b_{\rm xc}^\alpha(\mathbf{r},t) = -\frac{\delta E_{\rm xc}}{\delta m^\alpha(\mathbf{r})}\Big|_{\substack{n(\mathbf{r})=n(\mathbf{r},t) \\ \mathbf{m}(\mathbf{r})=\mathbf{m}(\mathbf{r},t)}} \,, \tag{2.51}$$

and no memory effects are taken into account.

2.2 Pseudopotentials

The *pseudopotential approximation* consists in building an effective potential for the outermost electrons of an atom, which mimics the scattering properties of the ion formed by the nucleus and the inner electrons. This approach relies on the assumption that the core electrons do not participate significantly in the formation of chemical bonds due to inter-atomic interactions. Apart from reducing the number of active electrons in a simulation, pseudopotentials are also fundamental in plane-wave calculations, since they can be built in such a way as to result *softer* (i.e. with lower Fourier-components) than the bare ionic potentials. Pseudopotentials play a key role also when relativistic effects are present, which usually involve core electrons in heavy elements. Relativistic pseudopotentials [40, 41, 42] can be built by solving Dirac's equations for the isolated atom and then used in the self-consistent non-relativistic calculations for the valence electrons only, so that effects such as spin-orbit coupling can be accounted for [43].

2.2.1 Norm-Conserving Pseudopotentials

If we treat an isolated atom within DFT, the Kohn-Sham effective potential can be shown to be spherically symmetric, so that the Kohn-Sham orbitals can be classified with the eigenvalues of the single-particle angular momentum operators $\hat{\ell}^2$ and $\hat{\ell}^z$, i.e.

$$\left[-\frac{\hbar^2}{2m}\nabla^2 + v_{\mathrm{KS}}[n](\mathbf{r})\right]\psi_i(\mathbf{r}) = \varepsilon_i\,\psi_i(\mathbf{r})\,, \qquad i \equiv \{n,l,m\}\,, \tag{2.52}$$

where l and m label the angular momentum eigenstates. In the formation of atomic bonds, not all the atomic states contribute, and some, the deeper and more localized, keep their isolated-atom character. These are called *core* states, whereas the ones responsible for the bonding are called *valence* states.

Since the density is a summation over the single-particle states, we can also define a core- and valence-charge

$$n_{\mathrm{c}}(\mathbf{r}) = \sum_i^{\mathrm{core}} \left|\psi_i(\mathbf{r})\right|^2, \qquad n_{\mathrm{v}}(\mathbf{r}) = \sum_i^{\mathrm{valence}} \left|\psi_i(\mathbf{r})\right|^2, \tag{2.53}$$

with $n = n_{\mathrm{c}} + n_{\mathrm{v}}$. When performing a DFT calculation, the self-consistency can be reduced to the valence charge only, since the core charge is not expected to change from the isolated-atom case (*frozen-core approximation*). It has been shown that, though the core wave functions are sensitive to changes of chemical environment with shifts of several eV, the total-energy error is instead of $\sim 0.1\,\mathrm{eV}$, due to its variational nature with respect to the density [44].

In the DFT framework, one can then extremize a "frozen-core" functional of the valence orbitals only:

$$E^{\mathrm{fc}}\left[\{\psi\}\right] = \sum_i^{\mathrm{valence}} \left\langle\psi_i, \left(\frac{\hat{p}^2}{2m} + \hat{v}^{\mathrm{fc}}_{\mathrm{ext}}\right)\psi_i\right\rangle + E_{\mathrm{Hxc}}\left[n_{\mathrm{v}}\right] - \sum_{ij}^{\mathrm{valence}} \Lambda_{ij}\Big(\langle\psi_i,\psi_j\rangle - \delta_{ij}\Big)\,, \tag{2.54}$$

where $\hat{v}_{\rm ext}^{\rm fc}$ is the potential felt by the valence electrons. In the *pseudopotential* approximation, $\hat{v}_{\rm ext}^{\rm fc}$ is replaced by a potential $\hat{v}_{\rm PP}$, built in such a way that the electrostatic and scattering properties of the atom described by the *all-electron* problem (2.52) are well-reproduced outside of a certain core radius $r_{\rm c}$ [45]. It is possible to build pseudopotentials with the properties above, which produce smooth wave functions inside the core radius $r_{\rm c}$ and which coincide with the *all-electron* wave functions of (2.52) outside $r_{\rm c}$. They satisfy the eigenvalue problem

$$\left[\frac{\hat{p}^2}{2m} + \hat{v}_{\rm Hxc}[\tilde{n}_{\rm v}] + \hat{v}_{\rm PP}\right] \tilde{\psi}_i(\mathbf{r}) = \tilde{\varepsilon}_i\, \tilde{\psi}_i(\mathbf{r})\,, \tag{2.55}$$

with the additional property that $\tilde{\varepsilon}_i \approx \varepsilon_i$ within few meV. The smoothness of the pseudo-orbitals $\tilde{\psi}_i$ turns out to be very useful in calculations which use plane-waves as a basis set, since fewer Fourier components are required to expand the $\tilde{\psi}_i$.

Unfortunately, the construction of such a potential is different for each l, and the total pseudopotential is non-local,[7] in the form of

$$v_{\rm PP}(r,\theta,\phi,\theta'\phi') = \sum_{lm} {\rm Y}_{lm}(\theta,\phi)\, v_l(r)\, {\rm Y}^*_{lm}(\theta',\phi')\,. \tag{2.56}$$

In actual calculations a summation of terms like (2.56) occurs, one for each ion, with the spherical coordinates referred to the position of the ion. This form, however, is particularly expensive in plane-wave calculations, where the fully separable Kleinman-Bylander reformulation [46] is used instead.

2.2.2 Nonlinear Core Corrections

The ab-initio construction of a pseudopotential begins with an all-electron reference calculation for the isolated atom, such as (2.52); then an effective potential $v^l_{\rm eff}(r)$ is built for each l of the valence: to this end, several recipies are present in the literature [45, 47, 48, 49]. At this stage, $v^l_{\rm eff}(r)$ contains also the Hartree and xc-contribution of the all-electron configuration; to unveil the potential given by the ion and core electrons only one has to *unscreen* $v^l_{\rm eff}(r)$, i.e.

$$v_l(r) = v^l_{\rm eff}(r) - v_{\rm H}[n_{\rm v}](r) - v_{\rm xc}[n_{\rm v}](r)\,. \tag{2.57}$$

This procedure, though working well in most of the cases, sometimes may prove to be poorly *transferable*, i.e. fails to reproduce the scattering properties of the atom when in a configuration different than the reference one (such as it may happen if using the atomic pseudopotential in a solid). To improve transferability, it has been noted that the unscreening procedure leaves some dependence on the starting configuration, since the xc-potential is not linear in density, therefore $v_{\rm xc}[n_{\rm c}]+v_{\rm xc}[n_{\rm v}] \neq v_{\rm xc}[n_{\rm c}+n_{\rm v}]$. The correct unscreening procedure is [50]

$$v_l(r) = v^l_{\rm eff}(r) - v_{\rm H}[n_{\rm v}](r) - v_{\rm xc}[n_{\rm v}+n_{\rm c}](r)\,. \tag{2.58}$$

[7] Pseudopotentials have then to be regarded as an approximation which gives results close to the original Kohn-Sham problem; their non-local nature, in fact, excludes them from proper DFT. It holds however the total-energy variational principle with respect to the orbitals $\tilde{\psi}_i$.

Since the core contribution to the exchange-correlation part is also removed from the pseudopotential, it has to be reintroduced in the self-consistent calculation every time that $v_{\rm xc}$ is computed. It has been shown, however, that a pseudo core density $\tilde{n}_{\rm c}$, smoothed below a cutoff radius r_0, can be used instead of the true one. The energy functional to minimize in the pseudopotential scheme, with nonlinear core correction, is then given by

$$E\big[\{\tilde{\psi}\}\big] = \sum_{i}^{\text{valence}} \langle \tilde{\psi}_i, \Big(\frac{\hat{p}^2}{2m} + \hat{v}_{\rm ext}^{\rm PP}\Big)\tilde{\psi}_i\rangle + E_{\rm H}\left[\tilde{n}_{\rm v}\right] + E_{\rm xc}\left[\tilde{n}_{\rm v}+\tilde{n}_{\rm c}\right] , \tag{2.59}$$

under the usual contraint $\langle\tilde{\psi}_i, \tilde{\psi}_j\rangle = \delta_{ij}$ for all the valence electrons. Nonlinear core corrections are particulary important in magnetic calculations, where the above procedure reads

$$v_l(r) = v_{\rm eff}^l(r) - v_{\rm H}[n_{\rm v}, \mathbf{m}_{\rm v}](r) - v_{\rm xc}[n_{\rm c}+n_{\rm v}, \mathbf{m}_{\rm c}+\mathbf{m}_{\rm v}](r) . \tag{2.60}$$

In these cases, in fact, the difference in the magnetization between the atomic and the condensed-matter case can be dramatic, hence a high transferability is required. From now on the 'tilde' will be dropped, yet keeping in mind that the orbitals and densities discussed in the following chapters are pseudo-orbitals and pseudo-densities.

2.2.3 Spin-Orbit Coupling

SOC is a one-body relativistic effect which would not emerge if one considered Hamiltonian (2.1). The correct starting point is the Dirac equation for a 4-component spinor under the action of external static quadri-potential $(v/c, \mathbf{A})$, which read (see [51], Ch. 15)

$$\begin{aligned} c\boldsymbol{\sigma}\cdot\hat{\boldsymbol{\pi}}\,\psi_i^{(s)}(\mathbf{r}) + \Big(mc^2 - ev(\mathbf{r})\Big)\psi_i^{(l)}(\mathbf{r}) &= \epsilon_i\,\psi_i^{(l)}(\mathbf{r}) \\ c\boldsymbol{\sigma}\cdot\hat{\boldsymbol{\pi}}\,\psi_i^{(l)}(\mathbf{r}) - \Big(mc^2 + ev(\mathbf{r})\Big)\psi_i^{(s)}(\mathbf{r}) &= \epsilon_i\,\psi_i^{(s)}(\mathbf{r}) , \end{aligned} \tag{2.61}$$

where $\hat{\boldsymbol{\pi}} = \hat{\mathbf{p}} + e\mathbf{A}(\mathbf{r})$. The 2-component spinors $\psi_i^{(s)}$ and $\psi_i^{(l)}$ are respectively called the small and large component of the 4-component Dirac spinor, where the name follows from the possibility to write $\psi_i^{(s)}$ as a Taylor expansion of $(v/c)^n$-order terms applied to $\psi_i^{(l)}$. Stopping at the $(v/c)^2$-terms one obtains that the large component has to satisfy

$$\Big[\hat{h}_{\rm Pauli} + \hat{h}_{\rm SO} + \hat{h}_{\rm Darwin} + \hat{h}_{\rm kinetic}\Big]\,\psi_i^{(l)} = \big(\epsilon_i - mc^2\big)\,\psi_i^{(l)} , \tag{2.62}$$

where

$$\hat{h}_{\text{Pauli}} = \frac{\hat{\pi}^2}{2m} - ev(\mathbf{r}) - \mu_B\, \boldsymbol{\sigma} \cdot \mathbf{b}(\mathbf{r}) \tag{2.63}$$

$$\hat{h}_{\text{SO}} = \frac{\mu_B}{2mc} \boldsymbol{\sigma} \cdot \Big[\nabla v(\mathbf{r}) \times \hat{\mathbf{p}}\Big] \tag{2.64}$$

$$\hat{h}_{\text{Darwin}} = -\frac{\hbar^2 e}{8m^2c^2} \nabla^2 v(\mathbf{r}) \tag{2.65}$$

$$\hat{h}_{\text{kinetic}} = -\frac{\hat{p}^4}{8m^3c^2} \tag{2.66}$$

and $\mathbf{b}(\mathbf{r}) = \nabla \times \mathbf{A}(\mathbf{r})$. The three corrections are responsible for the so called *fine structure* of the electronic levels in atomic physics[8] we notice that the spin-orbit term acquires its well-known form in the case of spherical scalar potentials, when $\nabla v(r) = \frac{\mathrm{d}v}{\mathrm{d}r}\frac{\mathbf{r}}{r}$, so that

$$\hat{h}_{\text{SO}} = \xi(r)\, \hat{\mathbf{s}} \cdot \hat{\boldsymbol{\ell}}\,, \tag{2.67}$$

where $\xi(r) = \frac{\mu_B}{\hbar mc}\frac{\mathrm{d}v}{\mathrm{d}r}\frac{1}{r}$ and $\hat{\boldsymbol{\ell}} = \hat{\mathbf{r}} \times \hat{\mathbf{p}}$ is the angular-momentum operator. It can be estimated that the splitting induce by spin-orbit on the atomic levels grows as $\sim Z^4$, with Z the nuclear charge, in fact its footprints are the more evident the heavier the atom.

In DFT calculations relativistic corrections are included via the pseudopotentials, and allow to solve Pauli-type Kohn-Sham equations for 2-component spinors also for systems where relativistic corrections become relevant. Relativistic DFT can be formulated in terms of the four-current variable [52], but it has been shown that non-relativistic xc-functionals, depending on charge- and magnetization-density only, can be used without major discrepancies [53, 54]. Once the all-electron, Dirac-like Kohn-Sham equations have been solved for the isolated atom, Pauli-like Kohn-Sham equations are solved for the valence electrons, tayloring the effective potentials in order to reproduce the all-electron large components outside of a cutoff radius. The main difference with the non-relativistic case is that the solution of the Dirac equation are classified by the quantum number l, j, m_j, with $j = l \pm \frac{1}{2}$ and $-j \leq m_j \leq j$, so that the pseudopotential acquires the form

$$v_{\text{PP}}(r, \theta, \phi, \theta'\phi') = \sum_{ljm_j} \tilde{\text{Y}}_{l,j,m_j}(\theta, \phi)\, v_{l,j}(r)\, \tilde{\text{Y}}^*_{l,j,m_j}(\theta', \phi')\,, \tag{2.68}$$

with $\tilde{\text{Y}}_{l,j,m_j}(\theta, \phi)$ being the spin-angle functions, eigenstates of $\hat{j}^2$, $\hat{j}^z$ and $\hat{\ell}^2$, $\hat{\mathbf{j}} = \hat{\boldsymbol{\ell}} + \hat{\mathbf{s}}$. The pseudopotentital (2.68) displays a dependence on the spin degrees of freedom, which can be shown to be [40]

$$v_{\text{PP}}(r, \theta, \phi, \theta'\phi') = \sum_{lm} \text{Y}_{lm}(\theta, \phi) \Big[v_l^{\text{ion}}(r)\sigma^\circ + v_l^{\text{SO}}(r)\, \hat{\mathbf{s}} \cdot \hat{\boldsymbol{\ell}}\Big]\, \text{Y}^*_{lm}(\theta', \phi')\,, \tag{2.69}$$

[8] The kinetic term is a relativistic correction to the kinetic energy coming from the Taylor expansion of $E = \sqrt{(mc^2)^2 + p^2c^2}$, the Darwin term produces shifts in the s-states, being proportional to $\delta(\mathbf{r})$ when $v(\mathbf{r})$ is the Coulomb potential. The vector-field terms contained in $\hat{\boldsymbol{\pi}}$ describe different physical phenomena, namely diamagnetism and absorbtion, scattering and emission of electromagnetic waves.

where the term $v_l^{\text{ion}}(r)$ is obtained in practice by j-averaging form (2.68), and is the only term used in scalar-relativistic pseudopotentials. A fully-separable Kleinamn-Bylander form for relativistic pseudopotentials have been devised in [43].

Ultra-Soft Pseudopotentials and PAW

The pseudopentials sketched in the previous sections are called *Norm-Conserving* (NC), since the sum of the square modulus of the pseudo-orbitals gives the same integral of the all-electron valence density. There are, however, more advanced pseudopontials in which the norm-conservation, and subsequently the orthonormality of the pseudo-orbitals, has been sacrificed to improve softness and transferability. These are the *Ultra-Soft* (US) pseudopotential [55] and the *Projector Augmented-Wave* (PAW) scheme [56], the former being a particular case of the latter [57]. PAW pseudopotentials display a lower transferability error with respect to US pseudopotentials, and provide a way to reconstruct the all-electron wave functions. Both the US-pseudopotential and PAW schemes have been extended to linear response, the interested reader may refer to [58] for the former and to [59] for the latter. Throughout this thesis only Norm-Conserving pseudopotentials will be used.

2.3 Extended Systems

We consider a crystal as a collection of $N_{\text{cells}} = N_x N_y N_z$ identical unit cells with periodic boundary conditions (known as Born-von Kármán (BvK) conditions), in order to avoid the explicit treatment of the surface.[9] The Kohn-Sham potential can be shown to have the same periodicity of the lattice defined by the position of the ions $\{\mathbf{R}_I\}$, resulting into the Kohn-Sham orbitals being Bloch states, i.e.

$$\psi_{n\mathbf{k}}(\mathbf{r}) = e^{i\mathbf{k}\cdot\mathbf{r}} u_{n\mathbf{k}}(\mathbf{r}) \,, \qquad u_{n\mathbf{k}}(\mathbf{r}+\mathbf{R}_I) = u_{n\mathbf{k}}(\mathbf{r}) \,. \tag{2.70}$$

where n is the band index and $\mathbf{k}$ has the discrete values

$$k_x = \frac{2\pi}{a_x N_x} n_x \,, \quad k_y = \frac{2\pi}{a_y N_y} n_y \,, \quad k_z = \frac{2\pi}{a_z N_z} n_z \,, \qquad n_x, n_y, n_z = 1, 2, \dots \,, \tag{2.71}$$

due to BvK conditions that we imposed on the Bloch orbitals. We notice that, when restricting into the Brillouin Zone (i.e. $n_\alpha^{\max} = N_\alpha$, $\alpha = x, y, z$), the number of $\mathbf{k}$-points equals the number of unit cells, therefore increasing the $\mathbf{k}$-sampling is another way of performing the limit $N_{\text{cells}} \to \infty$. For this reason, in the following $N_{\mathbf{k}}$ will be used instead of N_{cells} Quantities such as the density and magnetization per unit cell are then given by

$$n(\mathbf{r}) = \frac{1}{N_{\mathbf{k}}} \sum_{\mathbf{k}}^{\text{BZ}} \sum_{n}^{\varepsilon_{n\mathbf{k}} \le \varepsilon_{\text{F}}} |u_{n\mathbf{k}}(\mathbf{r})|^2 \,, \qquad \mathbf{m}(\mathbf{r}) = \frac{\mu_{\text{B}}}{N_{\mathbf{k}}} \sum_{\mathbf{k}}^{\text{BZ}} \sum_{n}^{\varepsilon_{n\mathbf{k}} \le \varepsilon_{\text{F}}} u_{n\mathbf{k}}^\dagger(\mathbf{r})\, \boldsymbol{\sigma}\, u_{n\mathbf{k}}(\mathbf{r}) \,. \tag{2.72}$$

where the periodic parts of the Bloch's functions are to be intended as 2-component spinors.

[9] Here we made use of the assumption that for a large enough N_{cells}, we expect the boundary conditions not to be relevant.

Eqs. (2.72) involve only the periodic part of the Bloch orbitals, the self-consistent equations are then usually rewritten in terms of $u_{n\mathbf{k}}$ only:

$$\int_{\Omega_0} \mathrm{d}^3 r' \delta(\mathbf{r}-\mathbf{r}') \Bigg[\left(-\frac{\hbar^2}{2m}(\nabla + i\mathbf{k})^2 + v_{\mathrm{Hxc}}[n,\mathbf{m}](\mathbf{r}) \right) + v_{\mathrm{PP}}(\mathbf{r},\mathbf{r}') e^{-i\mathbf{k}\cdot(\mathbf{r}-\mathbf{r}')} \Bigg] u_{n\mathbf{k}}(\mathbf{r}') = \varepsilon_{n\mathbf{k}}\, u_{n\mathbf{k}}(\mathbf{r}) \,, \tag{2.73}$$

where Ω_0 is the volume of the unit cell and we denote the $\mathbf{k}$-dependent Hamiltonian in square brackets as $\hat{h}_{\mathbf{k}}$. From now on we restore the general notation ψ_i and ε_i, where $i = \{n\mathbf{k}\}$ and $\sum_i \to \frac{1}{N_{\mathbf{k}}} \sum_{n\mathbf{k}}$ in the case of extended systems.

2.3.1 Smearing the Fermi Function

The summation over the Brillouin Zone as in (2.72) yields the correct thermodynamic limit if tending to the integral of the discretized function

$$\lim_{N_{\mathbf{k}}\to\infty} \frac{1}{N_{\mathbf{k}}} \sum_{\mathbf{k}}^{\mathrm{BZ}} f(\mathbf{k}) = \int_{\mathrm{BZ}} \mathrm{d}^3 k\, f(\mathbf{k}) \,, \tag{2.74}$$

which cannot be true when $f(\mathbf{k})$ is a discontinuos function. A very important case of these can be seen by rewriting the electron density as

$$n(\mathbf{r}) = \sum_n \int \mathrm{d}^3 k\; \vartheta(\varepsilon_F - \varepsilon_{n\mathbf{k}}) \left| u_{n\mathbf{k}}(\mathbf{r}) \right|^2 , \tag{2.75}$$

where $\vartheta(\varepsilon_F - \varepsilon_{n\mathbf{k}})$ is the step-function referred to the Fermi level ε_F. In metals there are bands $\varepsilon_{n\mathbf{k}}$ crossing the Fermi level, therefore the integrand of (2.75) is discontinuous and cannot be discretized. This issue is solved by noting that the Fermi occupation function is actually continuous at any finite temperature, therefore adding a (fictitious) temperature σ to the system allows to discretize the BZ-integrals. The price to pay is that the results might depend on the (fictitious) temperature, and the convergence of the properties of interest with respect to σ has to be checked.

To see how to reach this goal, let us start by *smearing* the Dirac's delta functions appearing in the density of states, i.e.

$$\tilde{n}(\varepsilon) = \sum_i \frac{1}{\sigma}\, \tilde{\delta}\left(\frac{\varepsilon - \varepsilon_i}{\sigma} \right) . \tag{2.76}$$

In this way, the knowledge at a given point is spread over a small area of neighbouring $\mathbf{k}$-points. The parameter σ is related to the width of the smearing function and

$$\lim_{\sigma\to 0} \frac{1}{\sigma} \tilde{\delta}\left(\frac{\varepsilon}{\sigma} \right) = \delta(\varepsilon) \,. \tag{2.77}$$

has to hold. Such a method is equivalent to the addition of a fictitious temperature to the electronic system, in fact the Kohn-Sham energy can be written as

$$E_{\mathrm{KS}} = \int_{-\infty}^{\varepsilon_{\mathrm{F}}} \mathrm{d}\varepsilon\, \varepsilon\, \tilde{n}(\varepsilon) \,, \tag{2.78}$$

substituting the smeared density of states one obtains

$$E_{\mathrm{KS}}(\sigma) = \sum_i \tilde{\vartheta}\left(\frac{\varepsilon_{\mathrm{F}} - \varepsilon_i}{\sigma}\right)\varepsilon_i - \sigma \sum_i S\left(\frac{\varepsilon_{\mathrm{F}} - \varepsilon_i}{\sigma}\right), \tag{2.79}$$

where

$$\tilde{\vartheta}(x) = \int_{-\infty}^{x} \mathrm{d}y\, \tilde{\delta}(y) \tag{2.80}$$

is a smeared step-function, i.e. an approximation of the Fermi function, and

$$S(x) = -\int_{-\infty}^{x} \mathrm{d}y\, y\, \tilde{\delta}(y) \tag{2.81}$$

can be interpreted as an entropic term which couples with the fictitious temperature σ: if we choose the Fermi distribution as $\tilde{\vartheta}$, and its derivative as $\tilde{\delta}$, one obtains the entropy of the free-electron gas, and $\sigma \equiv k_{\mathrm{B}}T$.

The definition of occupied single-particle states changes accordingly to the occupation function, so that the density and magnetization are now defined as

$$n(\mathbf{r}) = \sum_i \tilde{\vartheta}\left(\frac{\varepsilon_{\mathrm{F}} - \varepsilon_i}{\sigma}\right)|\psi_i(\mathbf{r})|^2, \tag{2.82}$$

$$\mathbf{m}(\mathbf{r}) = \mu_{\mathrm{B}} \sum_i \tilde{\vartheta}\left(\frac{\varepsilon_{\mathrm{F}} - \varepsilon_i}{\sigma}\right)\psi_i^\dagger(\mathbf{r})\,\boldsymbol{\sigma}\,\psi_i(\mathbf{r}). \tag{2.83}$$

The free-energy functional to extremize when smeared occupations are used is therefore

$$\begin{aligned} E_\sigma\big[\{\psi\},\{\tilde{\vartheta}_i\}\big] = {} & \sum_i \tilde{\vartheta}_i \left\langle \psi_i, \left(\frac{\hat{p}^2}{2m} + \hat{v}_{\mathrm{ext}}^{\mathrm{PP}}\right)\psi_i\right\rangle + E_{\mathrm{H}}\left[n_{\mathrm{v}}, \mathbf{m}_{\mathrm{v}}\right] + E_{\mathrm{xc}}\left[n_{\mathrm{v}}+n_{\mathrm{c}}, \mathbf{m}_{\mathrm{v}}+\mathbf{m}_{\mathrm{c}}\right] \\ & - \sigma \sum_i S(\tilde{\vartheta}_i) - \sum_{ij} \Lambda_{ij}\Big(\langle\psi_i,\psi_j\rangle - \delta_{ij}\Big) + \mu\Big(N - \sum_i \tilde{\vartheta}_i\Big), \end{aligned} \tag{2.84}$$

with

$$n_{\mathrm{v}}(\mathbf{r}) = \sum_i \tilde{\vartheta}_i\,|\psi_i(\mathbf{r})|^2, \qquad \mathbf{m}_{\mathrm{v}}(\mathbf{r}) = \mu_{\mathrm{B}} \sum_i \tilde{\vartheta}_i\,\psi_i^\dagger(\mathbf{r})\,\boldsymbol{\sigma}\,\psi_i(\mathbf{r}). \tag{2.85}$$

Notice that the functional is variational also with respect to the occupations $\tilde{\vartheta}_i$, in fact the stationarity condition reads

$$\frac{\delta E_\sigma}{\delta \tilde{\vartheta}_i} = 0 \qquad \Longrightarrow \qquad \frac{\partial S}{\partial \tilde{\vartheta}_i} = \frac{\varepsilon_i - \mu}{\sigma}, \tag{2.86}$$

which is true for any occupation function $\tilde{\vartheta}(x)$ and entropy $S(x)$ satisfying Eqs. (2.80) and (2.81) with $x = \frac{\mu-\varepsilon}{\sigma}$. In practice, during the constrained-minimization procedure, the approximate eigenvalues ε_i and chemical potential μ are computed, and with them the approximate $\tilde{\vartheta}_i = \tilde{\vartheta}((\varepsilon_i - \mu)/\sigma)$; when convergence is reached, the

orbitals $\{\psi_i\}$ and the occupations $\{\tilde{\vartheta}_i\}$ minimize the free-energy functional at a fixed smearing function and σ.

Different types of smearing functions have been proposed, from a simple Gaussian form [60], to the Methfessel-Paxton's expansion of the Dirac's delta in Hermite polynomials [61], the latter endowed with better-behaved convergency features. The Methfessel-Paxton's smearing, however, displays a negative bump and non-monotonic behaviour in the occupation function $\tilde{\vartheta}(x)$. The Marzari-Vanderbilt *cold-smearing* [62] heals the negative-bump feature, at the price of $\tilde{\delta}(x)$ not being an even function anymore. A thorough discussion of the derivations sketched above, and of the subtleties of the smearing approach can be found in Ch. 4 of [63], whereas for the generalization to the linear-response case the reader is referred to [64].

CHAPTER

THREE

LINEAR RESPONSE

The time-evolution induced by a time-dependent external perturbation drives a system into a dynamical superposition of all its unperturbed eigenstates. Consequently, the dynamics contains information about the excited states of the unperturbed system. Linear response theory encodes this information into the response functions, which, as shown in Ch. 1, are the theoretical tools needed to interpret inelastic scattering experiments. In the first part of this chapter, response functions, or susceptibilities, will be introduced in the general linear response theory framework; the second part is instead devoted to the definition of response functions in TDDFT, and to the numerical approaches used for their computation.

3.1 Linear Response Theory

Susceptibilities are equilibrium properties of a physical system which characterize its reaction to external perturbations. They are defined as the first-order response of an observable $\hat{\mathcal{A}}$ to a time-dependent external field $f_{\text{ext}}(t)$,

$$\delta\mathcal{A}(t) = \int_{t_0}^{t} \mathrm{d}t' \; \chi(t-t')\, f_{\text{ext}}(t')\,, \tag{3.1}$$

where $f_{\text{ext}}(t) = 0$ for $t < t_0$. Time-translational invariance, which ensures χ to be an equilibrium property, is explicit in its definition (3.1), and so is causality: $\chi(t-t')$ is defined only for $t > t'$.

In quantum mechanics, an expression for the susceptibility can be found by considering the time-evolution of a system, initially in the ground state, undergoing the perturbation

$$\hat{\mathcal{H}}_{\text{ext}}(t) = \hat{\mathcal{B}} f_{\text{ext}}(t)\,, \tag{3.2}$$

which describes the interaction between the system and the external field $f_{\text{ext}}(t)$. To make an example, $f_{\text{ext}}(t)$ can be a magnetic field, and $\hat{\mathcal{B}}$ the spin operator. After a first-order expansion of the time-evolution operator in the external perturbation (see, e.g., Ch. 3 of [28], or Ch. 5 of [65]), one obtains

$$\chi_{\mathcal{AB}}(\tau) = \frac{1}{i\hbar}\theta(\tau)\big\langle \Psi^{\circ}_{\text{GS}}, \Big[\hat{\mathcal{A}}^{\text{H}}(\tau), \hat{\mathcal{B}}^{\text{H}}(0)\Big]\, \Psi^{\circ}_{\text{GS}}\big\rangle \tag{3.3}$$

where "H" denotes the Heisenberg representation of an operator with respect to the unperturbed Hamiltonian

$$\hat{\mathcal{A}}^{\mathrm{H}}(t) = e^{i\frac{t}{\hbar}\hat{\mathcal{H}}^{\circ}}\,\hat{\mathcal{A}}\,e^{-i\frac{t}{\hbar}\hat{\mathcal{H}}^{\circ}}\,. \tag{3.4}$$

The susceptibility in the form of (3.3) is also known as *retarted correlation function*, due to the presence of the step function $\theta(\tau)$ which ensures causality. To distinguish the response of different observables to different perturbations, the two operators appearing in the commutator of (3.3) will be reported as subscript in the susceptibility.

Finite Temperature Formalism

At finite temperature, for $t < t_0$, the system is assumed to be in the thermal equilibrium with a reservoir, so that the eigenstates of the unperturbed Hamiltonian are populated with probability

$$p_n = \frac{e^{-\beta E_n}}{Z}\,, \tag{3.5}$$

where $\beta = 1/k_{\mathrm{B}}T$, $Z = \sum_n e^{-\beta E_n}$ is the canonical partition function and E_n are the eigenvalues of $\hat{\mathcal{H}}^{\circ}$. The expectation value of an observable $\hat{\mathcal{A}}$ is given by the thermal average

$$\langle\hat{\mathcal{A}}\rangle_{\mathrm{th}} = \sum_n p_n\,\langle\Psi_n^{\circ}, \hat{\mathcal{A}}\,\Psi_n^{\circ}\rangle\,. \tag{3.6}$$

When the external field $f_{\mathrm{ext}}(t)$ is turned on, the interaction Hamiltonian between the bath and the system should participate in the time-evolution, leading to coupled bath-system dynamics which is, in practice, unfeasible, either for the size of the problem or for the ignorance of the interaction Hamiltonian. However, when the typical frequencies of the external field are much higher than the inverse of the thermal equilibration time, the unperturbed states can be considered to evolve independently long enough to write

$$\langle\hat{\mathcal{A}}\rangle(t) = \sum_n p_n\,\langle\Psi_n(t), \hat{\mathcal{A}}\,\Psi_n(t)\rangle\,. \tag{3.7}$$

where the populations p_n have been kept frozen. Within this adiabatic assumption, the retarded response function is found to be

$$\chi_{\mathcal{AB}}(\tau) = \frac{1}{i\hbar}\theta(\tau)\sum_n p_n\,\left\langle\Psi_n^{\circ}, \left[\hat{\mathcal{A}}^{\mathrm{H}}(\tau), \hat{\mathcal{B}}^{\mathrm{H}}(0)\right]\Psi_n^{\circ}\right\rangle. \tag{3.8}$$

At zero-temperature, $p_n = 1$ for the ground state and vanishes for the remaining others, recovering Eq. (3.3).

3.1.1 Excited States and Energy Dissipation

The Fourier transform of (3.1) reads

$$\delta\mathcal{A}(\omega) = \chi(\omega)\,f_{\mathrm{ext}}(\omega)\,, \tag{3.9}$$

and describes the response of the system to a monochromatic perturbation in the form of

$$\hat{\mathcal{H}}^{\omega}_{\rm ext}(t) = \left[\hat{\mathcal{A}}^{\dagger} f_{\rm ext}(\omega) e^{-i\omega t} + \hat{\mathcal{A}} f^{*}_{\rm ext}(\omega) e^{i\omega t}\right] e^{\eta t} \,. \tag{3.10}$$

Making use of the completeness of the unperturbed eigenstates, the Fourier transform of the susceptibility can be written as[1]

$$\chi_{\mathcal{A}\mathcal{A}^{\dagger}}(\omega) = \lim_{\eta\to 0^{+}} \sum_{nm} \big(p_n - p_m\big) \frac{\langle \Psi^{\circ}_n, \hat{\mathcal{A}}\, \Psi^{\circ}_m\rangle \langle \Psi^{\circ}_m, \hat{\mathcal{A}}^{\dagger}\, \Psi^{\circ}_n\rangle}{\hbar\omega - (E_n - E_m) + i\eta} \,, \tag{3.12}$$

and its imaginary part reads

$$\mathrm{Im}\chi_{\mathcal{A}\mathcal{A}^{\dagger}}(\omega) = -\frac{\pi}{\hbar} \sum_{nm} p_n \Big[|\langle \Psi^{\circ}_n, \hat{\mathcal{A}}\, \Psi^{\circ}_m\rangle|^2 \delta(\omega - \omega_{mn}) - |\langle \Psi^{\circ}_n, \hat{\mathcal{A}}^{\dagger}\, \Psi^{\circ}_m\rangle|^2 \delta(\omega + \omega_{mn}) \Big] \,, \tag{3.13}$$

with $\omega_{mn} = (E_m - E_n)/\hbar$ being the *eigenmodes* of the system. Eq. (3.13) contains the density of excitations of the system, and is stricly linked to the power dissipation $W(\omega)$ via (cf. with Eq. (2.9) of [66])

$$W(\omega) = -2\omega |f_{\rm ext}(\omega)|^2 \, \mathrm{Im}\chi_{\mathcal{A}\mathcal{A}^{\dagger}}(\omega) \,. \tag{3.14}$$

The excitations act as absorption channels for the energy delivered by an external field, but only when the frequency of the latter equals one of the eigenmodes of the system. It can be further shown that

$$\mathrm{Im}\chi_{\mathcal{A}\mathcal{A}^{\dagger}}(\omega) = -\frac{\pi}{\hbar}(1 - e^{-\beta\hbar\omega}) S_{\mathcal{A}\mathcal{A}^{\dagger}}(\omega) \,, \tag{3.15}$$

where the *dynamical structure factor* $S_{\mathcal{A}\mathcal{A}^{\dagger}}(\omega)$ is defined as the Fourier transform of the auto-correlation function

$$\begin{aligned} S_{\mathcal{A}\mathcal{A}^{\dagger}}(\omega) &= \frac{1}{2\pi} \int_{-\infty}^{+\infty} \mathrm{d}t\, e^{i\omega t} \langle \hat{\mathcal{A}}^{\rm H}(t) \hat{\mathcal{A}}^{\dagger} \rangle_{\rm th} \\ &= |\langle \hat{\mathcal{A}} \rangle_{\rm th}|^2 \delta(\omega) + \frac{1}{2\pi} \int_{-\infty}^{+\infty} \mathrm{d}t\, e^{i\omega t} \langle \delta\hat{\mathcal{A}}^{\rm H}(t) \delta\hat{\mathcal{A}}^{\dagger} \rangle_{\rm th} \,, \end{aligned} \tag{3.16}$$

with $\delta\hat{\mathcal{A}} = \hat{\mathcal{A}} - \langle \hat{\mathcal{A}} \rangle_{\rm th}$. The last term in Eq. (3.16), the only one active for non-zero frequencies, is the autocorrelation function of the fluctuations of the observable $\hat{\mathcal{A}}$; the energy absorbed by the system through its eigenmodes is therefore fed into the fluctuations of the coupling variable. The link between $W(\omega)$ and $S_{\mathcal{A}\mathcal{A}^{\dagger}}(\omega)$, realized through $\mathrm{Im}\chi_{\mathcal{A}\mathcal{A}^{\dagger}}(\omega)$, goes by the name of *fluctuation-dissipation theorem* [66].

[1] Here we notice that in Eq. (3.10) an *adiabatic switching-on* has been introduced in order to extend linear response to the case of perturbations that do not vanish for $t \to -\infty$, such as periodic ones. The switching-on time scale has to be much longer than the period of the perturbation, i.e. $\omega >> \eta$, so that the system can actually experience the periodic field for finite times. On the other hand, the switching-on has to be faster than the thermal equilibration time γ^{-1}, not to break the adiabatic approximation, therefore $\eta > \gamma$. We also remind that

$$\int_{-\infty}^{+\infty} \mathrm{d}t\, \theta(t) f(t) = \lim_{\eta\to 0^{+}} \int_{0}^{+\infty} \mathrm{d}t\, e^{i(\omega - i\eta)t} f(t) \,. \tag{3.11}$$

can be used to obtain (3.12) directy from (3.8). In this sense, the $e^{\eta t}$ factor and the step function play the same role in the Fourier transform.

Multiple Fields

If the system is subject to multiple periodic fields of the same frequency, coupling with the operators $\mathcal{A}_\alpha$ (such, e.g., the three component of a magnetic field coupled with the three components of the spin operator), the perturbing Hamiltonian reads

$$\hat{\mathcal{H}}^{\omega}_{\text{ext}}(t) = \sum_{\alpha} \left[\hat{\mathcal{A}}^{\dagger}_{\alpha} f_\alpha(\omega) e^{-i\omega t} + \hat{\mathcal{A}}_\alpha f^*_\alpha(\omega) e^{i\omega t} \right] e^{\eta t} \,. \tag{3.17}$$

The average power absorption can be found to be equal to [67, 28]

$$W(\omega) = -2\omega \sum_{\alpha\beta} f^*_\alpha(\omega)\, L_{\alpha\beta}(\omega)\, f_\beta(\omega) \,, \tag{3.18}$$

where the *loss tensor* $L_{\alpha\beta}(\omega)$ is nothing but the *anti-hermitian* part of the Fourier transform of the susceptibility

$$L_{\alpha\beta}(\omega) = \frac{1}{2i} \left[\chi_{\mathcal{A}_\alpha \mathcal{A}^{\dagger}_\beta}(\omega) - \chi^*_{\mathcal{A}_\beta \mathcal{A}^{\dagger}_\alpha}(\omega) \right] . \tag{3.19}$$

The fluctuation-dissipation theorem generalizes to

$$L_{\alpha\beta}(\omega) = -\frac{\pi}{\hbar} \left(1 - e^{-\beta\hbar\omega}\right) S_{\mathcal{A}_\alpha \mathcal{A}^{\dagger}_\beta}(\omega) \,. \tag{3.20}$$

In the case of one external field only, the anti-hermitian part coincides with the imaginary part, recovering the previous results.

3.1.2 External Fields and Extended Systems

When the typical spatial modulations of the external field $f_{\text{ext}}(\mathbf{r}, t)$ are comparable with the size of the physical system, the inhomogeneity of $f_{\text{ext}}(\mathbf{r}, t)$ (and, in case, of the system) has to be accounted for. This is always the case for extended systems.

The perturbing Hamiltonian for multiple, inhomogeneous fields, reads

$$\hat{\mathcal{H}}_{\text{ext}}(t) = \sum_{\alpha} \int_{\mathbb{R}^3} \mathrm{d}^3 r \; \hat{\mathcal{A}}_\alpha(\mathbf{r})\, f_\alpha(\mathbf{r}, t) \,; \tag{3.21}$$

the position-dependent susceptibilities are defined as

$$\chi_{\mathcal{A}_\alpha \mathcal{A}_\beta}(\mathbf{r}, \mathbf{r}', \tau) = \frac{1}{i\hbar} \theta(\tau) \sum_n p_n \left\langle \Psi^\circ_n, \left[\hat{\mathcal{A}}^{\text{H}}_\alpha(\mathbf{r}, \tau), \hat{\mathcal{A}}_\beta(\mathbf{r}') \right] \Psi^\circ_n \right\rangle , \tag{3.22}$$

they relate the response of an observable in $\mathbf{r}'$ at the time τ to a perturbation intervened in $\mathbf{r}$ at time $\tau = 0$.

If the system were homogeneous, one would have $\chi_{\mathcal{A}_\alpha \mathcal{A}_\beta}(\mathbf{r} - \mathbf{r}', \tau)$, and consequently

$$\delta\mathcal{A}_\alpha(\mathbf{Q}, \omega) = \sum_{\beta} \chi_{\mathcal{A}_\alpha \mathcal{A}^{\dagger}_\beta}(\mathbf{Q}, \omega)\, f_\beta(\mathbf{Q}, \omega) \,, \tag{3.23}$$

so that the response to different spatial periodicities would be completely decoupled. In the case of periodic systems, translational invariance is only discrete and one obtains

$$\delta\mathcal{A}_\alpha(\mathbf{q}+\mathbf{G},\omega) = \sum_\beta \sum_{\mathbf{G}'}^{\mathrm{BZ}} \chi_{\mathcal{A}_\alpha\mathcal{A}_\beta^\dagger}(\mathbf{q}+\mathbf{G},\mathbf{q}+\mathbf{G}',\omega)\, f_\beta(\mathbf{q}+\mathbf{G}',\omega)\,, \tag{3.24}$$

where $\mathbf{q} \in \mathrm{BZ}$. Therefore, in a periodic system all the wavevectors connected by a $\mathbf{G}$-vector contribute to the same excitation. The susceptibility appearing in Eq. (3.24) is often denoted as $\chi^{\mathbf{G}\mathbf{G}'}_{\mathcal{A}_\alpha\mathcal{A}_\beta^\dagger}(\mathbf{q},\omega)$.

3.2 Linear Response in TDDFT and TD-SDFT

Let a system described via the DFT-densities $n^\circ(\mathbf{r})$ and $\mathbf{m}^\circ(\mathbf{r})$ be subjet to the time-dependent perturbation

$$\hat{\mathcal{H}}_{\mathrm{ext}} = \int_{\mathbb{R}^3} \left[\hat{\mathcal{N}}(\mathbf{r})\, v_{\mathrm{ext}}(\mathbf{r},t) - \hat{\boldsymbol{\mathcal{M}}}(\mathbf{r}) \cdot \mathbf{b}_{\mathrm{ext}}(\mathbf{r},t)\right]. \tag{3.25}$$

As a result, the densities acquire some dynamics, that is considered in the Fourier space:

$$\begin{aligned} n(\mathbf{r},\omega) &= n^\circ(\mathbf{r}) + n'(\mathbf{r},\omega) \\ m_\alpha(\mathbf{r},\omega) &= m^\circ_\alpha(\mathbf{r}) + m'_\alpha(\mathbf{r},\omega)\,. \end{aligned} \tag{3.26}$$

The Hartree and xc-potentials will change accordingly, and can be expanded at the first order in response densities:

$$\begin{aligned} v_{\mathrm{Hxc}}(\mathbf{r},\omega) &= v^\circ_{\mathrm{Hxc}}(\mathbf{r}) + v'_{\mathrm{Hxc}}(\mathbf{r},\omega) \\ b^\alpha_{\mathrm{xc}}(\mathbf{r},\omega) &= b^{\circ\alpha}_{\mathrm{xc}}(\mathbf{r}) + b'^\alpha_{\mathrm{xc}}(\mathbf{r},\omega)\,, \end{aligned} \tag{3.27}$$

with

$$\begin{aligned} v'_{\mathrm{Hxc}}(\mathbf{r},\omega) &= \int_{\mathbb{R}^3} \mathrm{d}^3r'\, K_{\mathrm{Hxc}}(\mathbf{r},\mathbf{r}',\omega) n'(\mathbf{r}',\omega) + \int_{\mathbb{R}^3} \mathrm{d}^3r'\, J^\alpha_{\mathrm{xc}}(\mathbf{r},\mathbf{r}',\omega) m'_\alpha(\mathbf{r}',\omega) \\ b'^\alpha_{\mathrm{xc}}(\mathbf{r},\omega) &= \int_{\mathbb{R}^3} \mathrm{d}^3r'\, J^\alpha_{\mathrm{xc}}(\mathbf{r},\mathbf{r}',\omega) n'(\mathbf{r}',\omega) + \int_{\mathbb{R}^3} \mathrm{d}^3r'\, I^{\alpha\beta}_{\mathrm{xc}}(\mathbf{r},\mathbf{r}',\omega) m'_\beta(\mathbf{r}',\omega)\,, \end{aligned} \tag{3.28}$$

where a summation on repeated indexes is intended. One can compactly write

$$\delta v_{\mathrm{Hxc}}(\mathbf{r},\omega) = \int_{\mathbb{R}^3} \mathrm{d}^3r'\, f_{\mathrm{Hxc}}(\mathbf{r},\mathbf{r}',\omega)\delta\rho(\mathbf{r}',\omega)\,, \tag{3.29}$$

where $\delta v^\top_{\mathrm{Hxc}} = \left(v'_{\mathrm{Hxc}}, b'^x_{\mathrm{xc}}, b'^y_{\mathrm{xc}}, b'^z_{\mathrm{xc}}\right)$, $\delta v^\top_{\mathrm{ext}} = \left(v_{\mathrm{ext}}, b^x_{\mathrm{ext}}, b^y_{\mathrm{ext}}, b^z_{\mathrm{ext}}\right)$, $\delta\rho^\top = \left(n', m'_x, m'_y, m'_z\right)$, and

$$f_{\mathrm{Hxc}} = \begin{pmatrix} K_{\mathrm{Hxc}} & J^x_{\mathrm{xc}} & J^y_{\mathrm{xc}} & J^z_{\mathrm{xc}} \\ J^x_{\mathrm{xc}} & I^{xx}_{\mathrm{xc}} & I^{xy}_{\mathrm{xc}} & I^{xz}_{\mathrm{xc}} \\ J^y_{\mathrm{xc}} & I^{yx}_{\mathrm{xc}} & I^{yy}_{\mathrm{xc}} & I^{yz}_{\mathrm{xc}} \\ J^z_{\mathrm{xc}} & I^{zx}_{\mathrm{xc}} & I^{zy}_{\mathrm{xc}} & I^{zz}_{\mathrm{xc}} \end{pmatrix}. \tag{3.30}$$

The 4×4 susceptibility of the non-interacting Kohn-Sham system $\chi^0(\omega)$ and the interacting system $\chi(\omega)$ are defined through

$$\delta\rho(\mathbf{r},\omega) = \int_{\mathbb{R}^3} \mathrm{d}^3 r' \chi^0(\mathbf{r},\mathbf{r}',\omega)\Big[\delta v_{\mathrm{Hxc}}(\mathbf{r}',\omega) + \delta v_{\mathrm{ext}}(\mathbf{r}',\omega)\Big] \tag{3.31}$$

$$\delta\rho(\mathbf{r},\omega) = \int_{\mathbb{R}^3} \mathrm{d}^3 r' \chi(\mathbf{r},\mathbf{r}',\omega)\delta v_{\mathrm{ext}}(\mathbf{r}',\omega)\,, \tag{3.32}$$

where $\chi^0(\omega)$ can be written in terms of the unperturbed Kohn-Sham orbitals as

$$\chi^0_{\alpha\beta}(\mathbf{r},\mathbf{r}',\omega) = \lim_{\eta\to 0^+} \sum_{ij} (\tilde{\vartheta}_{F,i} - \tilde{\vartheta}_{F,j}) \frac{\Big[\psi_i^{\circ\dagger}(\mathbf{r})\sigma^\alpha\psi_j^\circ(\mathbf{r})\Big]\,\Big[\psi_j^{\circ\dagger}(\mathbf{r}')\sigma^\beta\psi_i^\circ(\mathbf{r}')\Big]}{\hbar\omega - (\varepsilon_j - \varepsilon_i) + i\eta}\,. \tag{3.33}$$

Notice that $\alpha = \circ, x, y, z$, where σ° denotes the 2×2 identiy in the spin space, therefore the charge operator. By combining (3.29), (3.31) and (3.32), one obtains the TDDFT Dyson equation

$$\chi(\omega) = \chi^0(\omega) + \chi^0(\omega)\, f_{\mathrm{Hxc}}(\omega)\, \chi(\omega)\,, \tag{3.34}$$

whose solution is, by definition (3.1), the Fourier transform of the charge-spin susceptibility of the system, a 4×4 tensor in the form of

$$\chi(\omega) = \left(\begin{array}{c|ccc} \chi_{\mathcal{N}\mathcal{N}^\dagger} & \chi_{\mathcal{N}\mathcal{M}_x^\dagger} & \chi_{\mathcal{N}\mathcal{M}_y^\dagger} & \chi_{\mathcal{N}\mathcal{M}_z^\dagger} \\ \hline \chi_{\mathcal{M}_x\mathcal{N}^\dagger} & \chi_{\mathcal{M}_x\mathcal{M}_x^\dagger} & \chi_{\mathcal{M}_x\mathcal{M}_y^\dagger} & \chi_{\mathcal{M}_x\mathcal{M}_z^\dagger} \\ \chi_{\mathcal{M}_y\mathcal{N}^\dagger} & \chi_{\mathcal{M}_y\mathcal{M}_x^\dagger} & \chi_{\mathcal{M}_y\mathcal{M}_y^\dagger} & \chi_{\mathcal{M}_y\mathcal{M}_z^\dagger} \\ \chi_{\mathcal{M}_z\mathcal{N}^\dagger} & \chi_{\mathcal{M}_z\mathcal{M}_x^\dagger} & \chi_{\mathcal{M}_z\mathcal{M}_y^\dagger} & \chi_{\mathcal{M}_z\mathcal{M}_z^\dagger} \end{array}\right)\,. \tag{3.35}$$

As seen in Ch. 1,the anti-hermitian component of (3.35) provides the density of charge-charge, spin-spin and spin-charge excitations of the system. The formalism of linear-response in TDDFT can be used to compute the susceptibility of any local one-particle operator, given that their expectation values can be expressed in term of $n(\mathbf{r},t)$ and $\mathbf{m}(\mathbf{r},t)$. To mention but one example, the response of the dipole operator $\hat{\mathbf{d}} = -e\,\hat{\mathbf{r}}$ to a time-dependent, homogeneous electric field can be computed in order to obtain the dynamical polarizability of finite systems [36].

3.2.1 The Adiabatic Kernel

In the TDDFT adiabatic approximation, the kernel f_{Hxc} becomes static and can be expressed via the second derivatives of the Hartree and xc-energy functional

$$K_{\mathrm{Hxc}}(\mathbf{r},\mathbf{r}') = \left.\frac{\delta^2 E_{\mathrm{Hxc}}}{\delta n(\mathbf{r})\delta n(\mathbf{r}')}\right|_{\substack{n=n^\circ \\ m_\alpha = m_\alpha^\circ}} \tag{3.36}$$

$$J^\alpha_{\mathrm{xc}}(\mathbf{r},\mathbf{r}') = \left.\frac{\delta^2 E_{\mathrm{xc}}}{\delta m_\alpha(\mathbf{r})\delta n(\mathbf{r}')}\right|_{\substack{n=n^\circ \\ m_\alpha = m_\alpha^\circ}} \tag{3.37}$$

$$I^{\alpha\beta}_{\mathrm{xc}}(\mathbf{r},\mathbf{r}') = \left.\frac{\delta^2 E_{\mathrm{xc}}}{\delta m_\alpha(\mathbf{r})\delta m_\beta(\mathbf{r}')}\right|_{\substack{n=n^\circ \\ m_\alpha = m_\alpha^\circ}}\,. \tag{3.38}$$

The lack of a frequency dependence means that f_{Hxc} is a real tensor, which, in turn, has implications in the physics that the adiabatic approximation can describe. In fact it can be seen from (3.34) that the imaginary part of $\chi^0(\omega)$, i.e. the independent-particle continuum of transitions, can be renormalized *but not shifted* in the full $\chi(\omega)$. This leaves room for only two scenarios: in the first one a new peak appears in χ at ω_0 outside of the independent-particle continuum, after the resummation of the Dyson equation: this has to be intended as a collective excitation of the system, for which the adiabatic approximation predicts infinite lifetime, being a genuine pole that satisfies $1 - f_{\text{Hxc}}\text{Re}\chi^0(\omega) = 0$. In the second scenario, the Dyson resummation enhances $\text{Im}\chi^0$ around a certain frequency ω_0, producing an excitation which stands out of the continuum and is endowed with a finite lifetime. These are considered as collective modes broadened by the continuum, i.e. well-defined excitations that decay after a certain lifetime in other single-particle excitations of similar energy.

3.2.2 Computing the TDDFT Susceptibility

In order to solve the Dyson equation, the non-interacting Kohn-Sham response function has to be computed. A straightforward approach involves the summation over the empty states in Eq. (3.33), which are virtually infinite in number. In practice, only a finite amount is included up to a cutoff ε_c, which becomes an additional convergence parameter. In extended systems, where empty states have to be included for each **k**-point, this turns out to be a serious bottleneck and additional approximations are required [68].

An alternative approach is to compute via the KKR method the spin-resolved Green's function of the Kohn-Sham Hamiltonian $G_{\sigma\sigma'}(\mathbf{r}, \mathbf{r}', \omega)$ [67, 69], then obtain $\chi^0(\mathbf{r}, \mathbf{r}', \omega)$ as a frequency-convolution of two Green's functions. The computation of $\chi^0(\omega)$ still remains the bottleneck of the method, and has to be repeated for different values of the frequency.

In order to avoid a direct solution of the Dyson equation, an equivalent approach is to apply perturbation theory to the linearized time-dependent Kohn-Sham equations. This results in a set of self-consistent Shrödinger equations for the response orbitals, named Sternheimer equations. This method is the time-dependent generalization of DFpT [70], and allows the computation of $\chi(\omega)$ without the explicit computation of empty states. The first TDDFT magnetic susceptibility has been computed by Savrasov [38] with this approach which, however, still requires the solution of a set of Sternheimer equations for each frequency ω.

Non-Collinearity

If a collinear system is magnetized along the z-direction, the non-interacting susceptibility $\chi^0(\omega)$ reads

$$\chi^0(\omega) = \left(\begin{array}{c|ccc} \chi^0_{\mathcal{N}\mathcal{N}^\dagger} & 0 & 0 & \chi^0_{\mathcal{N}\mathcal{M}_z^\dagger} \\ \hline 0 & \chi^0_{\mathcal{M}_x\mathcal{M}_x^\dagger} & \chi^0_{\mathcal{M}_x\mathcal{M}_y^\dagger} & 0 \\ 0 & -\chi^0_{\mathcal{M}_x\mathcal{M}_y^\dagger} & \chi^0_{\mathcal{M}_x\mathcal{M}_x^\dagger} & 0 \\ -\chi^0_{\mathcal{N}\mathcal{M}_z^\dagger} & 0 & 0 & \chi^0_{\mathcal{M}_z\mathcal{M}_z^\dagger} \end{array}\right), \tag{3.39}$$

whereas the LSDA kernel becomes

$$f_{\mathrm{Hxc}} = \left(\begin{array}{c|ccc} K_{\mathrm{Hxc}} & 0 & 0 & J^z_{\mathrm{xc}} \\ \hline 0 & I^{xx}_{\mathrm{xc}} & 0 & 0 \\ 0 & 0 & I^{yy}_{\mathrm{xc}} & 0 \\ J^z_{\mathrm{xc}} & 0 & 0 & I^{zz}_{\mathrm{xc}} \end{array}\right). \tag{3.40}$$

It follows that the transverse xy-sector is decoupled from the longitudinal charge-spin sector, and a Dyson equation involving only the 2×2 xy-blocks in Eqs. (3.39) and (3.40) can be solved. All the methods mentioned in the last section have been implemented within this collinear-magnetization framework, and cannot aim at describing the non-collinear physics mentioned in Ch. 1. When SOC is accounted for in the ground-state problem, the non-interacting susceptibility $\chi^0(\omega)$ is not decoupled anymore in a two-block struture such as in (3.39), and the whole 4×4 matricial Dyson equation has to be solved.

To the best of our knowledge, only a KKR-based code at present features the possibility of computing magnetic susceptibilities for non-collinear systems [9], though only on the Atomic-Sphere Approximation (ASA) level.[2] In the following chapter, we present a method to compute the spin-charge susceptibility tensor (3.35) in a fully non-collinear framework, which does not require the explicit computation of empty states and whose bottleneck is independent of the frequency ω.

3.3 Other Methods

Here we briefly review other methods used to compute *ab initio* or partially *ab initio* magnon dispersions.

Adiabatic Spin Dynamics

In the Adiabatic Spin Dynamics Approximation, the charge and the magnetic-moment evolutions are decoupled; the spin dynamics is studied by mapping the

[2] In the ASA approximation the direction of the spin-density is taken to be collinear inside spherical regions centered on the atoms. SOC is a source of intra-atomic non-collinearity and the reliability of this approximation strongly depends on the system [9].

many-body system onto a Heisenberg Hamiltonian

$$\hat{\mathcal{H}} = -\frac{1}{2}\sum_{\mathbf{R}\mathbf{R}'} J_{\mathbf{R}\mathbf{R}'}\, \hat{\mathbf{s}}_{\mathbf{R}} \cdot \hat{\mathbf{s}}_{\mathbf{R}'}\,, \tag{3.41}$$

which is let evolve under a transverse, time-dependent, magnetic field [71]. The *exchange parameters* $J_{\mathbf{R}\mathbf{R}'}$ are usually derived from ab-initio ground-state calculations. This approximation turns out to be appropriate for the long wave-length part of the acoustic modes, in which the spin dynamics is some orders of magnitude slower than the ones of the faster Stoner excitations. An important drawback is that only a finite number of infinite-lifetime modes is given by the Heisenberg Hamiltonian, therefore no spin-wave damping can be studied within this approximation.

Empirical Tight Binding

In the Empirical Tight Binding (ETB) scheme, a model Hamiltonian of multi-band Hubbard type is built

$$\hat{\mathcal{H}} = \sum_{\mathbf{R}\mathbf{R}'}\sum_{ij\sigma} t^{ij}_{\mathbf{R}\mathbf{R}'}\, c^{\dagger}_{\mathbf{R}i\sigma} c_{\mathbf{R}'j\sigma} + \frac{1}{2}\sum_{\mathbf{R}}\sum_{ijkl}\sum_{\sigma\sigma'} U^{ij,kl}_{\mathbf{R}}\, c^{\dagger}_{\mathbf{R}i\sigma} c^{\dagger}_{\mathbf{R}j\sigma'} c_{\mathbf{R}l\sigma'} c_{\mathbf{R}k\sigma} \tag{3.42}$$

where $\mathbf{R}$, $\mathbf{R}'$ label the lattice sites, $ijkl$ the orbitals and $\sigma\sigma'$ the spin. The parameters t and U are usually obtained by fitting ab-initio ground-state calculations, and only a subspace of the orbitals enters the effective Hamiltonian, e.g. the d-orbitals for ordinary ferromagnetism. The equation of motion for the spin operator is then solved in the RPA approximation, yielding a Dyson equation whose solution is the dynamical susceptibility. ETB is the least expensive approach that features a true dynamical susceptibility, and historically has always been the first tool used to model and understand new systems of interest. As an example, the spin-wave damping due to SOC in ultrathin ferromagnets has been first studied with the ETB approach [6], with the appropriate inclusion of a spin-orbit term in (3.42). We notice that the Dyson equation in the ETB approach has a static kernel, linked to the U-parameters appearing in the Hamiltonian.

Many-Body Pertubation Theory

The Bethe-Salpeter Equation (BSE) is a set of self-consistent equations for the 2-particle Green's function, whose partial traces can produce all the correlators of one- and two-body operators. A formulation of the BSE in terms of spin-resolved Green's functions has been applied to collinear systems [72]; the self-consistency over the 1-particle Green's function is neglected and the screening $W(\mathbf{r}, \mathbf{r}', \omega)$ is first calculated solving the Dyson equation

$$W(\omega) = v + v\,\chi^0(\omega) W(\omega)\,, \tag{3.43}$$

and then fed into the BSE for the 2-particle Green's function. The starting χ^0 has always been chosen as the Kohn-Sham one, represented in some localized basis set. In spite of the heavy formalism, this formulation of the BSE equations is equivalent

to a Sternheimer formulation of TDDFT with a non-local, frequency-dependent response potential [73]. To the best of our knowledge, so far only calculations on BCC-Fe and FCC-Ni have been performed by using static, non-local screenings $W(\mathbf{r}, \mathbf{r}')$ and a DFT $\chi^0(\omega)$. In these cases the main discrepancies with experiments have been attributed to the deficiencies of the starting χ^0, and the non-locality of the response potential has been argued to act as a small correction to the adiabatic TDDFT results [68].

CHAPTER

FOUR

LIOUVILLE-LANCZOS APPROACH TO MAGNETIC EXCITATIONS

In this chapter we present a method to compute magnetic excitations in a fully non-collinear framework, without explicit reference to the empty states. The chapter is organized as follows: in Sec. 4.1 we introduce the general framework of the method. In Sec. 4.2 we review the Liouville-Lanczos (LL) formalism in the cases of non-magnetic finite systems [74, 75], and non-magnetic, non-metallic, extended systems [37, 76, 77]; in Sec. 4.3, we present the generalization of the LL approch to finite magnetic systems and extended magnetic systems; this is the central part of the chapter. Finally, in Sec. 4.4, we discuss the usage of the Lanczos algorithm in our approach.

4.1 Linear Response and Density Matrix

The expectation values of a local, one-particle operator $\hat{\mathcal{A}}$ can be computed in terms of the spin-resolved one-particle density matrix $\rho_{\sigma\sigma'}(\mathbf{r}, t)$

$$\mathcal{A}(t) = \mathrm{T}r\Big[\hat{A}\,\hat{\rho}(t)\Big]\,, \tag{4.1}$$

where the trace is meant over one-particle spin and space coordinates. In. (4.1) we have defined one-particle operators as

$$\hat{\mathcal{A}} = \sum_{i=1}^{N} \hat{A}_i\,, \tag{4.2}$$

with $\hat{A}_i$ acting on the spin and space degrees of freedom of the i-th electron.[1] Examples of operators as such are the charge- and magnetization densities $\hat{\mathcal{N}}(\mathbf{r})$ and $\hat{\boldsymbol{\mathcal{M}}}(\mathbf{r})$ defined in the previous chapters.

[1] When there is only one set of single-particle degrees of freedom, the subscript i will be dropped, since no ambiguity arises. This is the case, e.g., of $\hat{A}$ in Eq. (4.1)

Link with the Reponse Functions

Let a system be in equilibrium, described by the one-particle density matrix $\hat{\rho}^\circ$, and subject to a time dependent perturbation due to a local field $f_{\text{ext}}(t)$. The first-order expansion of the resulting density matrix

$$\hat{\rho}(t) = \hat{\rho}^\circ + \hat{\rho}'(t) + \mathcal{O}\left(f_{\text{ext}}^2\right) , \tag{4.3}$$

is immediately related to the susceptibilities of the system. In fact, by substituting (4.3) into (4.1) and Fourier-transforming in time, one obtains

$$\delta\mathcal{A}(\omega) = \mathrm{T}r\left[\hat{A}\,\hat{\tilde{\rho}}'(\omega)\right] = \chi_{\mathcal{AB}}(\omega)\, f_{\text{ext}}(\omega)\,, \tag{4.4}$$

where $\hat{\mathcal{B}} = \sum_{i=1}^{N} \hat{B}_i$ is the one-particle operator coupling with the field $f_{\text{ext}}(t)$ in the perturbing Hamiltonian. The knowledge of the response density matrix $\hat{\tilde{\rho}}'(\omega)$ is therefore enough to compute the response functions of any one-particle, local operator $\hat{\mathcal{A}}$.

Single-Particle Framework

In a single-particle theory, the time-dependent density matrix can be written in terms of the one-particle wave functions[2]

$$\hat{\rho}(t) = \sum_{i}^{\text{occ.}} \psi_i(t)\psi_i^\dagger(t)\,, \tag{4.5}$$

so that the response density matrix reads

$$\hat{\rho}'(t) = \sum_{i}^{\text{occ.}} \left[\psi_i'(t)\,\psi_i^{\circ\dagger} + \psi_i^\circ\,\psi_i'^\dagger(t)\right] . \tag{4.6}$$

The $\psi_i'(t)$ are defined as

$$e^{\frac{i}{\hbar}\varepsilon_i t}\,\psi_i(t) = \psi_i^\circ + \psi_i'(t) + \mathcal{O}\left(f_{\text{ext}}^2\right) \tag{4.7}$$

as the first-order correction to the unperturbed ψ_i°, and can be computed via time-dependent perturbation theory.

Self-Consistency

In a self-consistent framework the unperturbed system is described by the orbitals ψ_i°, solution of

$$\hat{h}^\circ\psi_i^\circ = \varepsilon_i\,\psi_i^\circ\,, \qquad \hat{h}^\circ = \frac{\hat{p}^2}{2m} + \hat{v}_{\text{eff}}^\circ\,, \tag{4.8}$$

with $\hat{v}_{\text{eff}}^\circ$ depending on the ψ_i°. In DFT, the last equations correspond to Eq. (2.17) in the spin-unpolarized case, to Eq. (2.40) in the case of collinear magnetism, and to

[2]The † symbol has to be inteded as complex conjugation and transposition over the spin indexes, in the case of spinorial ψ_i.

Eq. (2.30) in the case of non-collinear magnetism. The time-evolution due to $f_{\text{ext}}(t)$ is instead described by

$$i\hbar\frac{\partial\psi_i(t)}{\partial t} = \hat{h}(t)\,\psi_i(t)\,, \qquad \hat{h}(t) = \frac{\hat{p}^2}{2m} + \hat{v}_{\text{eff}}(t) + \hat{v}_{\text{ext}}(t)\,, \tag{4.9}$$

with $\hat{v}_{\text{eff}}(t)$ depending on the $\psi_i(t)$. Eqs. (4.5)–(4.7) still apply and the $\psi_i'(t)$ can be computed via perturbation theory, with the difference that $\mathcal{O}\left(f_{\text{ext}}\right)$-terms arise also from the linearization of $\hat{v}_{\text{eff}}(t)$, i.e.

$$\hat{v}_{\text{eff}}(t) = \hat{v}_{\text{eff}}^{\circ} + \hat{v}_{\text{eff}}'(t) + \mathcal{O}\left(f_{\text{ext}}^2\right)\,. \tag{4.10}$$

Perturbation theory has then to be applied considering

$$\hat{v}'(t) \equiv \hat{v}_{\text{eff}}'(t) + \hat{v}_{\text{ext}}(t) \tag{4.11}$$

as the time-dependent perturbation.

Summary

A one-to-one relation between the susceptibilities and the response orbitals $\psi_i'(t)$ has been established through the linearized density matrix. In the following, we shall write a set of linear equations for the Fourier transform of the response orbitals $\tilde{\psi}_i'(\omega)$, which determine $\hat{\tilde{\rho}}'(\omega)$ via[3]

$$\hat{\tilde{\rho}}'(\omega) = \sum_i^{\text{occ.}} \left[\tilde{\psi}_i'(\omega)\,\psi_i^{\circ\dagger} + \psi_i^{\circ}\,\tilde{\psi}_i'^{\dagger}(-\omega)\right]\,. \tag{4.12}$$

We shall then relate the solution of the linear system to the susceptibility $\chi_{\mathcal{AB}}(\omega)$. The linear equations turn out to be considerably different when magnetic systems are considered, therefore we shall first review the non-magnetic case, before we develop our method in detail.

4.2 The LL Approach to Non-Magnetic Systems

4.2.1 Non-Magnetic Finite Systems

We review the formalism of the Liouville-Lanczos approach in the case of non-magnetic, finite systems. Only a set of real orbitals is necessary, since no thermodynamic limit is required and Time-Reversal Symmetry (TRS) is assumed to hold.

[3]Note that $\tilde{\psi}_i'^{\dagger}(-\omega)$ is the Fourier transform of $\psi_i'(t)$ computed at $-\omega$, then hermitian conjugated.

Linearized Density Matrix and Empty States

We know by standard time-dependent perturbation theory that the Fourier transform of $\psi_i'(t)$ reads

$$\tilde{\psi}_i'(\omega) = \lim_{\eta\to 0^+} \sum_j \frac{\tilde{v}'_{ji}(\omega)}{\hbar\omega - (\varepsilon_j - \varepsilon_i) + i\eta} \psi_j^\circ \,, \tag{4.13}$$

where

$$\tilde{v}'_{ji}(\omega) = \frac{1}{2\pi} \int_{-\infty}^{+\infty} \mathrm{d}t \, e^{i\omega t} \big\langle \psi_j^\circ, \hat{v}'(t)\, \psi_i^\circ \big\rangle \,. \tag{4.14}$$

Substituting (4.13) into (4.12) we obtain

$$\hat{\tilde{\rho}}'(\omega) = \lim_{\eta\to 0^+} \sum_i^{\text{occ.}} \sum_j \left[\frac{\tilde{v}'_{ji}(\omega)}{\hbar\omega - (\varepsilon_j - \varepsilon_i) + i\eta} \psi_j^\circ \psi_i^{\circ *} - \frac{\tilde{v}'^*_{ji}(-\omega)}{\hbar\omega + (\varepsilon_j - \varepsilon_i) + i\eta} \psi_i^\circ \psi_j^{\circ *} \right] . \tag{4.15}$$

Given that the potential $\hat{v}'(t) = \hat{v}'_{\text{Hxc}}(t) + \hat{v}_{\text{ext}}(t)$ is hermitian,[4] one has $\tilde{v}'^*_{ji}(-\omega) = \tilde{v}'_{ij}(\omega)$. By writing $\sum_j = \sum_j^{\text{occ.}} + \sum_j^{\text{empty}}$, one can see from (4.15) that the terms where ψ_j° is an occupied orbital identically cancel, thus we can rewrite

$$\hat{\tilde{\rho}}'(\omega) = \sum_i^{\text{occ.}} \left[\Big(\hat{P}_{\mathcal{C}} \tilde{\psi}'_i(\omega) \Big)\, \psi_i^{\circ *} + \psi_i^\circ \, \Big(\hat{P}_{\mathcal{C}} \tilde{\psi}'_i(-\omega) \Big)^* \right] , \tag{4.16}$$

where the projector over the empty-state manifold has been introduced

$$\hat{P}_{\mathcal{C}} = \mathbb{1} - \sum_i^{\text{occ.}} \psi_i^\circ \, \psi_i^{\circ *} \,. \tag{4.17}$$

We conclude that, in order to compute any response property, only the projection of the response orbitals $\tilde{\psi}'_i(\omega)$ over the unperturbed empy-state manifold are required.

Use of Time-Reversal Symmetry

In non-magnetic systems, the Kohn-Sham Hamiltonian commutes with the time-reversal operator, and in the case of scalar wavefunctions one has

$$\psi_i^{\circ *} = \hat{\mathrm{T}} \psi_i^\circ = \psi_i^\circ \in \mathbb{R} \,. \tag{4.18}$$

Eq. (4.16) can therefore be rewritten as

$$\hat{\tilde{\rho}}'(\omega) = \sum_i^{\text{occ.}} \psi_i^\circ \left[\hat{P}_{\mathcal{C}}\, \tilde{\psi}'_i(\omega) + \hat{P}_{\mathcal{C}}\, \tilde{\psi}'^*_i(-\omega) \right] . \tag{4.19}$$

[4] The linearized Hxc-potential $\hat{v}'_{\text{Hxc}}(t)$ is hermitian, given the symmetry of the kernel $K(\mathbf{r}, \mathbf{r}')$ and the hermiticity of $\hat{\rho}'(t)$.

Linearized Time-Dependent Kohn-Sham Equations

By virtue of (4.16), we look for the equations whose solutions are

$$x_i(\omega) \equiv \hat{P}_{\mathcal{C}}\tilde{\psi}'_i(\omega)\,, \qquad y_i(\omega) \equiv \hat{P}_{\mathcal{C}}\tilde{\psi}'^{*}_i(-\omega) \tag{4.20}$$

In Eq. (4.13), the fraction is a complex number which weighs the unperturbed orbitals, hence one can see that by applying $\big[\hbar\omega - (\hat{h}^\circ - \varepsilon_i) + i\eta\big]$ to $\hat{P}_{\mathcal{C}}\tilde{\psi}'_i(\omega)$ and $\big[\hbar\omega + (\hat{h}^\circ - \varepsilon_i) + i\eta\big]$ to $\hat{P}_{\mathcal{C}}\tilde{\psi}'^{*}_i(-\omega)$ the denominators cancel out, obtaining

$$\begin{aligned}
\Big[(\hat{h}^\circ - \varepsilon_i) - (\hbar\omega + i\eta)\Big]x_i(\omega) + \hat{P}_{\mathcal{C}}\,\hat{\tilde{v}}'_{\mathrm{Hxc}}\big[X,Y\big](\omega)\psi_i^\circ &= -\hat{P}_{\mathcal{C}}\,\hat{\tilde{v}}_{\mathrm{ext}}(\omega)\psi_i^\circ \\
\Big[(\hat{h}^\circ - \varepsilon_i) + (\hbar\omega + i\eta)\Big]y_i(\omega) + \hat{P}_{\mathcal{C}}\,\hat{\tilde{v}}'_{\mathrm{Hxc}}\big[X,Y\big](\omega)\psi_i^\circ &= -\hat{P}_{\mathcal{C}}\,\hat{\tilde{v}}_{\mathrm{ext}}(\omega)\psi_i^\circ\,.
\end{aligned} \tag{4.21}$$

In Eq. (4.21) we have defined the sets of orbitals,

$$X \equiv \Big\{x_i(\omega)\Big\} \qquad Y \equiv \Big\{y_i(\omega)\Big\}\,, \tag{4.22}$$

called *batches* [74]; each set contains $N_{\mathcal{V}}$ orbitals, with $N_{\mathcal{V}}$ being the number of the occupied unperturbed states. The linearized Hartree and xc-potential reads, in term of the batches,[5]

$$\begin{aligned}
\tilde{v}'_{\mathrm{Hxc}}\big[X,Y\big](\mathbf{r},\omega) &= \int_{\mathbb{R}^3} \mathrm{d}^3r\, K_{\mathrm{Hxc}}(\mathbf{r},\mathbf{r}')\, n'(\mathbf{r}',\omega) \\
&= 2\int_{\mathbb{R}^3} \mathrm{d}^3r\, K_{\mathrm{Hxc}}(\mathbf{r},\mathbf{r}') \sum_i^{\mathrm{occ.}} \psi_i^\circ\Big[x_i(\omega) + y_i(\omega)\Big]\,.
\end{aligned} \tag{4.23}$$

The whole set of equations (4.21) can be recast in the more compact form by introducing the $\mathcal{D}$ and $\mathcal{K}$ *superoperators*,[6] whose action over the batch space reads

$$\mathcal{D}X(\mathbf{r}) \equiv \Big\{(\hat{h}^\circ - \varepsilon_i)x_i(\mathbf{r},\omega)\Big\} \tag{4.24}$$

$$\mathcal{K}X(\mathbf{r}) \equiv \Big\{2\sum_j^{\mathrm{occ.}} \hat{P}_{\mathcal{C}}\int_{\mathbb{R}^3} \mathrm{d}^3r'\,\psi_i^\circ(\mathbf{r})\,K_{\mathrm{Hxc}}(\mathbf{r},\mathbf{r}')\,\psi_j^\circ(\mathbf{r}')\,x_j(\mathbf{r}',\omega)\Big\}\,. \tag{4.25}$$

We can then write (4.21) as

$$\begin{pmatrix} \mathcal{D}+\mathcal{K} & \mathcal{K} \\ -\mathcal{K} & -\mathcal{D}-\mathcal{K} \end{pmatrix}\begin{pmatrix} X \\ Y \end{pmatrix} - \hbar\omega\begin{pmatrix} X \\ Y \end{pmatrix} = \begin{pmatrix} \Big\{-\hat{P}_{\mathcal{C}}\,\hat{\tilde{v}}_{\mathrm{ext}}(\omega)\psi_i^\circ\Big\} \\ \Big\{\hat{P}_{\mathcal{C}}\,\hat{\tilde{v}}_{\mathrm{ext}}(\omega)\psi_i^\circ\Big\} \end{pmatrix}\,. \tag{4.26}$$

We conclude by noting that a rotation of the batches can be performed by defining [78]

$$Q = \frac{1}{2}\,(X+Y)\,, \qquad P = \frac{1}{2}\,(X-Y)\,, \tag{4.27}$$

[5]The factor of 2 in Eq. (4.23) comes from the spin-degeneracy which enters the charge density.

[6]Superoperators are objects which map an operator into another one, such as a commutator with a fixed operator. Why $\mathcal{D}$ and $\mathcal{K}$ are (representations of) superoperators will become clear in the next section.

so to obtain the even simpler form

$$\begin{pmatrix} \mathbb{0} & \mathcal{D} \\ \mathcal{D}+2\mathcal{K} & \mathbb{0} \end{pmatrix} \begin{pmatrix} Q \\ P \end{pmatrix} - \hbar\omega \begin{pmatrix} Q \\ P \end{pmatrix} = \begin{pmatrix} 0 \\ \left\{ -\hat{P}_{\mathcal{C}}\, \hat{\tilde{v}}_{\mathrm{ext}}(\omega)\psi_i^{\circ} \right\} \end{pmatrix} . \tag{4.28}$$

The simplification due to the rotation (4.27), which will be referred to as Standard Batch Rotation, is due to the TRS, which allows to write the response density as a function of the Q only (cf. (4.19)).

Quantum Liouville Equation and Batch Representation

An alternative way to derive Eqs. (4.26) is to start from the time-evolution equation for the density matrix

$$i\hbar \frac{\partial \hat{\rho}(t)}{\partial t} = \left[\hat{h}(t), \hat{\rho}(t) \right] , \tag{4.29}$$

known as the quantum Liouville equation. Linearizing $\hat{h}(t) = \hat{h}^{\circ} + \hat{v}'(t) + \mathcal{O}(f_{\mathrm{ext}}^2)$ and $\hat{\rho}(t) = \hat{\rho}^{\circ} + \hat{\rho}'(t) + \mathcal{O}(f_{\mathrm{ext}}^2)$ like it was done in last section, we obtain, after Fourier transforming,

$$\mathcal{L}\, \hat{\tilde{\rho}}'(\omega) = \hbar\omega\, \hat{\tilde{\rho}}'(\omega) - \left[\hat{\tilde{v}}_{\mathrm{ext}}(\omega), \hat{\rho}^{\circ} \right] , \tag{4.30}$$

where the *Liouvillian superoperator* has been introduced

$$\mathcal{L}\, \hat{\tilde{\rho}}'(\omega) \equiv \left[\hat{h}^{\circ}, \hat{\tilde{\rho}}'(\omega) \right] + \left[\hat{\tilde{v}}'_{\mathrm{Hxc}}(\omega), \hat{\rho}^{\circ} \right] . \tag{4.31}$$

Note, by considering Eq. (4.30) with a vanishing external field, that the eigenvalues of the Liouvillian are the excitation energies of the system.

Now we introduce a mapping between one-particle operators defined in (4.2) and two batches of orbitals, which we shall call *batch representation* of an operator:

$$\hat{\mathcal{A}} \to \begin{pmatrix} A^x \\ \\ A^y \end{pmatrix} = \begin{pmatrix} \left\{ a_i^x \right\} \\ \\ \left\{ a_i^y \right\} \end{pmatrix} , \tag{4.32}$$

where

$$a_i^x \equiv \hat{P}_{\mathcal{C}}\, \hat{A}\, \psi_i^{\circ} , \qquad a_i^y \equiv \left(\hat{P}_{\mathcal{C}}\, \hat{A}^{\dagger} \psi_i^{\circ} \right)^* . \tag{4.33}$$

It can be easily shown that the batch representation of Eq. (4.30) is exactly Eq. (4.26): In particular it is worth noting

$$\hat{\tilde{\rho}}'(\omega) \xrightarrow{\mathrm{BR}} \begin{pmatrix} X \\ Y \end{pmatrix} \tag{4.34}$$

$$\mathcal{L}\, \hat{\tilde{\rho}}'(\omega) \xrightarrow{\mathrm{BR}} \begin{pmatrix} \mathcal{D}+\mathcal{K} & \mathcal{K} \\ -\mathcal{K} & -\mathcal{D}-\mathcal{K} \end{pmatrix} \begin{pmatrix} X \\ Y \end{pmatrix} . \tag{4.35}$$

Response Functions

The external potential field couples with the one-particle operator $\hat{\mathcal{B}}$, so that

$$\hat{v}_{\text{ext}}(\omega) = \hat{B}^{\dagger} f_{\text{ext}}(\omega) , \tag{4.36}$$

and we can invert the Liouville equation obtaining

$$\hat{\tilde{\rho}}'(\omega) = (\hbar\omega - \mathcal{L})^{-1} \left[\hat{B}^{\dagger}, \hat{\rho}^{\circ} \right] f_{\text{ext}}(\omega) . \tag{4.37}$$

Substituting (4.37) into (4.4) one obtains

$$\chi_{\mathcal{AB}}(\omega) = \text{Tr}\left[\hat{A} \, (\hbar\omega - \mathcal{L})^{-1} \left[\hat{B}^{\dagger}, \hat{\rho}^{\circ} \right] \right] . \tag{4.38}$$

To make an example, if $\hat{A}$ and $\hat{B}$ are two components of the dipole operator, i.e. $\hat{A} = \hat{d}^{\alpha}$ and $\hat{B} = \hat{d}^{\beta}$, then $\chi_{\mathcal{AB}}(\omega) \equiv \alpha_{\alpha\beta}(\omega)$ willa be the dynamical polarizabiliy, defined as the response function of the dipole operator to a homogeneous electric field. We conclude by noting that the batch representation maps the trace into a scalar product, defined as

$$\text{Tr}\left[\hat{\mathcal{A}}, \hat{\mathcal{B}} \right] \equiv \left\langle \hat{\mathcal{A}}, \hat{\mathcal{B}} \right\rangle \equiv \sum_{i}^{\text{occ.}} \left[\langle a_i^x, b_i^x \rangle + \langle a_i^y, b_i^y \rangle \right] , \tag{4.39}$$

4.2.2 Non-Magnetic Extended Systems

The LL approach has been generalized to extended systems in [37, 76]. In the following only insulating extended system will be treated, the discussion of metallic systems is delayed to Sec. 4.3. The Kohn-Sham unperturbed system reads

$$\hat{h}^{\circ} \psi^{\circ}_{n\mathbf{k}} = \varepsilon_{n\mathbf{k}} \, \psi^{\circ}_{n\mathbf{k}} \tag{4.40}$$

and the Kohn-Sham orbitals are Bloch orbitals. It immediately follows

$$\hat{\tilde{\rho}}'(\omega) = \sum_{n\mathbf{k}}^{\text{occ.}} \left[\tilde{\psi}'_{n\mathbf{k}}(\omega) \, \psi^{\circ *}_{n\mathbf{k}} + \psi^{\circ}_{n\mathbf{k}} \, \tilde{\psi}'^{*}_{n\mathbf{k}}(-\omega) \right] , \tag{4.41}$$

where $\mathbf{k} \in \text{BZ}$.

Response Density Matrix and Empty States

By using (4.13) with $i \to n\mathbf{k}$ we have

$$\hat{\tilde{\rho}}'(\omega) = \lim_{\eta \to 0^+} \sum_{n\mathbf{k}}^{\text{occ.}} \sum_{n'\mathbf{k}'} \left[\frac{\tilde{v}'_{n'\mathbf{k}',n\mathbf{k}}(\omega)}{\hbar\omega - (\varepsilon_{n'\mathbf{k}'} - \varepsilon_{n\mathbf{k}}) + i\eta} \psi^{\circ}_{n'\mathbf{k}'} \psi^{\circ *}_{n\mathbf{k}} \right.$$
$$\left. - \frac{\tilde{v}'_{n\mathbf{k},n'\mathbf{k}'}(\omega)}{\hbar\omega + (\varepsilon_{n'\mathbf{k}'} - \varepsilon_{n\mathbf{k}}) + i\eta} \psi^{\circ}_{n\mathbf{k}} \psi^{\circ *}_{n'\mathbf{k}'} \right] , \tag{4.42}$$

where the hermiticity of $\hat{v}'(t)$, i.e. $\tilde{v}'^{*}_{n'\mathbf{k}',n\mathbf{k}}(-\omega) = \tilde{v}'_{n\mathbf{k},n'\mathbf{k}'}(\omega)$ has been considered in the second term. Likewise in the finite-system case, the terms in which $n\mathbf{k}$ and $n'\mathbf{k}'$ are both occupied cancel out, and we can write

$$\hat{\tilde{\rho}}'(\omega) = \sum_{n\mathbf{k}}^{\text{occ.}} \left[\left(\hat{P}_{\mathcal{C}} \tilde{\psi}'_{n\mathbf{k}}(\omega) \right) \psi^{\circ *}_{n\mathbf{k}} + \psi^{\circ}_{n\mathbf{k}} \left(\hat{P}_{\mathcal{C}} \tilde{\psi}'_{n\mathbf{k}}(-\omega) \right)^{*} \right], \tag{4.43}$$

where

$$\hat{P}_{\mathcal{C}} = \mathbb{1} - \sum_{n'\mathbf{k}'}^{\text{occ.}} \psi^{\circ}_{n'\mathbf{k}'} \psi^{\circ *}_{n'\mathbf{k}'} \,. \tag{4.44}$$

Perturbation at Finite Wave Vector

The crucial difference with respect to finite systems is the that for extended systems one is interested in the response to specific single-wavelength perturbations

$$\hat{\tilde{v}}_{\text{ext},\mathbf{Q}}(\omega) = \hat{B}^{\dagger}_{\mathbf{Q}} \, f_{\text{ext}}(\mathbf{Q}, \omega) \,, \tag{4.45}$$

where $\hat{B}^{\dagger}_{\mathbf{Q}}$ bears a phase $e^{i\mathbf{Q}\cdot\mathbf{r}}$, and $\mathbf{Q} = \mathbf{q} + \mathbf{G}$, with $\mathbf{q} \in \text{BZ}$. It can be shown that

$$\left\langle \psi_{n'\mathbf{k}'}, \hat{\tilde{v}}'_{\text{ext},\mathbf{Q}}(\omega) \, \psi^{\circ}_{n\mathbf{k}} \right\rangle = \delta_{\mathbf{k}',\mathbf{k}+\mathbf{q}} \left\langle \psi_{n'\mathbf{k}+\mathbf{q}}, \hat{\tilde{v}}'_{\text{ext},\mathbf{Q}}(\omega) \, \psi^{\circ}_{n\mathbf{k}} \right\rangle, \tag{4.46}$$

which demonstrates that the response density can be characterized only by the wave vector $\mathbf{q} \in \text{BZ}$. Given that one can always decompose a function into Bloch components, if we write[7]

$$\hat{\tilde{v}}'_{\text{Hxc}}(\omega) = \sum_{\mathbf{q}}^{\text{BZ}} \hat{\tilde{v}}'_{\text{Hxc},\mathbf{q}}(\omega) \,, \tag{4.48}$$

with $\hat{\tilde{v}}'_{\text{Hxc},\mathbf{q}}(\omega)$ being a Bloch function of wave vector $\mathbf{q}$, we obtain from (4.42), (4.43), and (4.46),

$$\hat{\tilde{\rho}}'(\omega) = \sum_{\mathbf{q}}^{\text{BZ}} \hat{\tilde{\rho}}'_{\mathbf{q}}(\omega) \,, \tag{4.49}$$

with

$$\hat{\tilde{\rho}}'_{\mathbf{q}}(\omega) = \sum_{n\mathbf{k}}^{\text{occ.}} \left[\left(\hat{P}_{\mathcal{C}} \tilde{\psi}'_{n\mathbf{k}+\mathbf{q}}(\omega) \right) \psi^{\circ *}_{n\mathbf{k}} + \psi^{\circ}_{n\mathbf{k}} \left(\hat{P}_{\mathcal{C}} \tilde{\psi}'_{n\mathbf{k}-\mathbf{q}}(-\omega) \right)^{*} \right], \tag{4.50}$$

and

$$\hat{P}_{\mathcal{C}} \tilde{\psi}'_{n\mathbf{k}+\mathbf{q}}(\omega) = \sum_{n'}^{\text{unocc.}} \frac{\left\langle \psi_{n'\mathbf{k}+\mathbf{q}}, \hat{\tilde{v}}'_{\mathbf{q}}(\omega) \, \psi^{\circ}_{n\mathbf{k}} \right\rangle}{\hbar\omega - (\varepsilon_{n'\mathbf{k}+\mathbf{q}} - \varepsilon_{n\mathbf{k}}) + i\eta} \psi^{\circ}_{n'\mathbf{k}+\mathbf{q}} \,, \tag{4.51}$$

where $\hat{\tilde{v}}'_{\mathbf{q}}(\omega) = \hat{\tilde{v}}'_{\text{Hxc},\mathbf{q}}(\omega) + \hat{\tilde{v}}'_{\text{ext},\mathbf{Q}}(\omega)$.

[7] When dealing with potentials decomposed into Bloch functions, the following notation will be used:

$$\tilde{v}(\mathbf{r}, \omega) = \sum_{\mathbf{q}}^{\text{BZ}} \bar{v}_{\mathbf{q}}(\mathbf{r}, \omega) = \sum_{\mathbf{q}}^{\text{BZ}} e^{i\mathbf{q}\cdot\mathbf{r}} \tilde{v}_{\mathbf{q}}(\mathbf{r}, \omega) \,, \tag{4.47}$$

where the $\tilde{v}_{\mathbf{q}}(\mathbf{r}, \omega)$ denotes the periodic part. The same notation applies for the density matrix. We prefer to work with the non-periodic quantities $\bar{v}_{\mathbf{q}}(\mathbf{r}, \omega)$ for a better readability, the final equations in terms of the periodic quantities can be found in App. B.

Use of Time-Reversal Symmetry

For Bloch Hamiltonians which commute with the time-reversal operator one has

$$\hat{\mathrm{T}}\psi^{\circ}_{n-\mathbf{k}} = \psi^{\circ}_{n\mathbf{k}}\,, \qquad \varepsilon_{n\mathbf{k}} = \varepsilon_{n-\mathbf{k}}\,. \tag{4.52}$$

By exchanging $\mathbf{k} \to -\mathbf{k}$ in the second term of (4.50) one obtains

$$\hat{\tilde{\rho}}'_{\mathbf{q}}(\omega) = \sum_{n\mathbf{k}}^{\text{occ.}} \Big[\Big(\hat{P}_{\mathcal{C}}\tilde{\psi}'_{n\mathbf{k}+\mathbf{q}}(\omega)\Big) + \Big(\hat{P}_{\mathcal{C}}\tilde{\psi}'_{n-\mathbf{k}-\mathbf{q}}(-\omega)\Big)^{*} \Big] \psi^{\circ *}_{n\mathbf{k}}\,. \tag{4.53}$$

Note that

$$\Big(\hat{P}_{\mathcal{C}}\tilde{\psi}'_{n-\mathbf{k}-\mathbf{q}}(-\omega)\Big)^{*} = \sum_{n'}^{\text{unocc.}} \frac{\big\langle \psi_{n'\mathbf{k}+\mathbf{q}}, \hat{\tilde{v}}'_{\mathbf{q}}(\omega)\,\psi^{\circ}_{n\mathbf{k}}\big\rangle}{\hbar\omega + (\varepsilon_{n'\mathbf{k}+\mathbf{q}} - \varepsilon_{n\mathbf{k}}) + i\eta} \psi^{\circ}_{n'\mathbf{k}+\mathbf{q}} \tag{4.54}$$

is a Bloch orbital of wave vector $\mathbf{k}+\mathbf{q}$ and that, thanks to TRS, only the knowledge of the unperturbed orbitals at $\mathbf{k}+\mathbf{q}$ is required.

Linearized Time-Dependent Kohn-Sham Equations

We seek solutions for

$$x_{n\mathbf{k}+\mathbf{q}}(\omega) \equiv \hat{P}_{\mathcal{C}}\tilde{\psi}'_{n\mathbf{k}+\mathbf{q}}(\omega)\,, \qquad y_{n\mathbf{k}+\mathbf{q}}(\omega) \equiv \Big(\hat{P}_{\mathcal{C}}\tilde{\psi}'_{n-\mathbf{k}-\mathbf{q}}(-\omega)\Big)^{*}\,, \tag{4.55}$$

so we apply $\big[\hbar\omega - (\hat{h}^{\circ} - \varepsilon_{n\mathbf{k}}) + i\eta\big]$ to $x_{n\mathbf{k}+\mathbf{q}}(\omega)$ and $\big[\hbar\omega + (\hat{h}^{\circ} - \varepsilon_{n\mathbf{k}}) + i\eta\big]$ to $y_{n\mathbf{k}+\mathbf{q}}(\omega)$, obtaining

$$\begin{aligned}
&\Big[(\hat{h}^{\circ} - \varepsilon_{n\mathbf{k}}) - (\hbar\omega + i\eta)\Big] x_{n\mathbf{k}+\mathbf{q}}(\omega) + \hat{P}_{\mathcal{C}}\,\hat{\tilde{v}}'_{\text{Hxc},\mathbf{q}}\big[X,Y\big](\omega)\psi^{\circ}_{n\mathbf{k}} = -\hat{P}_{\mathcal{C}}\,\hat{\tilde{v}}_{\text{ext},\mathbf{Q}}(\omega)\psi^{\circ}_{n\mathbf{k}} \\
&\Big[(\hat{h}^{\circ} - \varepsilon_{n\mathbf{k}}) + (\hbar\omega + i\eta)\Big] y_{n\mathbf{k}+\mathbf{q}}(\omega) + \hat{P}_{\mathcal{C}}\,\hat{\tilde{v}}'_{\text{Hxc},\mathbf{q}}\big[X,Y\big](\omega)\psi^{\circ}_{n\mathbf{k}} = -\hat{P}_{\mathcal{C}}\,\hat{\tilde{v}}_{\text{ext},\mathbf{Q}}(\omega)\psi^{\circ}_{n\mathbf{k}}\,.
\end{aligned} \tag{4.56}$$

As done for finite systems, the batches

$$X_{\mathbf{q}} \equiv \Big\{x_{n\mathbf{k}+\mathbf{q}}(\omega)\Big\} \qquad Y_{\mathbf{q}} \equiv \Big\{y_{n\mathbf{k}+\mathbf{q}}(\omega)\Big\}\,, \tag{4.57}$$

have been introduced, where each batch contain as many orbitals as the number of occupied states *considering all the* $\mathbf{k}$*-points*. This means that the dimension of a batch increases if a finer BZ-sampling is considered. The linearized response potential in the terms of the batch elements reads as

$$\begin{aligned}
\bar{v}'_{\text{Hxc},\mathbf{q}}\big[X,Y\big](\mathbf{r},\omega) &= \int_{\mathbb{R}^3} \mathrm{d}^3 r\, K_{\text{Hxc}}(\mathbf{r},\mathbf{r}')\,\bar{n}'_{\mathbf{q}}(\mathbf{r}',\omega) \\
&= 2\int_{\mathbb{R}^3} \mathrm{d}^3 r\, K_{\text{Hxc}}(\mathbf{r},\mathbf{r}') \sum_{n\mathbf{k}}^{\text{occ.}} \psi^{\circ *}_{n\mathbf{k}} \Big[x_{n\mathbf{k}+\mathbf{q}}(\omega) + y_{n\mathbf{k}+\mathbf{q}}(\omega)\Big]\,.
\end{aligned} \tag{4.58}$$

One can perform the same batch rotation as (4.27), and obtain the compact form

$$\begin{pmatrix} \mathbb{0} & \mathcal{D} \\ \mathcal{D}+2\mathcal{K} & \mathbb{0} \end{pmatrix} \begin{pmatrix} Q_{\mathbf{q}} \\ P_{\mathbf{q}} \end{pmatrix} - \hbar\omega \begin{pmatrix} Q_{\mathbf{q}} \\ P_{\mathbf{q}} \end{pmatrix} = \begin{pmatrix} 0 \\ \Big\{-\hat{P}_{\mathcal{C}}\,\hat{\tilde{v}}_{\text{ext},\mathbf{Q}}(\omega)\psi^{\circ}_{n\mathbf{k}}\Big\} \end{pmatrix}\,. \tag{4.59}$$

where

$$\mathcal{D}X_{\mathbf{q}}(\mathbf{r}) \equiv \left\{ (\hat{h}^{\circ} - \varepsilon_{n\mathbf{k}}) x_{n\mathbf{k}+\mathbf{q}}(\mathbf{r},\omega) \right\} \tag{4.60}$$

$$\mathcal{K}X_{\mathbf{q}}(\mathbf{r}) \equiv \left\{ 2 \sum_{n'\mathbf{k}'}^{\text{occ.}} \hat{P}_{\mathcal{C}} \int_{\mathbb{R}^3} \mathrm{d}^3 r' \, \psi^{\circ}_{n\mathbf{k}}(\mathbf{r}) \, K_{\text{Hxc}}(\mathbf{r},\mathbf{r}') \, \psi^{\circ *}_{n'\mathbf{k}'}(\mathbf{r}') \, x_{n'\mathbf{k}'+\mathbf{q}}(\mathbf{r}',\omega) \right\}. \tag{4.61}$$

Batch Representation and Response Functions

The quantum-Liouville equation for a monochromatic perturbation of wave length $\mathbf{Q}$ reads

$$\mathcal{L}\,\hat{\tilde{\rho}}'_{\mathbf{q}}(\omega) = \hbar\omega\,\hat{\tilde{\rho}}'_{\mathbf{q}}(\omega) - \left[\hat{\tilde{v}}_{\text{ext},\mathbf{Q}}(\omega), \hat{\rho}^{\circ} \right], \tag{4.62}$$

with

$$\mathcal{L}\,\hat{\tilde{\rho}}'_{\mathbf{q}}(\omega) \equiv \left[\hat{h}^{\circ}, \hat{\tilde{\rho}}'_{\mathbf{q}}(\omega) \right] + \left[\hat{\tilde{v}}'_{\text{Hxc},\mathbf{q}}(\omega), \hat{\rho}^{\circ} \right]. \tag{4.63}$$

The straightforward generalization of the batch representation (4.32) is found to be

$$\hat{\mathcal{A}}_{\mathbf{Q}} \to \begin{pmatrix} \left\{ a^{x}_{n\mathbf{k}+\mathbf{Q}} \right\} \\ \left\{ a^{y}_{n\mathbf{k}+\mathbf{Q}} \right\} \end{pmatrix} = \begin{pmatrix} \left\{ \hat{P}_{\mathcal{C}}\, \hat{A}_{\mathbf{Q}}\, \psi^{\circ}_{n\mathbf{k}} \right\} \\ \left\{ \left(\hat{P}_{\mathcal{C}}\, \hat{A}^{\dagger}_{\mathbf{Q}} \psi^{\circ}_{n-\mathbf{k}} \right)^{*} \right\} \end{pmatrix}. \tag{4.64}$$

One can check that Eqs. (4.56) are recovered once (4.64) is applied to (4.62), and, following the same route as for finite systems one can conclude that

$$\chi_{\mathcal{A}_{\mathbf{Q}}\mathcal{B}^{\dagger}_{\mathbf{Q}}}(\omega) = \mathrm{T}r \left\{ \hat{A}_{\mathbf{Q}} \, (\hbar\omega - \mathcal{L})^{-1} \left[\hat{B}^{\dagger}_{\mathbf{Q}}, \hat{\rho}^{\circ} \right] \right\}, \tag{4.65}$$

where

$$\left\langle \hat{\mathcal{A}}_{\mathbf{Q}}, \hat{\mathcal{B}}_{\mathbf{Q}} \right\rangle \equiv \sum_{n\mathbf{k}}^{\text{occ.}} \left[\langle a^{x}_{n\mathbf{k}+\mathbf{Q}}, b^{x}_{n\mathbf{k}+\mathbf{Q}} \rangle + \langle a^{y}_{n\mathbf{k}+\mathbf{Q}}, b^{y}_{n\mathbf{k}+\mathbf{Q}} \rangle \right]. \tag{4.66}$$

As an example, if $\hat{\mathcal{A}}_{\mathbf{Q}} = \hat{\mathcal{B}}_{\mathbf{Q}} = \hat{\mathcal{N}}(\mathbf{Q})$, with $\hat{\mathcal{N}}(\mathbf{Q})$ being the Fourier transform of the charge-density operator $\hat{\mathcal{N}}(\mathbf{r})$,

4.3 Liouville-Lanczos Approach Goes Magnetic

Here we present the generalization of the methodology exposed above to the case of non-collinear magnetic systems. Two major complications arise: the unperturbed Kohn-Sham equations

$$\hat{h}^{\circ}\psi^{\circ}_{i} = \varepsilon_{i}\,\psi^{\circ}_{i}, \tag{4.67}$$

which have to be intended as spinorial equations now, are not time-reversal invariant anymore, in fact

$$\hat{\mathrm{T}}\hat{h}^{\circ}\psi^{\circ}_{i} = \hat{h}^{\circ[-\mathbf{b}]}\hat{\mathrm{T}}\psi^{\circ}_{i} = \varepsilon_{i}\,\hat{\mathrm{T}}\psi^{\circ}_{i}, \tag{4.68}$$

i.e. the time-reversed wave function is eigenstate of the Hamiltonian with a reversed magnetic field. The second complication is given by the metallic character of the most ordinary solid-state magnetic systems, which forces us to use the smearing techniques explained in Sec. 2.3.1. The LL approach to non-magnetic metallic systems has already been faced in [37], here we shall generalize it to magnetic systems.

4.3.1 The Linearized Density Matrix and Empty States

The unperturbed one-particle density-matrix of a metallic system reads[8]

$$\hat{\rho}^\circ = \sum_i \tilde{\vartheta}_{F,i}\, \psi_i^\circ\, \psi_i^{\circ\dagger}\,, \tag{4.69}$$

where $\tilde{\vartheta}_{F,i} \equiv \tilde{\vartheta}((\varepsilon_F - \varepsilon_i)/\sigma)$ are the *ground-state* occupations. When the system is evolved under an external perturbation, we consider the time-dependent density-matrix

$$\hat{\rho}(t) = \sum_i \tilde{\vartheta}_{F,i}\, \psi_i(t)\psi_i^\dagger(t)\,, \tag{4.70}$$

i.e. we neglect the change in the occupations with respect to time, which corresponds to the *adiabatic approximation* of linear response theory discussed in Sec. 3.1. This approximation is justified when the inverse of the thermal relaxation time γ is much smaller than the frequency of the perturbation. Typical thermal relaxation times of the electrons in metals are of 10^{-9}–$10^{-10}\,\mathrm{s}$ at $T = 5\,\mathrm{K}$, and tend to decrease for lower temperatures [79]; this corresponds to $\gamma \approx 10^{-5}$–$10^{-6}\,\mathrm{eV}$, which is safely smaller than the typical magnetic excitations, in the order of 10^{-2}–$10^{-1}\,\mathrm{eV}$.

As done in the non-magnetic case, we define the time-dependent response orbitals via

$$e^{\frac{i}{\hbar}\varepsilon_i t}\psi_i(t) = \psi_i^\circ + \psi_i'(t)\,, \tag{4.71}$$

that we compute at the first-order level of time-dependent perturbation theory. Their Fourier transform reads

$$\tilde{\psi}_i'(\omega) = \lim_{\eta\to 0^+} \sum_j \frac{\tilde{v}_{ji}'(\omega)}{\hbar\omega - (\varepsilon_j - \varepsilon_i) + i\eta}\psi_j^\circ\,, \tag{4.72}$$

with

$$\tilde{v}_{ji}'(\omega) = \frac{1}{2\pi}\int_{-\infty}^{+\infty} \mathrm{d}t\, e^{i\omega t}\big\langle \psi_j^\circ, \hat{v}'(t)\,\psi_i^\circ\big\rangle\,. \tag{4.73}$$

Substituting (4.71) into (4.70) and taking the Fourier transform to get

$$\hat{\tilde{\rho}}(\omega) = \hat{\rho}^\circ + \hat{\tilde{\rho}}'(\omega) + \mathcal{O}(f_{\mathrm{ext}}^2)\,, \tag{4.74}$$

where

$$\hat{\tilde{\rho}}'(\omega) = \lim_{\eta\to 0^+} \sum_{ij} \tilde{\vartheta}_{F,i}\left[\frac{\tilde{v}_{ji}'(\omega)}{\hbar\omega - (\varepsilon_j - \varepsilon_i) + i\eta}\psi_j^\circ\psi_i^{\circ\dagger} - \frac{\tilde{v}_{ij}'(\omega)}{\hbar\omega + (\varepsilon_j - \varepsilon_i) + i\eta}\psi_i^\circ\psi_j^{\circ\dagger}\right]. \tag{4.75}$$

[8]Note that the Kohn-Sham wave functions are now spinors, therefore the hermitian conjugation takes the place of the complex conjugation.

The hermiticity of the perturbation has been taken into account as usual in the second term of (4.75).

When dealing with fractional occupations, the demarcation between occupied and empty states becomes blurred in a strip around the Fermi level, and a neat separation in occupied-to-empty transitions is not possible anymore. To face this problem, we pursue the idea of de Gironcoli [64] in the treatment of the occupation factors *without assuming time-reversal invariance* for the ground-state system: first we exchange $i \leftrightarrow j$ in the second term of (4.75), then we introduce $\vartheta_{i,j} + \vartheta_{j,i} = 1$, where $\vartheta_{i,j} = \vartheta(\varepsilon_i - \varepsilon_j)$ is a non-smeared occupation function, and switch again $i \leftrightarrow j$ in the second term, so to obtain

$$\hat{\tilde{\rho}}'(\omega) = \sum_i \left[\left(\hat{P}_{\mathcal{C}(i)}\, \tilde{\psi}'_i(\omega) \right) \psi_i^{\circ\dagger} + \psi_i^{\circ} \left(\hat{P}_{\mathcal{C}(i)}\, \tilde{\psi}'_i(-\omega) \right)^{\dagger} \right] , \tag{4.76}$$

where

$$\hat{P}_{\mathcal{C}(i)}\, \tilde{\psi}'_i(\omega) \equiv \lim_{\eta \to 0^+} \sum_j \left(\tilde{\vartheta}_{F,i} - \tilde{\vartheta}_{F,j} \right) \vartheta_{j,i}\, \frac{\tilde{v}'_{ji}(\omega)}{\hbar\omega - (\varepsilon_j - \varepsilon_i) + i\eta}\, \psi_j^{\circ} . \tag{4.77}$$

Note that $\tilde{\psi}_i'^{\dagger}(-\omega)$ is the hermitian conjugate of the Fourier transform of $\tilde{\psi}'_i(\omega)$, computed at $-\omega$ and that the operator

$$\hat{P}_{\mathcal{C}(i)} = \left[\tilde{\vartheta}_{F,i} - \hat{P}_i \right] = \left[\tilde{\vartheta}_{F,i} - \sum_j \left(\tilde{\vartheta}_{F,i} \vartheta_{i,j} + \tilde{\vartheta}_{F,j} \vartheta_{j,i} \right) \psi_j^{\circ} \psi_j^{\circ\dagger} \right] \tag{4.78}$$

is *not* a projector, i.e. $\hat{P}_{\mathcal{C}(i)} \hat{P}_{\mathcal{C}(i)} \neq \hat{P}_{\mathcal{C}(i)}$, as long as fractional occupations are used. Before we proceed, we note that

$$\begin{aligned} \delta\mathcal{A}(\omega) &\equiv \mathrm{Tr} \left[\hat{\mathcal{A}}\, \hat{\tilde{\rho}}'(\omega) \right] \\ &= \sum_i \left[\left\langle \psi_i^{\circ}, \hat{A}\, \hat{P}_{\mathcal{C}(i)}\, \tilde{\psi}'_i(\omega) \right\rangle + \left\langle \hat{P}_{\mathcal{C}(i)}\, \tilde{\psi}'_i(-\omega), \hat{A} \psi_i^{\circ} \right\rangle \right] \\ &= \sum_i \left[\left\langle \hat{A}^{\dagger} \psi_i^{\circ},\, \hat{P}_{\mathcal{C}(i)}\, \tilde{\psi}'_i(\omega) \right\rangle + \left\langle \hat{\mathrm{T}} \hat{A} \psi_i^{\circ}, \hat{\mathrm{T}} \hat{P}_{\mathcal{C}(i)}\, \tilde{\psi}'_i(-\omega) \right\rangle \right] , \end{aligned} \tag{4.79}$$

where in second-to-last line we used the anti-unitarity of the time-reversal operator:

$$\langle u, v \rangle = \langle \hat{\mathrm{T}} u, \hat{\mathrm{T}} v \rangle^* . \tag{4.80}$$

The most natural choice for the unknowns of the linearized equations seems then

$$x_i(\omega) \equiv \hat{P}_{\mathcal{C}(i)}\, \tilde{\psi}'_i(\omega) \tag{4.81}$$

$$y_i(\omega) \equiv \hat{\mathrm{T}} \hat{P}_{\mathcal{C}(i)}\, \tilde{\psi}'_i(-\omega) , \tag{4.82}$$

so that we can express the trace as a standard scalar product

$$\mathrm{Tr} \left[\hat{\mathcal{A}}\, \hat{\tilde{\rho}}'(\omega) \right] = \sum_i \left[\left\langle \hat{A}^{\dagger} \psi_i^{\circ},\, x_i(\omega) \right\rangle + \left\langle \hat{\mathrm{T}} \hat{A} \psi_i^{\circ}, y_i(\omega) \right\rangle \right] . \tag{4.83}$$

4.3.2 The Linearized Response Equations

By applying $[\hat{h}^\circ - \varepsilon_i - (\hbar\omega + i\eta)]$ to $x_i(\omega)$ and $[\hat{h}^{\circ[-\mathbf{b}]} - \varepsilon_i + (\hbar\omega + i\eta)]$ to $y_i(\omega)$ one obtains

$$\left[\hat{h}^\circ - \varepsilon_i - (\hbar\omega + i\eta)\right] x_i(\omega) = -\sum_j \left(\tilde{\vartheta}_{F,i} - \tilde{\vartheta}_{F,j}\right) \vartheta_{j,i} \left\langle \psi_j^\circ, \hat{\tilde{v}}'(\omega)\, \psi_i^\circ \right\rangle \psi_j^\circ \,, \quad (4.84)$$

$$\left[\hat{h}^{\circ[-\mathbf{b}]} - \varepsilon_i + (\hbar\omega + i\eta)\right] y_i(\omega) = -\sum_j \left(\tilde{\vartheta}_{F,i} - \tilde{\vartheta}_{F,j}\right) \vartheta_{j,i} \left\langle \psi_i^\circ, \hat{\tilde{v}}'(\omega)\, \psi_j^\circ \right\rangle \hat{\mathrm{T}} \psi_j^\circ \,. \quad (4.85)$$

We now make again use of the anti-unitarity of $\hat{\mathrm{T}}$ to rewrite the second equation

$$\left[\hat{h}^\circ - \varepsilon_i - (\hbar\omega + i\eta)\right] x_i(\omega) = -\sum_j \left(\tilde{\vartheta}_{F,i} - \tilde{\vartheta}_{F,j}\right) \vartheta_{j,i} \left\langle \psi_j^\circ, \hat{\tilde{v}}'(\omega)\, \psi_i^\circ \right\rangle \psi_j^\circ \,, \quad (4.86)$$

$$\left[\hat{h}^{\circ[-\mathbf{b}]} - \varepsilon_i + (\hbar\omega + i\eta)\right] y_i(\omega) = -\sum_j \left(\tilde{\vartheta}_{F,i} - \tilde{\vartheta}_{F,j}\right) \vartheta_{j,i} \left\langle \hat{\mathrm{T}}\psi_j^\circ, \hat{\mathrm{T}}\hat{\tilde{v}}'^{\dagger}(\omega)\psi_i^\circ, \right\rangle \hat{\mathrm{T}} \psi_j^\circ \quad (4.87)$$

which allows to write

$$\left[\hat{h}^\circ - \varepsilon_i - (\hbar\omega + i\eta)\right] x_i(\omega) = -\hat{P}_{\mathcal{C}(i)}\, \hat{\tilde{v}}'(\omega)\, \psi_i^\circ \,, \quad (4.88)$$

$$\left[\hat{h}^{\circ[-\mathbf{b}]} - \varepsilon_i + (\hbar\omega + i\eta)\right] y_i(\omega) = -\hat{\Pi}_{\mathcal{C}(i)}\, \hat{\mathrm{T}}\hat{\tilde{v}}'^{\dagger}(\omega)\psi_i^\circ \,. \quad (4.89)$$

In Eq. (4.89) we have defined the operator

$$\hat{\Pi}_{\mathcal{C}(i)} \equiv \left[\tilde{\vartheta}_{F,i} - \hat{\Pi}_i\right] \equiv \left[\tilde{\vartheta}_{F,i} - \sum_j \left(\tilde{\vartheta}_{F,i}\, \vartheta_{i,j} + \tilde{\vartheta}_{F,j}\, \vartheta_{j,i}\right) \left(\hat{\mathrm{T}}\psi_j^\circ\right) \left(\hat{\mathrm{T}}\psi_j^\circ\right)^\dagger\right] \,, \quad (4.90)$$

which is nothing but the $\hat{P}_{\mathcal{C}(i)}$ operator acting on the manifold of the time-reversed orbitals. We notice here that a) both $\hat{P}_{\mathcal{C}(i)}$ and $\hat{\Pi}_{\mathcal{C}(i)}$ become true projectors when the smearing width $\sigma \to 0$, and b) $\hat{\Pi}_{\mathcal{C}(i)}$ spans the same manifold of $\hat{P}_{\mathcal{C}(i)}$ when the time-reversal symmetry holds, and can be replaced by the latter.

The Response and External Potentials

The external and linearized effective potentials are hermitian in the time-domain, hence

$$\hat{\tilde{v}}'^{\dagger}(\omega) = \hat{\tilde{v}}'(-\omega) \,. \quad (4.91)$$

We first consider explicitly the linearized effective potential, since it contains new terms with respect to the non-magnetic case

$$\tilde{v}'_{\mathrm{eff}}(\omega) = \sigma^\circ \left(\frac{\delta^2 E_{\mathrm{Hxc}}}{\delta n\, \delta n}\, \tilde{n}'(\omega) + \sum_\alpha \frac{\delta^2 E_{\mathrm{Hxc}}}{\delta n\, \delta m^\alpha}\, \tilde{m}'^{\alpha}(\omega)\right) + \sum_\alpha \sigma^\alpha \left(\frac{\delta^2 E_{\mathrm{Hxc}}}{\delta m^\alpha\, \delta n}\, \tilde{n}'(\omega) + \sum_\beta \frac{\delta^2 E_{\mathrm{Hxc}}}{\delta m^\alpha\, \delta m^\beta}\, \tilde{m}'^{\beta}(\omega)\right) \,. \quad (4.92)$$

where the density- and magnetization-response

$$\tilde{n}'(\mathbf{r},\omega) = \sum_i \left[\psi_i^{\circ\dagger}(\mathbf{r}) x_i(\mathbf{r},\omega) + \left(\hat{\mathrm{T}}\psi_i^\circ(\mathbf{r})\right)^\dagger y_i(\mathbf{r},\omega) \right] \tag{4.93}$$

$$\tilde{m}'^\alpha(\mathbf{r},\omega) = \mu_B \sum_i \left[\psi_i^{\circ\dagger}(\mathbf{r}) \sigma^\alpha \, x_i(\mathbf{r},\omega) - \left(\hat{\mathrm{T}}\psi_i^\circ(\mathbf{r})\right)^\dagger \sigma^\alpha \, y_i(\mathbf{r},\omega) \right] \tag{4.94}$$

are meant to be integrated with the kernels given by the second derivatives in Eq. (4.92). If we focus on the spin structure of the potential we can write it as

$$\tilde{v}'_{\mathrm{eff}}(\omega) = \sigma^\circ \tilde{v}'_{\mathrm{Hxc}}(\omega) - \mu_B \boldsymbol{\sigma} \cdot \tilde{\mathbf{b}}'_{\mathrm{xc}}(\omega) \,, \tag{4.95}$$

The second derivatives are real, symmetric functions, whereas from (4.93) and (4.94) it follows

$$\tilde{n}'^*(\mathbf{r},-\omega) = \tilde{n}'(\mathbf{r},\omega) \,, \qquad \tilde{\mathbf{m}}'^*(\mathbf{r},-\omega) = \tilde{\mathbf{m}}'(\mathbf{r},\omega) \,. \tag{4.96}$$

Putting all together we find

$$\hat{\mathrm{T}}\hat{\tilde{v}}'_{\mathrm{eff}}(-\omega) = \sigma^\circ \tilde{v}'_{\mathrm{Hxc}}(\omega) + \mu_B \boldsymbol{\sigma} \cdot \tilde{\mathbf{b}}'_{\mathrm{xc}}(\omega) \equiv \hat{\tilde{v}}'^{[-\mathbf{b}]}_{\mathrm{eff}}(\omega)\hat{\mathrm{T}} \,. \tag{4.97}$$

The same holds for the external potential, which reads

$$v_{\mathrm{ext}}(t) = \sigma^\circ v'_{\mathrm{ext}}(t) - \mu_B \boldsymbol{\sigma} \cdot \mathbf{b}'_{\mathrm{ext}}(t) \,, \tag{4.98}$$

with $v'_{\mathrm{ext}}(t)$ and $\mathbf{b}'_{\mathrm{ext}}(t)$ being real fields.

The Final Form

The linearized time-dependent Kohn-Sham equations can eventually be written as

$$\left[\hat{h}^\circ - \varepsilon_i - (\hbar\omega + i\eta)\right] x_i(\omega) + \hat{P}_{\mathcal{C}(i)} \, \hat{\tilde{v}}'_{\mathrm{eff}}[X,Y](\omega) \, \psi_i^\circ = -\hat{P}_{\mathcal{C}(i)} \, \hat{\tilde{v}}_{\mathrm{ext}}(\omega) \, \psi_i^\circ \tag{4.99}$$

$$\left[\hat{h}^{\circ[-\mathbf{b}]} - \varepsilon_i + (\hbar\omega + i\eta)\right] y_i(\omega) + \hat{\Pi}_{\mathcal{C}(i)} \, \hat{\tilde{v}}'^{[-\mathbf{b}]}_{\mathrm{eff}}[X,Y](\omega) \, \hat{\mathrm{T}}\psi_i^\circ = -\hat{\Pi}_{\mathcal{C}(i)} \, \hat{\tilde{v}}^{[-\mathbf{b}]}_{\mathrm{ext}}(\omega) \, \hat{\mathrm{T}}\psi_i^\circ \,. \tag{4.100}$$

We refrain from writing down the batch representation of the linearized equations straight away, since, as it happened for the non-magnetic case, it would be a particular case of what we are going to present in the next section (namely the $\mathbf{k} = \mathbf{q} = 0$ one).

4.3.3 Extended Systems

We start from the response density matrix defined in Eqs. (4.76) and (4.77), in exteded systems one has

$$\hat{\tilde{\rho}}'(\omega) = \sum_{n\mathbf{k}}^{\mathrm{BZ}} \left[\left(\hat{P}_{\mathcal{C}(n\mathbf{k})} \, \tilde{\psi}'_{n\mathbf{k}}(\omega) \right) \psi_{n\mathbf{k}}^{\circ\dagger} + \psi_{n\mathbf{k}}^\circ \left(\hat{P}_{\mathcal{C}(n\mathbf{k})} \, \tilde{\psi}'_{n\mathbf{k}}(-\omega) \right)^\dagger \right] , \tag{4.101}$$

and

$$\hat{P}_{\mathcal{C}(n\mathbf{k})}\,\tilde{\psi}'_{n\mathbf{k}}(\omega) \equiv \lim_{\eta\to 0^+}\sum_{n'\mathbf{k}'}\left(\tilde{\vartheta}_{F,n\mathbf{k}}-\tilde{\vartheta}_{F,n\mathbf{k}'}\right)\vartheta_{n'\mathbf{k}',n\mathbf{k}}\,\frac{\tilde{v}'_{n'\mathbf{k}',n\mathbf{k}}(\omega)}{\hbar\omega-(\varepsilon_{n'\mathbf{k}'}-\varepsilon_{n\mathbf{k}})+i\eta}\,\psi^{\circ}_{n'\mathbf{k}'}\,. \tag{4.102}$$

We consider an external perturbation in the form of

$$\hat{\tilde{v}}_{\mathrm{ext},\mathbf{Q}}(\omega) = \sum_{\alpha}\hat{B}^{\alpha\dagger}_{\mathbf{Q}}\,f^{\alpha}_{\mathrm{ext}}(\mathbf{Q},\omega)\,, \tag{4.103}$$

where α labels operators of wave vector $\mathbf{Q}=\mathbf{q}+\mathbf{G}$, with $\mathbf{q}\in$ BZ. In our case, they will be the Fourier transform of the magnetization- and charge-density, and $\mathbf{Q}=\mathbf{q}+\mathbf{G}$. By performing a $\mathbf{q}$-separation of the effective potential into Bloch functions, by virtue of (4.46), one obtains one obtains

$$\hat{P}_{\mathcal{C}(n\mathbf{k})}\,\tilde{\psi}'_{n\mathbf{k}}(\omega) = \sum_{\mathbf{q}}^{\mathrm{BZ}}\hat{P}_{\mathcal{C}(n\mathbf{k})}\,\tilde{\psi}'_{n\mathbf{k}+\mathbf{q}}(\omega)\,, \tag{4.104}$$

where

$$\hat{P}_{\mathcal{C}(n\mathbf{k})}\,\tilde{\psi}'_{n\mathbf{k}+\mathbf{q}}(\omega)\equiv\lim_{\eta\to 0^+}\sum_{n'}\left(\tilde{\vartheta}_{F,n\mathbf{k}}-\tilde{\vartheta}_{F,n\mathbf{k}+\mathbf{q}}\right)\vartheta_{n'\mathbf{k}+\mathbf{q},n\mathbf{k}}\,\frac{\tilde{v}'_{n'\mathbf{k}+\mathbf{q},n\mathbf{k}}(\omega)}{\hbar\omega-(\varepsilon_{n'\mathbf{k}+\mathbf{q}}-\varepsilon_{n\mathbf{k}})+i\eta}\,\psi^{\circ}_{n'\mathbf{k}+\mathbf{q}}\,. \tag{4.105}$$

is a Bloch function of wave vector $\mathbf{k}+\mathbf{q}$. We also notice that

$$\hat{\mathrm{T}}\hat{P}_{\mathcal{C}(n-\mathbf{k})}\,\tilde{\psi}'_{n-\mathbf{k}}(\omega) = \sum_{\mathbf{q}}^{\mathrm{BZ}}\hat{\mathrm{T}}\hat{P}_{\mathcal{C}(n-\mathbf{k})}\,\tilde{\psi}'_{n-\mathbf{k}-\mathbf{q}}(-\omega)\,, \tag{4.106}$$

with $\hat{\mathrm{T}}\hat{P}_{\mathcal{C}(n-\mathbf{k})}\,\tilde{\psi}'_{n-\mathbf{k}-\mathbf{q}}(-\omega)$ being a Bloch function of wave vector $\mathbf{k}+\mathbf{q}$. We are then lead to the choice of the unknows in the same spirit of (4.55), i.e.

$$\begin{aligned} x_{n\mathbf{k}+\mathbf{q}}(\omega) &\equiv \hat{P}_{\mathcal{C}(n\mathbf{k})}\,\tilde{\psi}'_{n\mathbf{k}+\mathbf{q}}(\omega)\\ y_{n\mathbf{k}+\mathbf{q}}(\omega) &\equiv \hat{\mathrm{T}}\hat{P}_{\mathcal{C}(n-\mathbf{k})}\,\tilde{\psi}'_{n-\mathbf{k}-\mathbf{q}}(-\omega)\,. \end{aligned} \tag{4.107}$$

Density- and Magnetization-Response

It can be shown by computing the trace of (4.101) with $\hat{\mathcal{N}}(\mathbf{r})$ and $\hat{\boldsymbol{\mathcal{M}}}(\mathbf{r})$ that

$$\tilde{n}'(\mathbf{r},\omega) = \sum_{\mathbf{q}}^{\mathrm{BZ}}\bar{n}'_{\mathbf{q}}(\mathbf{r},\omega)\,,\qquad \tilde{\mathbf{m}}'(\mathbf{r},\omega) = \sum_{\mathbf{q}}^{\mathrm{BZ}}\bar{\mathbf{m}}'_{\mathbf{q}}(\mathbf{r},\omega)\,, \tag{4.108}$$

where a) $\bar{n}'_{\mathbf{q}}(\mathbf{r},\omega)$ and $\bar{\mathbf{m}}'_{\mathbf{q}}(\mathbf{r},\omega)$ are Bloch functions of wave vector $\mathbf{q}$ and b) the relations $\bar{n}'^{*}_{-\mathbf{q}}(\mathbf{r},-\omega)=\bar{n}'_{\mathbf{q}}(\mathbf{r},\omega)$ and $\bar{\mathbf{m}}'^{*}_{-\mathbf{q}}(\mathbf{r},-\omega)=\bar{\mathbf{m}}'_{\mathbf{q}}(\mathbf{r},\omega)$ hold. The charge- and magnetization densities in terms of the x- and y-spinors read

$$\bar{n}'_{\mathbf{q}}(\mathbf{r},\omega) = \sum_{n\mathbf{k}}^{\mathrm{BZ}}\left[\psi^{\circ\dagger}_{n\mathbf{k}}(\mathbf{r})x_{n\mathbf{k}+\mathbf{q}}(\mathbf{r},\omega)+\left(\hat{\mathrm{T}}\psi^{\circ}_{n-\mathbf{k}}(\mathbf{r})\right)^{\dagger}y_{n\mathbf{k}+\mathbf{q}}(\mathbf{r},\omega)\right] \tag{4.109}$$

$$\bar{m}'^{\alpha}_{\mathbf{q}}(\mathbf{r},\omega) = \mu_B\sum_{n\mathbf{k}}^{\mathrm{BZ}}\left[\psi^{\circ\dagger}_{n\mathbf{k}}(\mathbf{r})\sigma^{\alpha}\,x_{n\mathbf{k}+\mathbf{q}}(\mathbf{r},\omega)-\left(\hat{\mathrm{T}}\psi^{\circ}_{n-\mathbf{k}}(\mathbf{r})\right)^{\dagger}\sigma^{\alpha}\,y_{n\mathbf{k}+\mathbf{q}}(\mathbf{r},\omega)\right]\,, \tag{4.110}$$

and the **q**-separation for the effective Kohn-Sham response potential reads

$$\bar{v}'_{\mathrm{eff},\mathbf{q}}(\omega) = \sigma^{\circ}\left(\frac{\delta^2 E_{\mathrm{Hxc}}}{\delta n\,\delta n}\,\bar{n}'_{\mathbf{q}}(\omega) + \sum_{\alpha}\frac{\delta^2 E_{\mathrm{Hxc}}}{\delta n\,\delta m^{\alpha}}\,\bar{m}'^{\alpha}_{\mathbf{q}}(\omega)\right) + \sum_{\alpha}\sigma^{\alpha}\left(\frac{\delta^2 E_{\mathrm{Hxc}}}{\delta m^{\alpha}\,\delta n}\,\bar{n}'_{\mathbf{q}}(\omega) + \sum_{\beta}\frac{\delta^2 E_{\mathrm{Hxc}}}{\delta m^{\alpha}\,\delta m^{\beta}}\,\bar{m}'^{\beta}_{\mathbf{q}}(\omega)\right). \tag{4.111}$$

The Linearized Equations

By applying $[\hat{h}^{\circ} - \varepsilon_{n\mathbf{k}} - (\hbar\omega + i\eta)]$ to $x_{n\mathbf{k}+\mathbf{q}}(\omega)$ and $[\hat{h}^{\circ[-\mathbf{b}]} - \varepsilon_{n-\mathbf{k}} + (\hbar\omega + i\eta)]$ to $y_{n\mathbf{k}+\mathbf{q}}(\omega)$ we obtain

$$\Big[\hat{h}^{\circ} - \varepsilon_{n\mathbf{k}} - (\hbar\omega + i\eta)\Big]\, x_{n\mathbf{k}+\mathbf{q}}(\omega) + \hat{P}_{\mathcal{C}(n\mathbf{k})}\,\hat{\bar{v}}'_{\mathrm{eff},\mathbf{q}}[X,Y](\omega)\,\psi^{\circ}_{n\mathbf{k}} = -\hat{P}_{\mathcal{C}(n\mathbf{k})}\,\hat{\bar{v}}_{\mathrm{ext},\mathbf{Q}}(\omega)\,\psi^{\circ}_{n\mathbf{k}} \tag{4.112}$$

$$\Big[\hat{h}^{\circ[-\mathbf{b}]} - \varepsilon_{n-\mathbf{k}} + (\hbar\omega + i\eta)\Big]\, y_{n\mathbf{k}+\mathbf{q}}(\omega) + \hat{\Pi}_{\mathcal{C}(n-\mathbf{k})}\,\hat{\bar{v}}'^{[-\mathbf{b}]}_{\mathrm{eff},\mathbf{q}}[X,Y](\omega)\,\hat{\mathrm{T}}\psi^{\circ}_{n-\mathbf{k}} = -\hat{\Pi}_{\mathcal{C}(n-\mathbf{k})}\,\hat{\bar{v}}^{[-\mathbf{b}]}_{\mathrm{ext},\mathbf{Q}}(\omega)\,\hat{\mathrm{T}}\psi^{\circ}_{n-\mathbf{k}}\,, \tag{4.113}$$

where we have defined the *batches*

$$X_{\mathbf{q}} \equiv \Big\{x_{n\mathbf{k}+\mathbf{q}}(\omega)\Big\}\,, \qquad Y_{\mathbf{q}} \equiv \Big\{y_{n\mathbf{k}+\mathbf{q}}(\omega)\Big\}\,. \tag{4.114}$$

Also in this case, the whole problem can be recast in a compact block-matrix form

$$\left[\begin{pmatrix} \mathcal{D}^X + \mathcal{P}^X\mathcal{K}^{XX} & \mathcal{P}^X\mathcal{K}^{XY} \\ -\mathcal{P}^Y\mathcal{K}^{YX} & -\left(\mathcal{D}^Y + \mathcal{P}^Y\mathcal{K}^{YY}\right)\end{pmatrix} - (\hbar\omega + i\eta)\right]\begin{pmatrix} X_{\mathbf{q}} \\ Y_{\mathbf{q}}\end{pmatrix} = \begin{pmatrix} \left\{-\hat{P}_{\mathcal{C}(n\mathbf{k})}\,\hat{\bar{v}}_{\mathrm{ext},\mathbf{Q}}(\omega)\,\psi^{\circ}_{n\mathbf{k}}\right\} \\ \left\{\hat{\Pi}_{\mathcal{C}(n-\mathbf{k})}\,\hat{\bar{v}}^{[-\mathbf{b}]}_{\mathrm{ext},\mathbf{Q}}(\omega)\,\hat{\mathrm{T}}\psi^{\circ}_{n-\mathbf{k}}\right\}\end{pmatrix}, \tag{4.115}$$

where the Liouvillian superoperator reads

$$\mathcal{L} = \begin{pmatrix} \mathcal{D}^X + \mathcal{P}^X\mathcal{K}^{XX} & \mathcal{P}^X\mathcal{K}^{XY} \\ -\mathcal{P}^Y\mathcal{K}^{YX} & -\left(\mathcal{D}^Y + \mathcal{P}^Y\mathcal{K}^{YY}\right)\end{pmatrix}, \tag{4.116}$$

and the action of each block is defines by

$$\mathcal{D}^X X_{\mathbf{q}} \equiv \left\{ \left[\hat{h}^\circ - \varepsilon_{n\mathbf{k}} \right] x_{n\mathbf{k}+\mathbf{q}} \right\} \tag{4.117}$$

$$\mathcal{D}^Y Y_{\mathbf{q}} \equiv \left\{ \left[\hat{h}^{\circ[-\mathbf{b}]} - \varepsilon_{n-\mathbf{k}} \right] y_{n\mathbf{k}+\mathbf{q}} \right\} \tag{4.118}$$

$$\mathcal{K}^{XX} X_{\mathbf{q}} + \mathcal{K}^{XY} Y_{\mathbf{q}} \equiv \left\{ \hat{\tilde{v}}'_{\mathrm{eff},\mathbf{q}} \left[X, Y \right] (\omega) \, \psi^\circ_{n\mathbf{k}} \right\} \tag{4.119}$$

$$\mathcal{K}^{YX} X_{\mathbf{q}} + \mathcal{K}^{YY} Y_{\mathbf{q}} \equiv \left\{ \hat{\tilde{v}}'^{[-\mathbf{b}]}_{\mathrm{eff},\mathbf{q}} \left[X, Y \right] (\omega) \, \hat{\mathrm{T}} \psi^\circ_{n-\mathbf{k}} \right\} \tag{4.120}$$

$$\mathcal{P}^X X_{\mathbf{q}} \equiv \left\{ \hat{P}_{\mathcal{C}(n\mathbf{k})} \, x_{n\mathbf{k}+\mathbf{q}} \right\} \tag{4.121}$$

$$\mathcal{P}^Y Y_{\mathbf{q}} \equiv \left\{ \hat{\Pi}_{\mathcal{C}(n-\mathbf{k})} \, y_{n\mathbf{k}+\mathbf{q}} \right\} . \tag{4.122}$$

4.3.4 The Response Functions

By specializing (4.79) to the case of a **Q**-perturbation one can write

$$\delta \mathcal{A}_{\mathbf{Q}}(\omega) = \mathrm{Tr} \left[\hat{A}_{\mathbf{Q}} \, \hat{\tilde{\rho}}'_{\mathbf{q}}(\omega) \right] , \tag{4.123}$$

$$= \sum_{n\mathbf{k}}^{\mathbf{k}\in \mathrm{BZ}} \left[\left\langle \hat{A}^\dagger_{\mathbf{Q}} \psi^\circ_{n\mathbf{k}}, \, x_{n\mathbf{k}+\mathbf{q}}(\omega) \right\rangle + \left\langle \hat{\mathrm{T}} \hat{A}_{\mathbf{Q}} \psi^\circ_{n-\mathbf{k}}, y_{n\mathbf{k}+\mathbf{q}}(\omega) \right\rangle \right] ,$$

$$= \langle A_{\mathbf{Q}}, \varrho_{\mathbf{q}}(\omega) \rangle \tag{4.124}$$

where the second line defines the scalar product between the two batches

$$A_{\mathbf{Q}} = \begin{pmatrix} \left\{ \hat{A}^\dagger_{\mathbf{Q}} \psi^\circ_{n\mathbf{k}} \right\} \\ \left\{ \hat{\mathrm{T}} \hat{A}_{\mathbf{Q}} \psi^\circ_{n-\mathbf{k}} \right\} \end{pmatrix} , \qquad \varrho_{\mathbf{q}}(\omega) = \begin{pmatrix} \left\{ x_{n\mathbf{k}+\mathbf{q}}(\omega) \right\} \\ \left\{ y_{n\mathbf{k}+\mathbf{q}}(\omega) \right\} \end{pmatrix} . \tag{4.125}$$

The second batch is solution of Eq (4.115), that we can rewrite as

$$\varrho_{\mathbf{q}}(\omega) = \Big(\hbar\omega - \mathcal{L} \Big)^{-1} B_{\mathbf{Q}} \, f_{\mathrm{ext}}(\mathbf{Q}, \omega) , \tag{4.126}$$

where

$$B_{\mathbf{Q}} = \begin{pmatrix} \left\{ \hat{P}_{\mathcal{C}} \hat{B}^\dagger_{\mathbf{Q}} \psi^\circ_{n\mathbf{k}} \right\} \\ \left\{ - \hat{\Pi}_{\mathcal{C}} \hat{\mathrm{T}} \hat{B}_{\mathbf{Q}} \psi^\circ_{n-\mathbf{k}} \right\} \end{pmatrix} , \tag{4.127}$$

we conclude that

$$\chi_{\mathcal{A}_{\mathbf{Q}} \mathcal{B}^\dagger_{\mathbf{Q}}}(\omega) = \Big\langle A_{\mathbf{Q}}, \Big(\hbar\omega - \mathcal{L} \Big)^{-1} B_{\mathbf{Q}} \Big\rangle . \tag{4.128}$$

4.4 Solving with the Lanczos Algorithm

Once the problem has been stated into the form

$$g(\omega) = \langle u, (\omega - \hat{\mathcal{A}})^{-1} v \rangle , \tag{4.129}$$

it can be tackled with linear-algebra iterative methods, which come in handy when one is interested only in some portion of the spectrum of large operators. The Lanczos algorithm is particularly suitable to the case of static kernels (i.e. when $\hat{A}$ does not depend on ω, such as in ALDA), where the problem can be solved for all the frequencies ω at once. In the following we briefly illustrate the reason why.

The Lanczos method for non-hermitian operators defines a biorthonormal basis through the recursion relations

$$\begin{aligned} \beta_{i+1} q_{i+1} &= \hat{\mathcal{A}}\, q_i - \alpha_i q_i - \gamma_i q_{i-1} \\ \gamma^*_{i+1} p_{i+1} &= \hat{\mathcal{A}}^\dagger p_i - \alpha^*_i p_i - \beta^*_i p_{i-1} \end{aligned} \tag{4.130}$$

with

$$q_1 = p_1 = v\,, \qquad q_0 = p_0 = 0\,, \tag{4.131}$$

where the biorthogonality reads

$$\langle p_i, q_j \rangle = \delta_{ij}\,. \tag{4.132}$$

The α_i, β_i and γ_i coefficients are computed on the fly through

$$\alpha_i = \langle p_i, \hat{\mathcal{A}}\, q_i \rangle \tag{4.133}$$

$$\beta_{i+1} = \sqrt{\left\langle \left(\hat{\mathcal{A}}^\dagger p_i - \alpha^*_i p_i - \beta^*_i p_{i-1}\right), \left(\hat{\mathcal{A}}\, q_i - \alpha_i q_i - \gamma_i q_{i-1}\right) \right\rangle} \tag{4.134}$$

$$\gamma_{i+1} = \frac{\left\langle \left(\hat{\mathcal{A}}^\dagger p_i - \alpha^*_i p_i - \beta^*_i p_{i-1}\right), \left(\hat{\mathcal{A}}\, q_i - \alpha_i q_i - \gamma_i q_{i-1}\right) \right\rangle}{\beta_{i+1}}\,. \tag{4.135}$$

It can be shown that the operator $\hat{\mathcal{A}}$ acquires the tridiagonal form if represented in the Lanczos basis $\langle p_i, \hat{\mathcal{A}}\, q_j \rangle = T^N_{ij}$, where

$$T^N = \begin{pmatrix} \alpha_1 & \gamma_2 & 0 & \cdots & 0 \\ \beta_2 & \alpha_2 & \gamma_3 & 0 & \vdots \\ 0 & \beta_3 & \alpha_3 & \ddots & 0 \\ \vdots & 0 & \ddots & \ddots & \gamma_N \\ 0 & \cdots & 0 & \beta_N & \alpha_N \end{pmatrix}\,. \tag{4.136}$$

Notice that the dimension of the representation has the number of Lanczos iterations N: the more iterations, the more accurate the representation of $\hat{\mathcal{A}}$ will be. Furthermore: the lower the eigenvalue, the faster the convergence. This feature makes Lanczos extremely appealing for linear-response computations, where the lowest-lying excitations are seeked.

If we insert into Eq. (4.129) the completeness

$$\mathbb{1} \approx \sum_{i=1}^{N} q_i\, p_i^\dagger\,, \tag{4.137}$$

which is, of course, approximate as long as N is smaller than the dimension of the operator $\hat{\mathcal{A}}$, we obtain

$$\begin{aligned} g(\omega) &\approx \sum_{i=1}^{N} \langle u, q_i \rangle \langle p_i, (\omega - \hat{\mathcal{A}})^{-1} q_1 \rangle \\ &\approx \sum_{i=1}^{N} \langle u, q_i \rangle \left[(\omega - T^N)^{-1} \right]_{i1} . \end{aligned} \tag{4.138}$$

Summing up, in order to compute a resolvent $g(\omega)$ with Lanczos we have to a) generate the Lanczos chain, storing at each step the α_i, β_i, γ_i and $\zeta_i = \langle u, q_i \rangle^*$, b) solve the tridiagonal problem $(\omega - T^N)\chi_i = e_1$, where $e_1^\top = (1, 0, 0 \ldots)$, c) compute $g(\omega) \approx \sum_{i=1}^{N} \zeta_i^* \chi_i$. Step a) is by-far the most time-consuming, involving the application of the operator $2N$ times. Steps b) and c) are particularly inexpensive, due to the tridiagonal nature of the problem, which scales linearly with N. The strength of Lanczos for frequency-independent kernels is precisely due to these reasons: the numerical bottleneck is the tridiagonalization of the operator, which is done only once, then the susceptibility can be computed for each ω at a negligible cost.

Conclusions

The formulation of the linearized time-dependent Kohn-Sham equations has been carried out in the case of finite and extended systems *without assuming time-reversal symmetry*, in a *fully non-collinear framework* and *without explicit reference to the empty states*. With a particular choice in the unknowns of the equations, namely (4.82) for finite systems and (4.107) for extended systems, we are able to recast the whole TDDFT linear-response problem into a linear form in the *batch space*, namely (4.115). This form is particularly suitable for the Lanczos algorithm, since the tridiagonalization of the operator $\mathcal{L}$ can be performed, at a given wave vector $\mathbf{Q}$, once and for all the frequencies; however, nothing forbids to apply other iterative methods such as the Davidson or the Conjugate Gradient algorithms. We remark that the equations we have obtained in Sec. 4.3 chapter are already accounting for SOC if present in $\hat{h}^\circ$, due to the fact that relativistic NC pseudopotentials commute with the time-reversal operator (see App. A).

CHAPTER

FIVE

IMPLEMENTATION AND BENCHMARKING

In this chapter we present the implementation and benchmarking of the method developed in the last sections. In the first part the algorithm and the implementation in a Plane-Wave (PW) framework are discussed. In the second part, after some numerical detail on the pseudopotential we have generated, we benchmark the performances and accuracy of the method via the computation of the magnon dispersion of Fe BCC.

5.1 Implementation

We have implemented the approach described in Ch. 4 in the TDDFPT-package of the QUANTUM ESPRESSO suite of computer codes [80], which uses a PW basis set with periodic boundary conditions on the simulation cell, together with the pseudopotential approximation. In the next two sections, first we comment on the general implementation strategy, then we go into some details of the PW-implementation.

5.1.1 The Algorithm

The Lanczos recursion for non-hermitian operators is illustrated in Algorithm 1. Two main operations need to be implemented: the application of the Liouvillian on a given vector, and the scalar product.

The Linear Space

The Liouvillian operator acts on the space spanned by *batches*. A *batch* is a set of $N_{\mathcal{V}}$ wave functions, where $N_{\mathcal{V}}$ is the number of the occupied Kohn-Sham orbitals. In extended systems, it means $N_{\mathbf{k}} \times N_b(\mathbf{k})$ orbitals, where $N_{\mathbf{k}}$ is the number of $\mathbf{k}$-points in the Brillouin Zone and $N_b(\mathbf{k})$ is the number of occupied bands for each $\mathbf{k}$-point. If smearing is used, states are considered occupied up to $\varepsilon_F + 3\sigma$, where σ is the broadening parameter.[1] The size of these vectors can increase very rapidly, in this

[1] Notice that, when smearing is used, the size of the batches would in principle be infinite. In practice, we are allowed to stop at $N_b(\mathbf{k})$ since the batches are built in such a way as to have a

Algorithm 1 Bi-orthogonalization Lanczos.

$\gamma_1 q_0 \leftarrow 0; \qquad \beta_1 p_0 \leftarrow 0;$
$q_1 \leftarrow v; \qquad p_1 \leftarrow v;$
for $j = 1, N_{\text{its}}$ **do**
▷ *Apply operator twice (bottleneck)*
$\bar{q} \leftarrow \mathcal{L} q_j; \qquad \bar{p} \leftarrow \mathcal{L}^\dagger p_j$
▷ *Compute and store β and γ*
$\beta_j \leftarrow \sqrt{|\langle p_j, q_j \rangle|}$
$\gamma_j \leftarrow \gamma_j / \beta_j$
▷ *Rescale vectors*
$q_j \leftarrow q_j / \beta_j; \qquad p_j \leftarrow p_j / \gamma_j^*$
$\bar{q} \leftarrow \bar{q} / \beta_j; \qquad \bar{p} \leftarrow \bar{p} / \gamma_j^*$
▷ *Compute and store α and ζ*
$\alpha_j \leftarrow \langle p_j, \bar{q} \rangle$
$\zeta_j \leftarrow \langle q_j, u \rangle$
▷ *Build the full (non-normalized) vectors*
$q_{j+1} \leftarrow \bar{q} - \alpha_j q_j - \gamma_j q_{j-1}$
$p_{j+1} \leftarrow \bar{p} - \alpha_j^* p_j - \beta_j p_{j-1}$
▷ *Prepare for the next iteration*
$q_{j-1} \leftarrow q_j; \qquad p_{j-1} \leftarrow p_j$
$q_j \leftarrow q_{j+1}; \qquad p_j \leftarrow p_{j+1}$
end for

regard Lanczos seems the most suitable choice to solve the problem in such a base, since it only needs the vectors at the previous two iterations, for a total of 6 vectors in memory for the recursion (3 for the right subspace and 3 for the left one) plus the $A_{\mathbf{q}}$ batch of Eq. (4.125) (the u vector in Alg. 1) needed to compute the ζ coefficients at each step.

Initialization

The starting vector of v of Algorithm 1 is the batch $B_{\mathbf{Q}}$ of Eq. (4.127), which depends on the external perturbation; e.g., in the case of magnetic field along the y-direction, $\hat{B}_{\mathbf{Q}} = \hat{m}^y(\mathbf{Q})$, i.e. the Fourier transform of the single-particle magnetization operator.[2] The perturbation defines which column of the susceptibility matrix (3.35) is computed: with one Lancozs chain, one has access to the entire column. The rows are instead defined by the batch $A_{\mathbf{Q}}$ of Eq. (4.125), which in Algorithm 1 is represented by the u vector, needed to compute the ζ_j coefficients. Since the scalar

vanishing norm for $\varepsilon_{n\mathbf{k}} > \varepsilon_F + 3\sigma$, due to the definition introduced by de-Gironcoli and explained in Sec. 4.3.1.

[2]The many-body magnetization reads as

$$\mathcal{M}^\alpha(\mathbf{r}) = \sum_{i=1}^{N} \hat{m}_i^\alpha(\mathbf{r}) \,, \tag{5.1}$$

which can be compared with Eq. (4.2).

product is quite inexpensive compared to the application of the Liouvillian, the ζ_j for the charge and the three magnetic polarizations can be computed at each step, without any appreciable lowering of the performance.

The Scalar Product

Given two batch-vectors

$$A_{\mathbf{q}} = \begin{pmatrix} \left\{ a^x_{n\mathbf{k}+\mathbf{q}} \right\} \\ \left\{ a^y_{n\mathbf{k}+\mathbf{q}} \right\} \end{pmatrix}, \qquad B_{\mathbf{q}} = \begin{pmatrix} \left\{ b^x_{n\mathbf{k}+\mathbf{q}} \right\} \\ \left\{ b^y_{n\mathbf{k}+\mathbf{q}} \right\} \end{pmatrix}, \tag{5.2}$$

where $a^x_{n\mathbf{k}+\mathbf{q}}$ are single-particle spinors, the scalar product on the batch space is defined as

$$\langle A_{\mathbf{q}}, B_{\mathbf{q}} \rangle \equiv \frac{1}{N_{\mathbf{k}}} \sum_{\mathbf{k}}^{N_{\mathbf{k}}} \sum_{n}^{N_b(\mathbf{k})} \left[\langle a^x_{n\mathbf{k}+\mathbf{q}}, b^x_{n\mathbf{k}+\mathbf{q}} \rangle_{1p} + \langle a^y_{n\mathbf{k}+\mathbf{q}}, b^y_{n\mathbf{k}+\mathbf{q}} \rangle_{1p} \right], \tag{5.3}$$

where $\langle \cdots \rangle_{1p}$ denotes the scalar product in the single-particle Hilbert space.

Post-Processing

Every M iterations, where M is a user-defined parameter, the α, β, γ and ζ coefficients are written to file. The inversion of the tri-diagonal problem for each value of $\omega + i\eta$ is performed by a serial post-processing code with a completely negligible effort with respect to the tridiagonalization.

The q-Decoupling and $\hat{P}$- and $\hat{\Pi}$-operators

In order to perform a linear-response calculation, the knowledge of the unperturbed Kohn-Sham states is required. In general, when TRS does not hold in the ground-state problem, the response of the unperturbed wave function $\psi^\circ_{n\mathbf{k}}$ to a $\mathbf{q}$-perturbation contains a Bloch-component with wave vector $\mathbf{k}+\mathbf{q}$ and another one of wave vector $\mathbf{k}-\mathbf{q}$. This results in the nuisance of treating three different Bloch states at a time, and even in the more cumbersome rebuilding all the non-local pseudopotential terms with the two different values of $\mathbf{q}$ and $-\mathbf{q}$. When TRS holds, this problem is avoided by considering the response of a $(-\mathbf{k})$-state to a $(-\mathbf{q})$-perturbation, (the response density is insentive to such a change, being integrated over the whole BZ), which belongs to the same degenerate space of $\mathbf{k}+\mathbf{q}$ vectors. When TRS does not hold, this is not true anymore, but still we can consider the response of a $(-\mathbf{k})$-state to a $(-\mathbf{q})$-perturbation and define the time-reversal of this state as our variable. This latter state will not in general be degenerate with another $\mathbf{k}+\mathbf{q}$ state, but will surely be of wave vector $\mathbf{k}+\mathbf{q}$, so that only 2 different sets of Bloch orbitals and one non-local $\mathbf{q}$-term enter the problem. These considerations are already included in the formulation given in Sec. 4.3.3, but have been explicitly reported here, where appropriate.

The price we pay is in disk-storage, in fact the unperturbed wave functions at $-\mathbf{k}-\mathbf{q}$ are needed throughout the calculation. To understand this point we first

consider the action of $\hat{P}_{\mathcal{C}(n\mathbf{k})}$ on a wave function of wave vector $\mathbf{k}'$. It can be shown that

$$\hat{P}_{\mathcal{C}(n\mathbf{k})}\,\psi_{\mathbf{k}'}(\mathbf{r}) = e^{i\mathbf{k}'\cdot\mathbf{r}}\,\hat{P}^{\mathbf{k}'}_{\mathcal{C}(n\mathbf{k})}\,u_{\mathbf{k}'}(\mathbf{r})\,, \tag{5.4}$$

where $u_{n\mathbf{k}}(\mathbf{r})$ is the periodic part of the Bloch orbitals, and

$$\hat{P}^{\mathbf{k}'}_{\mathcal{C}(n\mathbf{k})} \equiv \left[\tilde{\vartheta}_{F,n\mathbf{k}} - \sum_{n'}\left(\tilde{\vartheta}_{F,n\mathbf{k}}\,\vartheta_{n\mathbf{k},n'\mathbf{k}'} + \tilde{\vartheta}_{F,n'\mathbf{k}'}\,\vartheta_{n'\mathbf{k}',n\mathbf{k}}\right) u^{\circ}_{n'\mathbf{k}'}u^{\circ\dagger}_{n'\mathbf{k}'}\right]\,. \tag{5.5}$$

On the other hand, the newly-defined projector $\hat{\Pi}_{\mathcal{C}(n\mathbf{k})}$ has the similar property

$$\hat{\Pi}_{\mathcal{C}(n\mathbf{k})}\,\psi_{\mathbf{k}'}(\mathbf{r}) = e^{i\mathbf{k}'\cdot\mathbf{r}}\,\hat{\Pi}^{\mathbf{k}'}_{\mathcal{C}(n\mathbf{k})}\,u_{\mathbf{k}'}(\mathbf{r})\,, \tag{5.6}$$

where

$$\hat{\Pi}^{\mathbf{k}'}_{\mathcal{C}(n\mathbf{k})} \equiv \left[\tilde{\vartheta}_{F,n\mathbf{k}} - \sum_{n'}\left(\tilde{\vartheta}_{F,n\mathbf{k}}\,\vartheta_{n\mathbf{k},n'-\mathbf{k}'} + \tilde{\vartheta}_{F,n'-\mathbf{k}'}\,\vartheta_{n'-\mathbf{k}',n\mathbf{k}}\right)\left(\hat{\mathrm{T}}u^{\circ}_{n'-\mathbf{k}'}\right)\left(\hat{\mathrm{T}}u^{\circ}_{n'-\mathbf{k}'}\right)^{\dagger}\right]\,. \tag{5.7}$$

since $\hat{P}^{\mathbf{k}'}_{\mathcal{C}(n\mathbf{k})}$ and $\hat{\Pi}^{\mathbf{k}'}_{\mathcal{C}(n-\mathbf{k})}$ are applied to wave functions of wave vector $\mathbf{k}+\mathbf{q}$, in order to compute the action of the $\hat{P}$-operator we need the functions $u^{\circ}_{n\mathbf{k}+\mathbf{q}}$, instead of computing the action of the $\hat{\Pi}$-operator the unperturbed $u^{\circ}_{n-\mathbf{k}-\mathbf{q}}$ are needed.

The Unperturbed Wave Functions

A customized **k**-point grid is built in such a way that the occupied wave functions

$$\begin{array}{ll} u^{\circ}_{n\mathbf{k}} & \hat{\mathrm{T}}u^{\circ}_{n\mathbf{k}} \\ u^{\circ}_{n\mathbf{k}+\mathbf{q}} & \hat{\mathrm{T}}u^{\circ}_{n\mathbf{k}+\mathbf{q}} \\ u^{\circ}_{n\mathbf{k}-\mathbf{q}} & \hat{\mathrm{T}}u^{\circ}_{n\mathbf{k}-\mathbf{q}} \\ u^{\circ}_{n-\mathbf{k}} & \hat{\mathrm{T}}u^{\circ}_{n-\mathbf{k}} \\ u^{\circ}_{n-\mathbf{k}+\mathbf{q}} & \hat{\mathrm{T}}u^{\circ}_{n-\mathbf{k}+\mathbf{q}} \\ u^{\circ}_{n-\mathbf{k}-\mathbf{q}} & \hat{\mathrm{T}}u^{\circ}_{n-\mathbf{k}-\mathbf{q}} \end{array} \tag{5.8}$$

are stored to disk in separate binary files with the above **k**-point order. Each block of orbitals of type (5.8) allows to build the operators $\hat{P}^{\mathbf{k}'}_{\mathcal{C}(n\mathbf{k})}$ and $\hat{\Pi}^{\mathbf{k}'}_{\mathcal{C}(n-\mathbf{k})}$ for two pairs of Eq. (4.113).

5.1.2 Details of the Implementation in a PW Code

The periodic part of the wave function is expanded in PWs

$$\psi_{n\mathbf{k}}(\mathbf{r}) = e^{i\mathbf{k}\cdot\mathbf{r}}u_{n\mathbf{k}}(\mathbf{r})\,, \qquad u_{n\mathbf{k}}(\mathbf{r}) = \sum_{\mathbf{G}}^{|\mathbf{k}+\mathbf{G}|^2\le\varepsilon_{\mathrm{cut}}} c_{n\mathbf{k}}(\mathbf{G})\frac{e^{i\mathbf{G}\cdot\mathbf{r}}}{\sqrt{\Omega}}\,, \tag{5.9}$$

where $\Omega = N_{\mathbf{k}}\Omega_0$ is the crystal volume. ε_{cut} is the user-defined cutoff for the wavefunctions. A wave function is then described by the set of complex numbers $c_{n\mathbf{k}}(\mathbf{G})$,[3] and a label recalling the $\mathbf{k}$-point. The scalar product when NC pseudopotentials are used is given by

$$\langle \psi_{n\mathbf{k}}, \psi_{n'\mathbf{k}} \rangle_{1p} = \sum_{\mathbf{G}}^{|\mathbf{k}+\mathbf{G}|^2 \leq \varepsilon_{\text{cut}}} c^*_{n\mathbf{k}}(\mathbf{G}) c_{n'\mathbf{k}}(\mathbf{G}) \,, \tag{5.10}$$

according to which wave functions are normalized to unity. A PW basis set greatly benefits from Fast Fourier Transform (FFT), which allow to switch between the $\mathbf{G}$-space and the $\mathbf{R}$-space at a $\mathcal{O}(N \log N)$-cost [80], with N the number of grid points.

Applying the Liouvillian

The application of the Liouvillian operator to a batch is performed via Eqs. (B.9)–(B.14). Given an input batch

$$q = \begin{pmatrix} \left\{ x_{n\mathbf{k}+\mathbf{q}} \right\} \\ \\ \left\{ y_{n\mathbf{k}+\mathbf{q}} \right\} \end{pmatrix} , \tag{5.11}$$

the output batch $\mathcal{L}q$ is computed by

1. Building n' and $\mathbf{m}'$ via Eqs. (4.109) and (4.110). The multiplication with the unperturbed orbitals is done in real space via FFT.
2. The response potentials v'_{eff} and $v'^{[-\mathbf{b}]}_{\text{eff}}$ are computed from n' and $\mathbf{m}'$ (Eq. (4.111)); the Hartree term in $\mathbf{G}$-space and the xc-one (local or semi-local) in $\mathbf{R}$-space.
3. The terms $v'_{\text{eff}}\psi^{\circ}_{n\mathbf{k}}$ and $v'^{[-\mathbf{b}]}_{\text{eff}}\hat{\mathrm{T}}\psi^{\circ}_{n-\mathbf{k}}$ are computed in $\mathbf{R}$-space.
4. The operators $\hat{P}_{\mathcal{C}}$ and $\hat{\Pi}_{\mathcal{C}}$ are applied in $\mathbf{G}$-space.
5. The terms $[\hat{h}^{\circ} - \varepsilon_{n\mathbf{k}}]x_{n\mathbf{k}+\mathbf{q}}$ and $[\hat{h}^{\circ[-\mathbf{b}]} - \varepsilon_{n-\mathbf{k}}]y_{n\mathbf{k}+\mathbf{q}}$ are computed and summed to $\hat{P}_{\mathcal{C}}v'_{\text{eff}}\psi^{\circ}_{n\mathbf{k}}$ and $\hat{\Pi}_{\mathcal{C}}v'^{[-\mathbf{b}]}_{\text{eff}}\hat{\mathrm{T}}\psi^{\circ}_{n-\mathbf{k}}$ respectively. The former summation gives the upper output batch, the latter the lower output batch.

We point out that the superoperators $\mathcal{D}$, $\mathcal{K}$ and $\mathcal{P}$ appearing in Eq. (4.115) are hermitian with the exception of $\mathcal{K}^{XY\dagger} = \mathcal{K}^{YX}$, (see App. B), therefore to compute $\mathcal{L}^{\dagger}p$ the same routines can be applied.

Parallelization

The code has inherited from the QUANTUM ESPRESSO environment a two-level parallelization via the MPI interface. The first parallelization level is the FFT grid ($\mathbf{R}$&$\mathbf{G}$ parallelization), the second over the $\mathbf{k}$-points (pool parallelization). In the pool parallelization, care has been exerted in order not to break blocks (5.8) among different pools.

[3] Notice that the number of coefficients $c_{n\mathbf{k}}(\mathbf{G})$ depends on the cutoff *and* on the size of the simulation cell. Moreover, at fixed ε_{cut} and simulation cell, the number of $c_{n\mathbf{k}}(\mathbf{G})$ may slightly vary from $\mathbf{k}$-point to $\mathbf{k}$-point, due to the different shift of the cutoff sphere of (5.9).

5.2 Testing

5.2.1 The Norm-Conserving Pseudopotential

Iron is a 3d transition element with atomic number $Z = 26$ and an electronic configuration [Ar] $3d^6$ $4s^2$. At ambient pressure and temperature, it is found in a ferromagnetic state with a BCC crystal symmetry (called Iron α-phase). Norm-Conserving pseudopotentials for transition elements tend to be very hard due to the nodeless, but localized, structure of the radial part of the 3d-orbitals. For this reason there is poor availability of such pseudopotentials, and we resorted to generating one ourselves via the `atomic` package of QUANTUM ESPRESSO.

Following [81], we have kept the 3d and 4s electrons in valence, with cutoff radii $r_c = 2.2$ bohr for $l = 0$, $r_c = 3.2$ bohr for $l = 1$ and $r_c = 1.5$ bohr for $l = 2$. $l = 0$ has been chosen as the local channel for the Kleinman-Bylander form [46]. The Troullier-Martins [48] pseudization scheme has been used and non-linear core corrections have been included. The LDA xc-functional with the Perdew-Zunger (PZ) parametrization has been chosen. We plot the Kohn-Sham band structure along the high-symmetry directions, as reported in Fig. 8. The two flat branches of opposite spin, right below and right above the Fermi level, are responsible for the Stoner transitions, which is expected to reach its maximum slightly above 2 eV. This can be seen more clearly by plotting the DoS projected on atomic orbitals (pDoS), as done in Fig. 9: the two flat bands are mainly of d-origin, and produce pronounced peaks of opposite spin-flavour at a distance of ~ 2.5 eV.

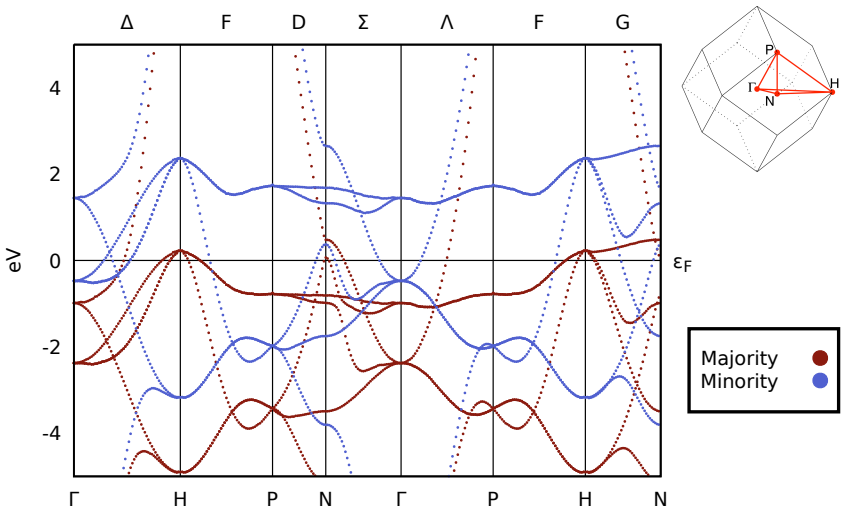

Figure 8. LSDA bands of Fe BCC along the high-symmetry directions, computed with $\varepsilon_{\text{cut}} = 90$ Ry, Gaussian smearing $\sigma = 0.005$ Ry and a $36 \times 36 \times 36$ Monkhorst-Pack grid for the BZ sampling. On this energy scale, bands are indistinguishable from the ones computed at lower BZ-sampling up to $16 \times 16 \times 16$ grids. We notice right below and right above the Fermi level very flat bands with opposite spin orientations, signal of a high-density of Stoner (spin-flip) transitions.

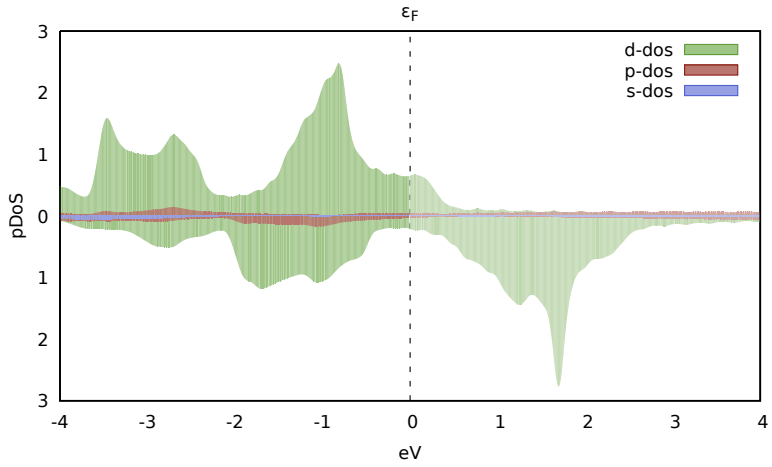

Figure 9. Projected Density of States (pDoS) of Fe BCC computed with the same parameters as the one used for Fig. 8 regarding the self-consistent calculation, plus a subsequent refinement via a non self-consistent calculation on a $60 \times 60 \times 60$ Monkhorst-Pack grid. The positive part represents the majority-spin pDos, the negative part the minority ones. We notice the predominance of the d-character and the peaked structure about 1 eV before and 1.5 eV after the Fermi level, which mark the presence of Stoner excitations.

In order to choose the energy cutoff for the wave functions, the behaviour of the ground-state magnetization as a function of a volumetric deformation is inspected, as done in Ref. [82]. The results are reported in the left panel of Fig. 10: already at $\varepsilon_{\text{cut}} = 90\,\text{Ry}$ the error in the magnetization per atom is within 1%, yielding a value of $2.12\,\mu_B$ (to be compared with the experimental value of $2.22\,\mu_B$ at 0 K). The equilibrium lattice constant results of $a = 2.81\,\text{Å}$ (vs. 2.86 Å from [82]) and the bulk modulus of 222 GPa, which overestimates of about 30% the extrapolated experimental value at 0 K of 170.35 GPa [83]; this is a well-known failure of the LSDA approximation [82]. In all the production calculations a cutoff of 90 Ry and a lattice constant of $a = 2.81\,\mathring{A}$ will be used.

5.2.2 The Non-Interacting Response Function

In the development of a code, intermediate steps are necessary in order to check the correctness of the work done. Dealing with magnetic systems introduces intricacies which affect the code in a widespread way, most of them coming from the handling of Bloch orbitals at different **k**-points and their time-reversed counterparts. The implementation of this aspect has been validated by computing the magnetic sector of the non-interacting Kohn-Sham susceptibility, i.e. $\chi^0_{\alpha\beta}(\mathbf{q},\omega)$ with $\alpha,\beta = x,y,z$. The $\chi^0_{\alpha\beta}(\mathbf{q},\omega)$ obtained with our LL method has been compared to the one given by the explicit summation over all the possible transitions between occupied and empty states of Eq. (3.33). Within the LL approach, χ^0 is obtained by tri-diagonalizing a Liouvillian whose $\mathcal{K}$-terms, responsible for the mixing of the independent-particle excitations, have been set to zero in Eq. (4.115), i.e.

$$\mathcal{L}_0 = \begin{pmatrix} \mathcal{D}^X & \mathbb{0} \\ \mathbb{0} & -\mathcal{D}^Y \end{pmatrix}, \tag{5.12}$$

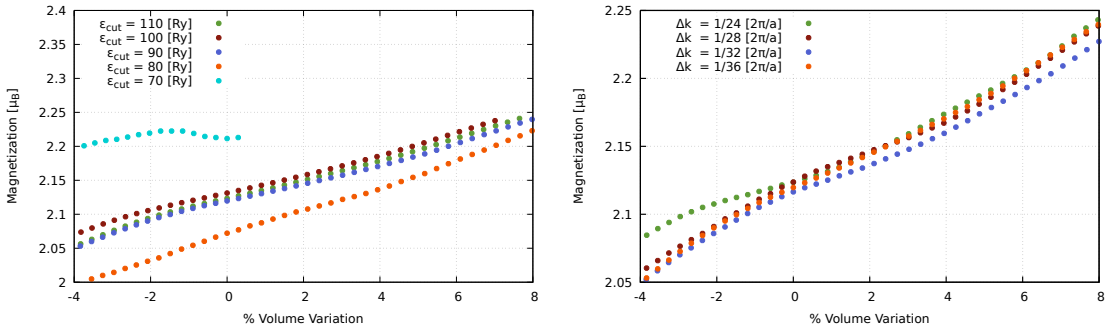

Figure 10. *Left panel*: modulus of the ground-state magnetization as a function of the volumetric deformation, i.e. a change in the lattice parameter a, for bulk Fe BCC. The curve for $\varepsilon_{\text{cut}} = 70\,\text{Ry}$ stops prematurely since it predicts an equilibrium lattice constant far too big than the better-converging cutoffs. The calculations have been performed with a Gaussian smearing of $\sigma = 0.005\,\text{Ry}$ and a $36 \times 36 \times 36$ Monkhorst-Pack grid for the BZ sampling. At about 90 Ry, the curves start to converge in an oscillatory fashion, with a width that lead us to estimate the error for the ground-state magnetization and lattice parameter $< 1\%$. *Right panel*: magnetization over volume at fixed $\varepsilon_{\text{cut}} = 90\,\text{Ry}$ for different Monkhorst-Pack grids. We notice that the agreement is maximum around equilibrium.

the direct approach consists instead in the evaluation of the Fourier transform of Eq. (3.33), which in the case of extended systems reads

$$\chi^0_{\alpha\beta}(\mathbf{q},\omega) = \sum_{\mathbf{k}\in\text{BZ}} \sum_{nn'}^{\varepsilon_c} (\tilde{\vartheta}_{F,n\mathbf{k}} - \tilde{\vartheta}_{F,n'\mathbf{k}+\mathbf{q}}) \frac{\langle u^\circ_{n\mathbf{k}}, \sigma^\alpha u^\circ_{n'\mathbf{k}+\mathbf{q}}\rangle \langle u^\circ_{n'\mathbf{k}+\mathbf{q}}, \sigma^\beta u^\circ_{n\mathbf{k}}\rangle}{\hbar\omega - (\varepsilon_{n'\mathbf{k}+\mathbf{q}} - \varepsilon_{n\mathbf{k}}) + i\eta}\,, \tag{5.13}$$

where the summation over n and n' is cut off at a certain energy value ε_c. In both the computations a small, finite imaginary frequency η is kept, so to produce a Lorentzian broadening of the Dirac deltas appearing in the imaginary part of the susceptibility (cf. Eq. (3.13)). Notice that the LL solution is equivalent to (5.13) with $\varepsilon_c = \varepsilon_{\text{cut}}$, the ground-state cutoff. In Figs. 11, 12 and 13 the convergence with respect to the Lanczos iterations of the real and imaginary parts of $\chi^0_{\alpha\beta}(\omega)$ is reported. It can be seen that the region around $\sim 2\,\text{eV}$, where the majority of Stoner-transitions resides, converges slower than the low-energy region. This is a well-known feature of the Lanczos algorithm, in which the lowest eigenvalues are the first to converge.

In Fig. 14 the comparison between the converged Lanczos result and the direct approach is reported. The two susceptibilities are one on top of each other, thus validating our implementation. In both cases, the real and imaginary part respect the correct symmetries. In fact, for a collinear system magnetized along the z-direction, the following relation holds

$$\chi^0(\omega) = \begin{pmatrix} \chi^0_{xx}(\omega) & \chi^0_{xy}(\omega) & 0 \\ -\chi^0_{xy}(\omega) & \chi^0_{xx}(\omega) & 0 \\ 0 & 0 & \chi^0_{zz}(\omega) \end{pmatrix}. \tag{5.14}$$

Note that also the stability relations (see, e.g., Sec. 3.2.4 of [28])

$$\mathrm{Im}\chi_{\alpha\beta}(0) = 0\,, \qquad \mathrm{Re}\chi_{\alpha\beta}(0) \leq 0 \tag{5.15}$$

are fulfilled.

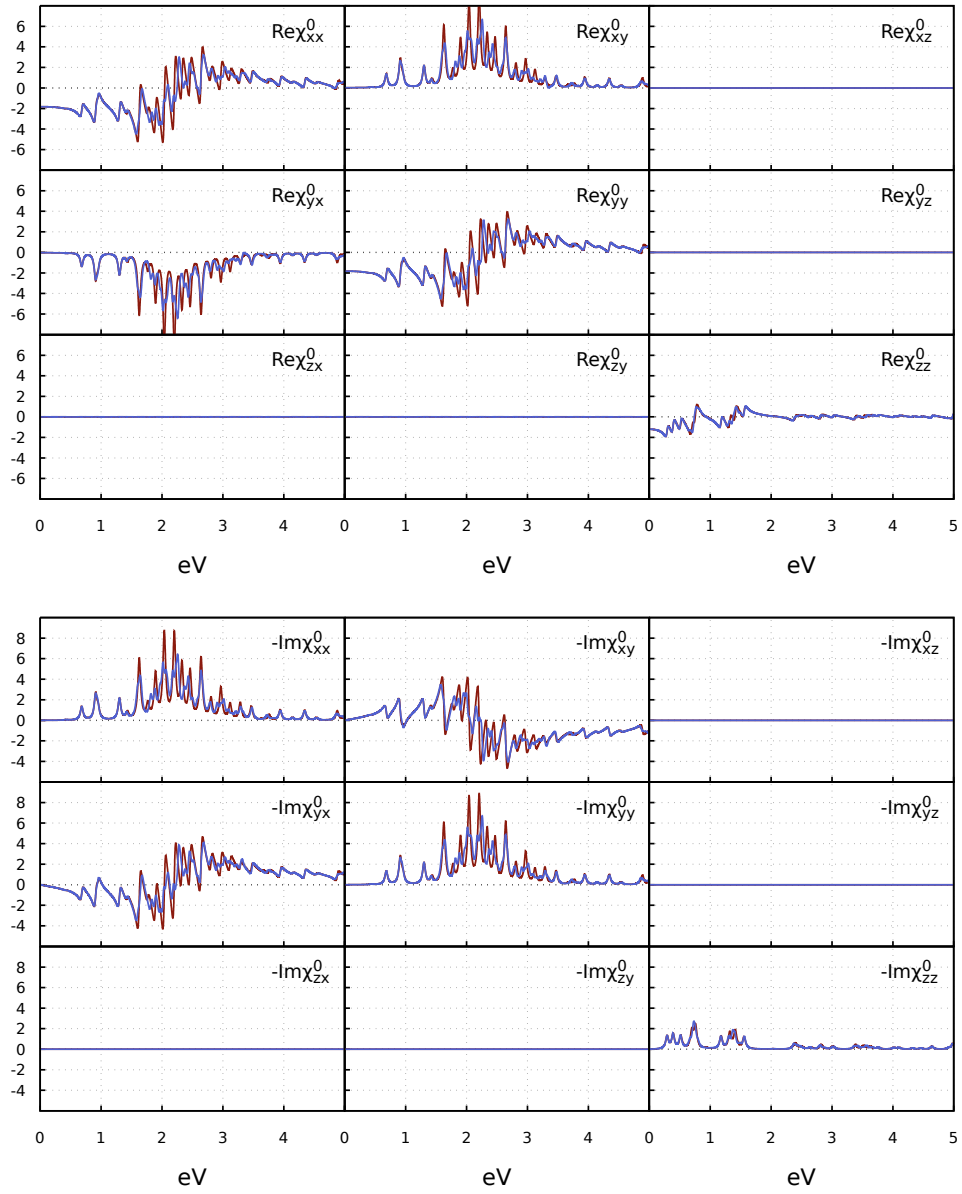

Figure 11. Real and imaginary part of $\chi^0_{\alpha\beta}(\mathbf{q},\omega)$ with $\mathbf{q} = (0.18, 0, 0)2\pi/a$, at 15000 (red) and 40000 (blue) Lanczos iterations. A lorentzian broadening of $\eta = 0.002\,\mathrm{Ry}$ has been used. The ground-state calculation has been performed with $\varepsilon_{\mathrm{cut}} = 60\,\mathrm{Ry}$, a smearing parameter of 0.01 Ry and a $4 \times 4 \times 4$ Monkhorst-Pack mesh.

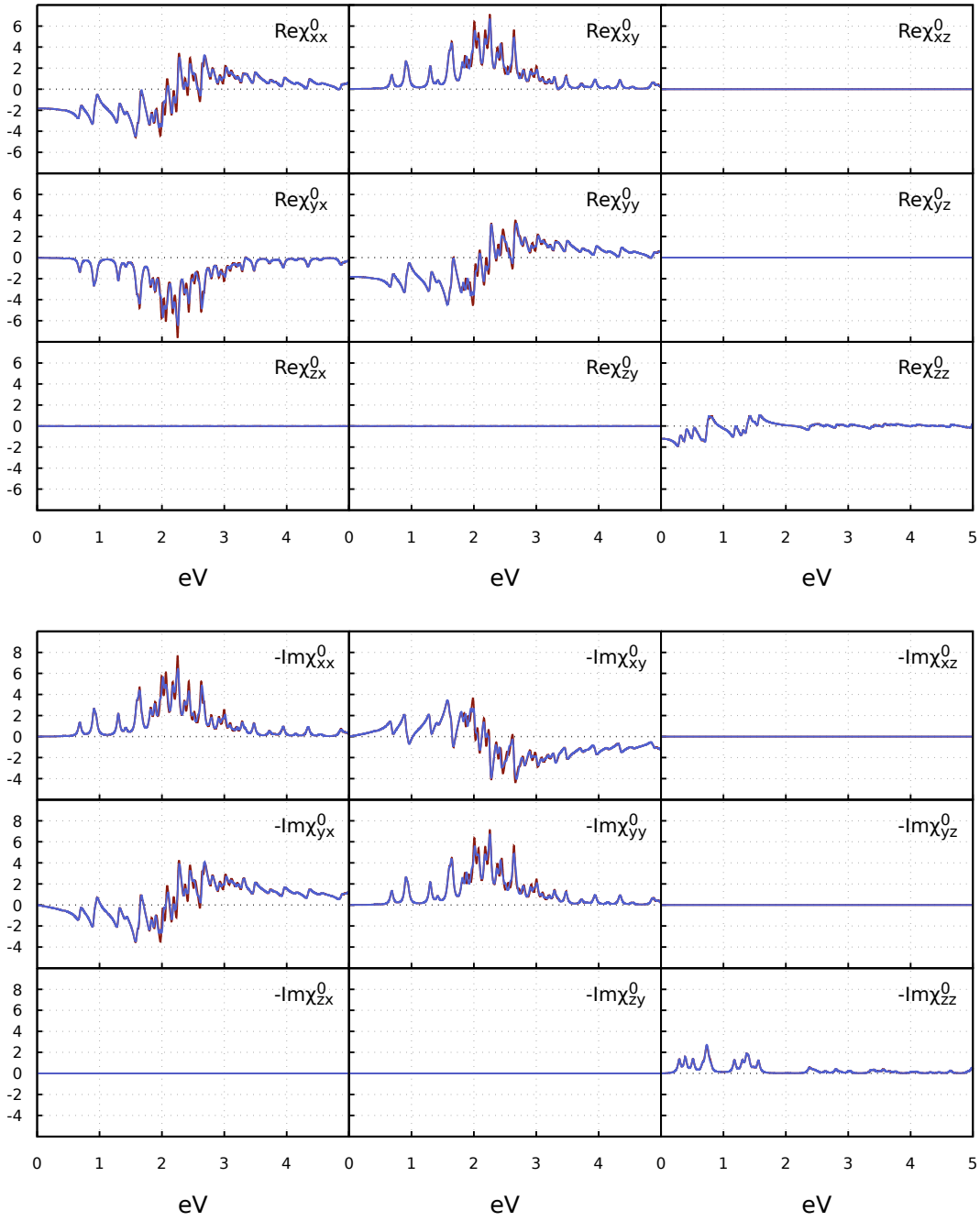

Figure 12. Real and imaginary part of $\chi^0_{\alpha\beta}(\mathbf{q},\omega)$ with $\mathbf{q} = (0.18, 0, 0)2\pi/a$, at 25000 (red) and 40000 (blue) Lanczos iterations. A lorentzian broadening of $\eta = 0.002\,\mathrm{Ry}$ has been used. The ground-state calculation has been performed with $\varepsilon_{\mathrm{cut}} = 60\,\mathrm{Ry}$, a smearing parameter of 0.01 Ry and a $4 \times 4 \times 4$ Monkhorst-Pack mesh.

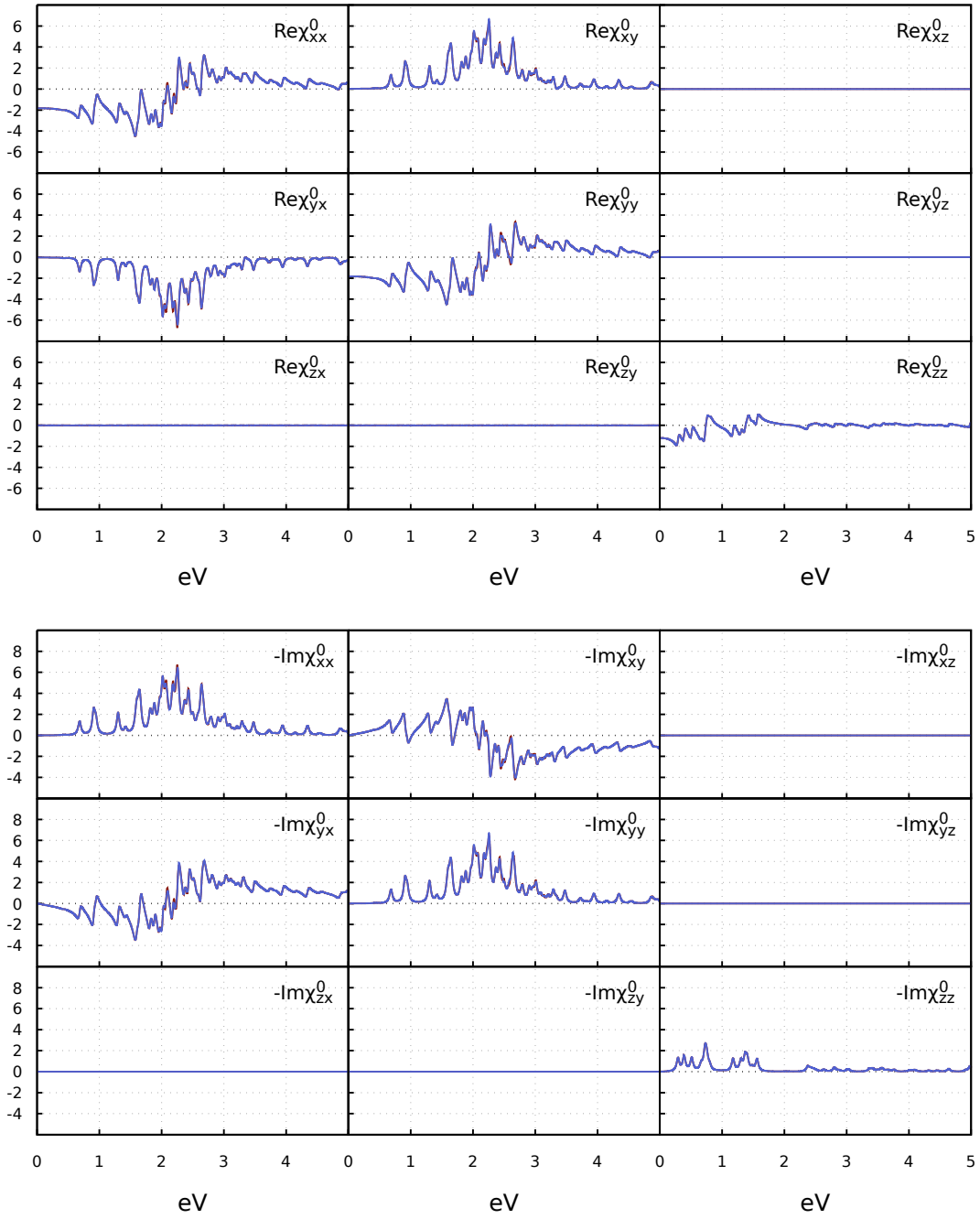

Figure 13. Real and imaginary part of $\chi^0_{\alpha\beta}(\mathbf{q},\omega)$ with $\mathbf{q} = (0.18, 0, 0)2\pi/a$, at 35000 (red) and 40000 (blue) Lanczos iterations. A lorentzian broadening of $\eta = 0.002\,\mathrm{Ry}$ has been used. The ground-state calculation has been performed with $\varepsilon_{\mathrm{cut}} = 60\,\mathrm{Ry}$, a smearing parameter of 0.01 Ry and a $4 \times 4 \times 4$ Monkhorst-Pack mesh.

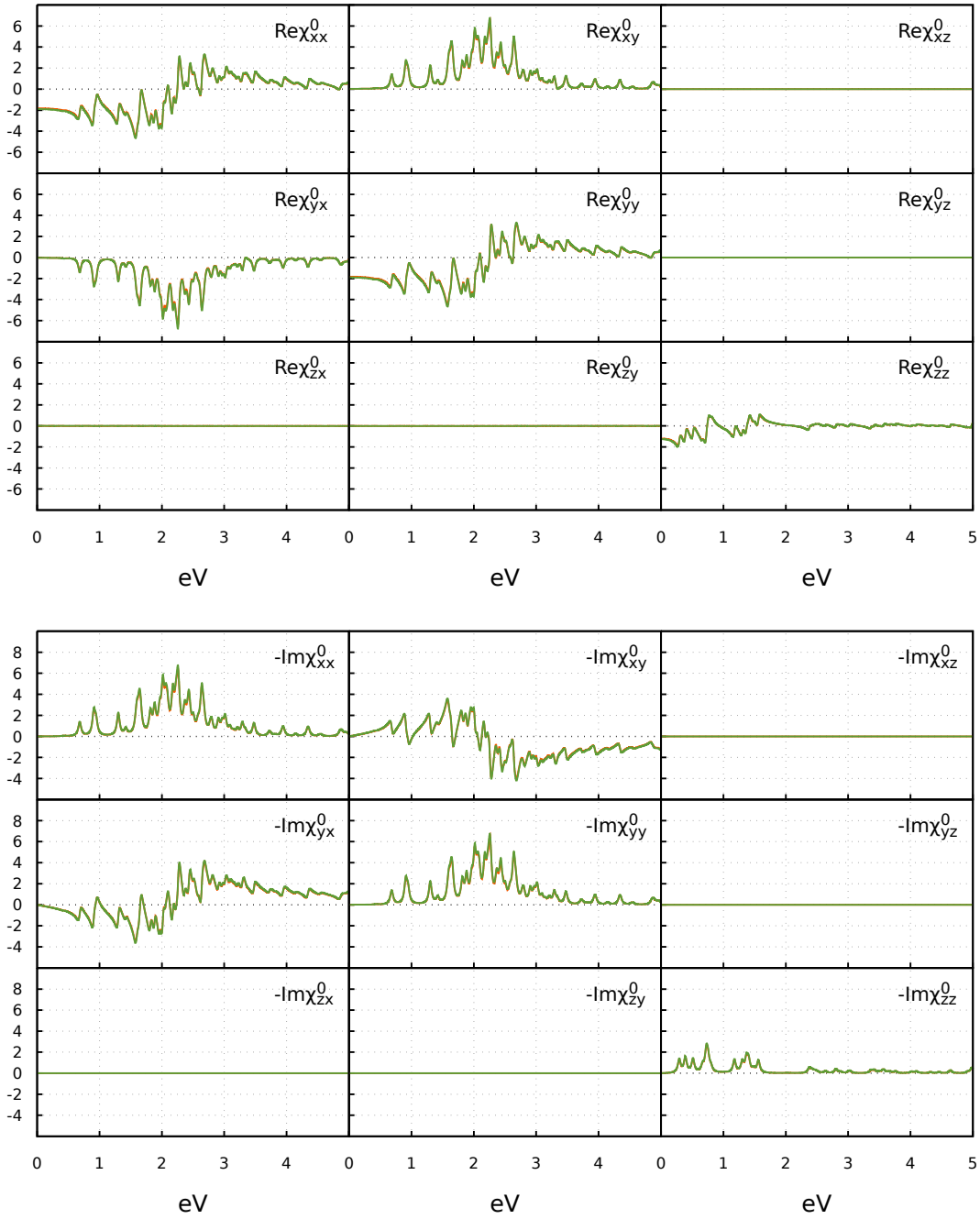

Figure 14. Comparison between the real and imaginary part of $\chi^0_{\alpha\beta}(\mathbf{q},\omega)$ at $\mathbf{q} = (0.18, 0, 0)2\pi/a$, computed with the LL approach (orange, 40000 iterations) and via the expicit form (5.13) (green, $\varepsilon_c = 3\,\mathrm{Ry}$). A lorentzian broadening of $\eta = 0.002\,\mathrm{Ry}$ has been used in both cases. The ground-state calculation has been performed with $\varepsilon_{\mathrm{cut}} = 60\,\mathrm{Ry}$, a smearing parameter of $0.01\,\mathrm{Ry}$ and a $4 \times 4 \times 4$ Monkhorst-Pack mesh.

5.3 Magnetic Excitations in Fe BCC

The final validation of our method is the computation of the full susceptibility of the collinear state of Fe BCC, within our non-collinear framework. We shall focus on the quantity

$$S(\mathbf{q},\omega) = -\sum_{\alpha\beta}\left(\delta_{\alpha\beta} - \frac{q^\alpha q^\beta}{q^2}\right) L_{\alpha\beta}(\mathbf{q},\omega)\,, \tag{5.16}$$

where $L_{\alpha\beta}(\mathbf{q},\omega)$ is the anti-hermitian component of the magnetic susceptibility $\chi_{\alpha\beta}(\mathbf{q},\omega)$ (see Eq. (1.9)). As already seen in Chs. 1 and 3, $S(\mathbf{q},\omega)$ is proportional to the scattering intensity of an INS experiment, and its peaks correspond to the magnetic excitations. The workflow reads as follows: a DFT, ground-state calculation is performed with a certain wave-function cutoff ε_{cut}, smearing σ, and BZ-sampling. Subsequently, a Lanczos recursion is performed as the one described in Algorithm. 1, using the same ε_{cut} to describe the wavefunctions, the same occupations defined by σ, and the same Δk to build the grid with the $\mathbf{k}$, $\mathbf{k}+\mathbf{q}$ and $\mathbf{k}-\mathbf{q}$ points. Results are reported and analyzed in the following.

Convergence over the Lanczos Iterations

In Fig. 15 the convergence of the magnon peak with respect to the Lanczos iterations is reported for two different values of $\mathbf{q}$ along the (100) direction. From 7000 to 15000 iterations may be necessary to reach a convergence of the position of the peak with a meV precision. A discussion of these results and possible improvements will be addressed in the conclusions.

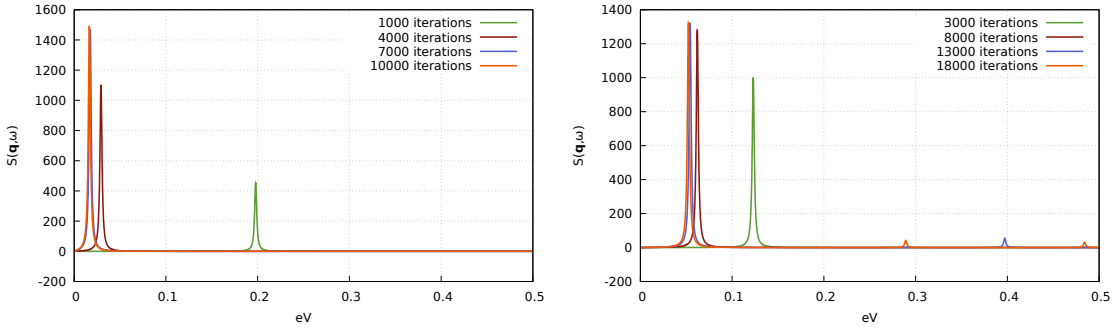

Figure 15. Convergence of the magnon peak in Fe BCC with respect to the Lanczos iterations for $\mathbf{q} = (0.09, 0, 0)2\pi/a$ on the left, $\mathbf{q} = (0.18, 0, 0)2\pi/a$ on the right. A cutoff of $\varepsilon_{\text{cut}} = 90\,\text{Ry}$, a smearing parameter $\sigma = 0.005\,\text{Ry}$ and a Monkhorst-Pack mesh of $28 \times 28 \times 28$ $\mathbf{k}$-points have been used in the ground-state calculations. The Lorentzian broadening of both the spectra is $\eta = 10^{-4}\,\text{Ry}$.

Behaviour of the Lanczos Coefficients

Information about the correct behaviour of the Lanczos chain can be inferred by inspecting the α, β, γ and ζ coefficients defined in Sec. 4.4, reported in Fig. 16 for the Lanczos chain corresponding to a magnetic perturbation along the y-direction. As noted in previous applications of the Lanczos algorithm [84, 76], and the β coefficients oscillate close to half of the energy cutoff, in this case 45 Ry; This is related to the bandwidth of the Liouvillian operator, which extends from minus

to plus the maximum excitation energy, roughly given by ε_{cut}. Moreover, the β coefficients averaged over the even and odd iterations should differ in the order of twice the gap of the system [84], in this case roughly twice the magnon energy, i.e. $\sim 10^{-1}$ eV, as shown in Fig. 17.

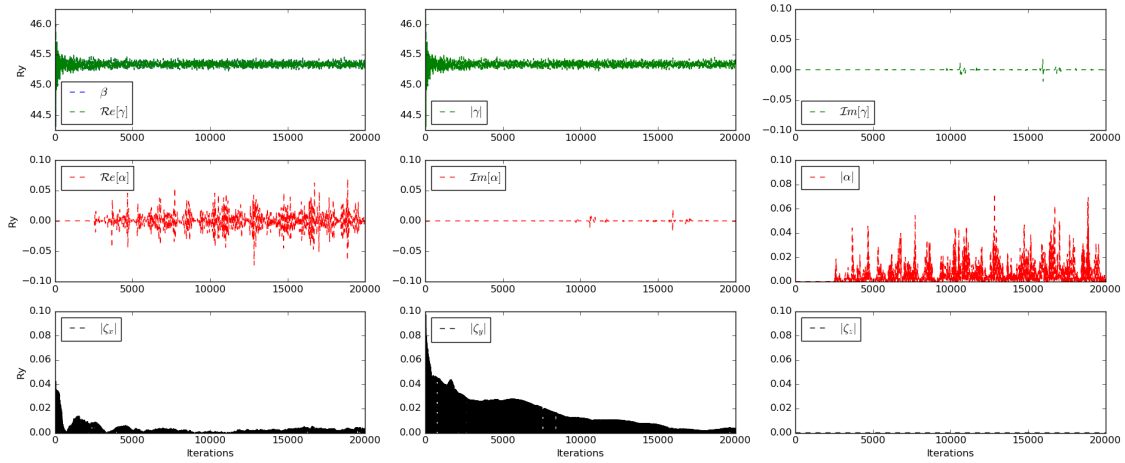

Figure 16. Lancozs coefficients relative to the calculation at $\mathbf{q} = (0.18, 0, 0)2\pi/a$ of Fig. 15. *Top panel*: β and real part of γ, modulus of γ, and imaginary part of γ. *Mid panel*: real, imaginary part and modulus of the α coefficients. *Lower panel*: modulus of ζ_x, ζ_y and ζ_z.

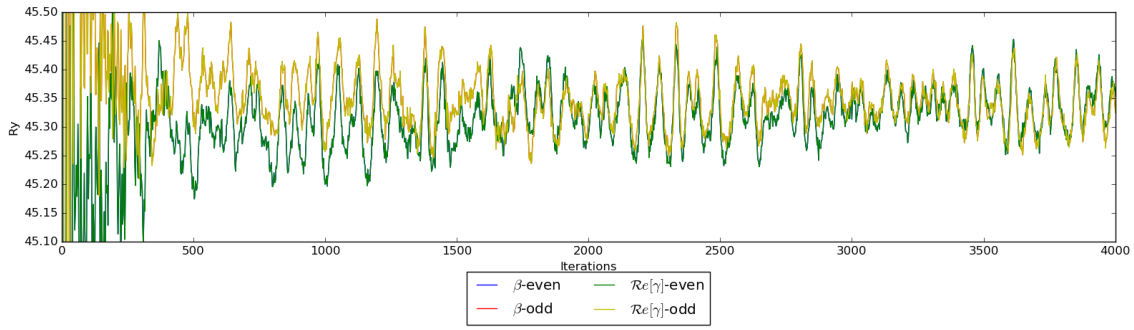

Figure 17. Magnification of the β coefficients as a function of the even and odd iterations.

Contrary to previous implementations of the LL approach, the lack of time-reversal invariance does not allow to conclude that $\alpha = 0$. From Fig. (16) the α coefficient appears negligible on the eV-energy scale for the first few thousands of iterations, then its real part starts to oscillate around zero, with amplitudes roughly on the magnon energy scale.

In the lower row of Fig. 16, the modulus of the ζ^x, ζ^y and ζ^z coefficients are reported. ζ^z is correctly negligible, being responsible for the $\chi_{zy}(\omega)$ component of magnetic susceptibility, which has to vanish for a ferromagnet polarized along the z direction described within LSDA. The ζ^x and ζ^y components, responsible for the transverse response, show a very slow decaying with respect to the number of iterations, if compared to other application of this algorithm [84, 76].

Convergence over the BZ-Sampling

In Fig. 18 the convergence of the peak position with respect to the BZ-sampling is reported for $\mathbf{q} = (0.18, 0, 0)2\pi/a$ and $\sigma = 0.005\,\mathrm{Ry}$. The position of the peak oscillates of about 6 meV around a central value up to 28^3-meshes, then already with a 32^3-mesh reaches a precision of about 2 meV.

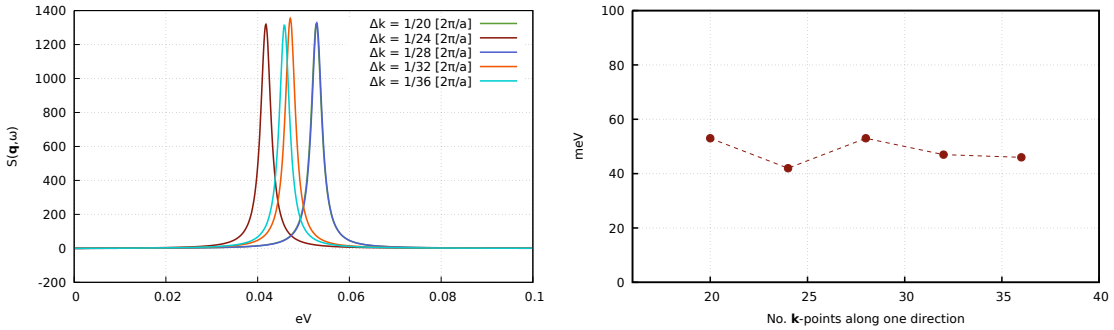

Figure 18. *Left*: convergence of the magnon peak for $\mathbf{q} = (0.18, 0, 0)2\pi/a$ with respect to the BZ-sampling at smearing parameter $\sigma = 0.005\,\mathrm{Ry}$. All the individual peaks have converged at 16000 Lanczos iterations. A Lorentzian broadening of $\eta = 10^{-4}\,\mathrm{Ry}$ has been used. *Right*: Position of the peak reported as a function of number of **k**-points used for the linear sampling of the BZ direction.

Dependence On Smearing

The investigation of the convergence of the magnon peak as a function of the BZ-sampling is compared for two different values of the ground-state smearing in Fig. 19. Though finer sampling for $\sigma = 0.01$ are missing, the overlapping region in Fig. 19 leads us to consider the position of the peak not significantly affected by the magnitude of the fictitious temperatures σ used. The overlapping region also tells us that the position of the peak loosely depends on the degree of convergence of the ground-state calculation at a fine level, and more on the fine sampling of the single-particle spin-flips.

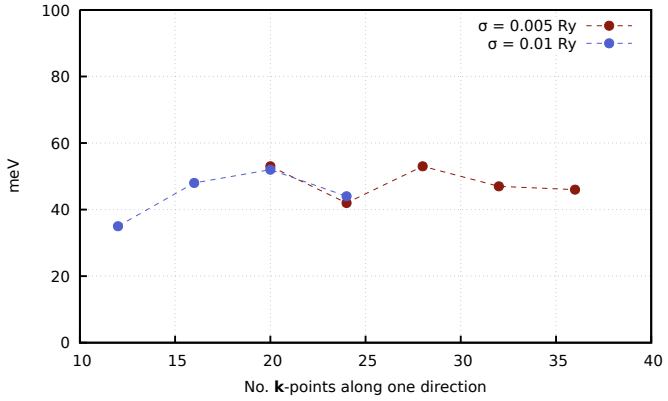

Figure 19. Position of the magnon peak at $\mathbf{q} = (0.18, 0, 0)2\pi/a$ as a function of the linear BZ-sampling, for two different ground-state smearings.

5.3.1 The Stoner Continuum

In order to investigate the continuum of Stoner excitations, the spectrum in the right panel of Fig. 15 is reported on a broader energy range in Fig. 20. The continuous part of an excitation spectrum computed with the LL method is known to converge the faster at the price of a lower resolution, i.e. the bigger the broadening η used to solve Eqs. (4.113).

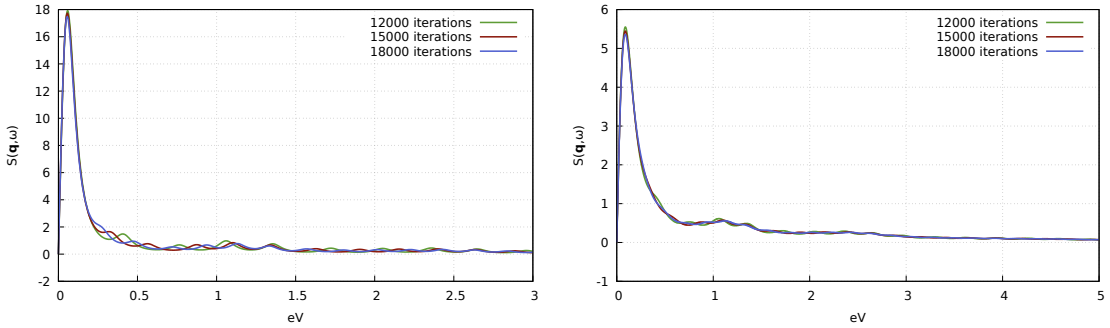

Figure 20. Convergence of $S(\mathbf{q},\omega)$ for $\mathbf{q} = (0.18, 0, 0)2\pi/a$ with two different broadening η. On the left, $\eta = 0.005\,\mathrm{Ry}$, on the right $\eta = 0.01\,\mathrm{Ry}$.

From Fig. 20 it can be seen that a broadening of about 0.01 Ry is necessary in order to converge the Stoner continuum with the same number of iterations needed to converge the spin-wave peak. This is not an issue as long as the two regions (spin-wave and Stoner) are well separated; instead, when the spin-wave energy becomes comparable to the one of the Stoner continuum, the value of η represents the resolution at which one can estimate the linewidth due to the Landau damping. If a finer resolution is desired, more Lanczos iterations are needed. This is the case when larger-wavevector excitations are explored, as reported in Fig. 21. In order to obtain a converged spectrum within 16000 iterations, the Lorentzian broadening needed is too big to infer the linewidth of the excitation with sufficient precision.

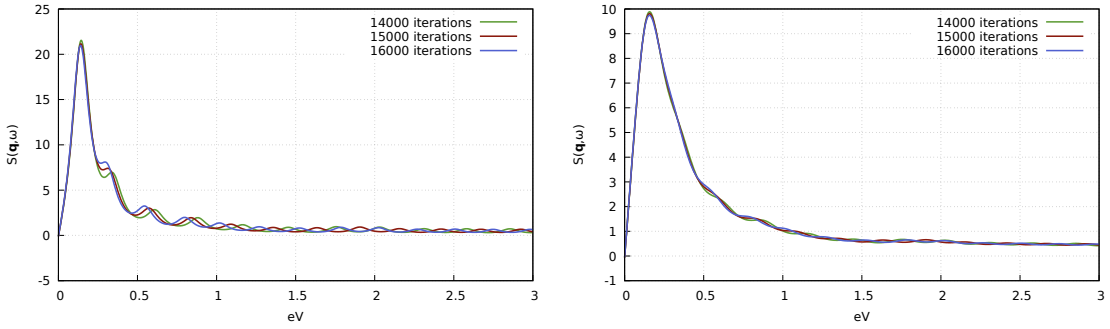

Figure 21. Convergence of $S(\mathbf{q},\omega)$ for $\mathbf{q} = (0.32, 0, 0)2\pi/a$ with a Lorentzian broadening of $\eta = 0.005\,\mathrm{Ry}$ (left) $\eta = 0.01\,\mathrm{Ry}$ (right). The shoulders on the right-hand side of the spin-wave peak reveal the presence of Stoner excitations competing with the collective excitation. A cutoff of $\varepsilon_{\mathrm{cut}} = 90\,\mathrm{Ry}$, a smearing parameter $\sigma = 0.005\,\mathrm{Ry}$ and a Monkhorst-Pack mesh of $28 \times 28 \times 28$ $\mathbf{k}$-points have been used in the ground-state calculations.

5.3.2 Dispersion along (100)

The results of the previous sections are summed up in Fig. 22, where experimental dispersions have been reported as well for comparison. The *spin stiffness* D, defined by the fit of the magnon dispersion for small $q = |\mathbf{q}|$ with the function

$$\hbar\omega(q) = Dq^2(1 - \beta q^2)\,, \tag{5.17}$$

has been computed taking into account the error bars as uncertainties. We obtain $D = 288 \pm 21\,\text{meV}\,\text{Å}^2$, in fair agreement with the experimental value of $D^{\text{exp}} = 325 \pm 10\,\text{meV}\,\text{Å}^2$ [85]. Other LDA calculations reported spin stiffnesses ranging from $D = 252\,\text{meV}\,\text{Å}^2$ [67] to $D = 304\,\text{meV}\,\text{Å}^2$ [81].

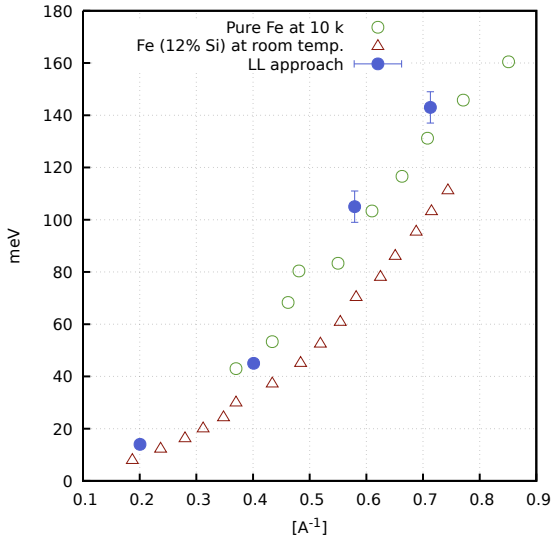

Figure 22. Spin-wave dispersion along the (100) direction obtained with the LL approach and compared with the experimental dispersion of pure Fe at 10 K [85], and Fe with a 12% of Si at room temperature [86]. All the calculations have been performed with $\varepsilon_{\text{cut}} = 90\,\text{Ry}$ and $\sigma = 0.005\,\text{Ry}$. Points with the error bar were converged with a $28 \times 28 \times 28$ Monkhorst-Pack mesh, therefore the magnitude of the oscillations for such a coarse BZ-sampling, discussed in Fig. 18 have been included to give an idea of the possible misplacement. The remaining points were converged with $36 \times 36 \times 36$ grid and the uncertainties of $\sim 1\,\text{meV}$ are not visible on this scale.

As seen in Sec. 5.3.1, already at energies of $\sim 150\,\text{meV}$ spin-waves start to feel the presence of the Stoner continuum and incur in Landau damping. Unfortunately, the high number of Lanczos iterations needed to converge the continuous portion of the spectrum forces us to use a Lorentzian broadening which does not allow to determine the linewidth of the excitations with a precision higher than 0.1 eV. In order to achive a greater accuracy, more iterations are needed with the present implementation. A more promising alternative, as discussed in the conclusions, is to use softer pseudopotentials, which would result in a faster convergence with respect to the iterations and in the subsequent more precise evaluation of the Landau damping.

CHAPTER

SIX

CONCLUSIONS AND PERSPECTIVES

A new computational approach to the study of magnetic excitations within TDDFT has been proposed, implemented in a PW-pseudopotential framework and tested on the magnon dispersion of Fe BCC. In our formulation the spin-charge susceptibility is computed as the resolvent of the Liouvillian superoperator by using Lanczos recursion, and, on contrary to the direct Dyson-equation approach, avoiding any explicit reference to the Kohn-Sham empty states. Our implementation allows to treat non-collinear magnetic structures and to account for spin-orbit effects; to the knowledge of the author, only another ab-initio code features the same possibilities at the present date [9].

The application of our method to non-collinear magnetic systems can already be carried out at the same computational effort as for BCC Iron, given that collinearity has not been assumed anywhere during the benchmarking, and layered systems with SOC can be studied with the present implementation. This represents one branch of the ongoing work. At the same time, efforts in order to improve the convergency speed have to be made, so that the high accuracy required by these systems can be reached within a lower number of iterations.

Due to the nature of the iterative solution, the computational cost of each Lanczos iteration is roughly 4–5 times the cost of one iteration in the ground-state calculation, given that $\hat{h}^{\circ}$ is applied to the batches twice per Liouvillian application. However, the number of iterations needed to reach convergency has resulted to be considerably high, if compared to similar implementations of the Lanczos algorithm for the computation of charge excitations; the reason why can be found in the very low energies at which magnetic excitations occur. The Lanczos algorithm, like many other iterative methods, is known to converge the slowlier, the higher the ratio between the highest and the lowest eigenvalue of the operator to tridiagonalize (striclty related to the so-called condition number); in our case a high cutoff forced by the NC-PP (highest eigenvalue) and a very low excitation energy (lowest eigenvalue) concur to produce a condition number of the Liouvillian from 2 to 3 order of magnitudes bigger than a typical calculation for charge excitations. The resulting slow damping of the ζ coefficients impedes the application of extrapolation techniques, which are particularly powerful in accelerating the convergence of the continuous parts of the excitation spectrum [84, 76]. This, for the time being, is the major

drawback of the Liouville-Lanczos approach to magnetic excitations, and causes an extremely slow convergence of the structures in the continuous portion of the spectrum.

For these reasons, the extension to US-PP is expected to have a big impact on the convergency speed, given that cutoffs in the order of half the NC-PP ones are typically used for transition elements in this scheme. Another direction to pursue is the implementation of symmetry in the linear-response calculation, although we expect a smaller gain with respect to US-PP, given the low number of equivalent point in BZ of the low-symmetry magnetic system we aim to study. A third option is to precondition the Lanczos algorithm by restricting the manifold in which the response orbitals are defined. This would result in a lower condition number of the Liouvillian and in a boost of Lanczos performances, as explained above. Ongoing work is pointing in this direction.

APPENDIX

A

TIME-REVERSAL SYMMETRY

In analogy with classical mechanics, the time reversal operator $\hat{\mathrm{T}}$ has the properties

$$\hat{\mathrm{T}}\,\hat{\mathbf{r}}\,\hat{\mathrm{T}}^{-1} = \hat{\mathbf{r}}\,, \qquad \hat{\mathrm{T}}\,\hat{\mathbf{p}}\,\hat{\mathrm{T}}^{-1} = -\hat{\mathbf{p}}\,. \tag{A.1}$$

The operator satisfying these properties is *anti-linear* and *anti-unitary*, i.e.

$$\hat{\mathrm{T}}\,(a_1\psi_1 + a_2\psi_2) = a_1^*\,\hat{\mathrm{T}}\psi_1 + a_2^*\,\hat{\mathrm{T}}\psi_2\,, \tag{A.2}$$

$$\langle\hat{\mathrm{T}}\psi_1, \hat{\mathrm{T}}\psi_2\rangle = \langle\psi_1, \psi_2\rangle^*\,; \tag{A.3}$$

both the properties are inherited from the complex-conjugation operator $\hat{K}$, in fact it can be shown that $\hat{\mathrm{T}} = \hat{U}\hat{K}$, where $\hat{U}$ is a unitary operator (see, e.g., Sec. 8.3 of [51]). From properties (A.1) it follows that the angular momentum changes sign as well under $\hat{\mathrm{T}}$, and in analogy also the spin-operator is assumed to have the same behaviour,

$$\hat{\mathrm{T}}\,\hat{\boldsymbol{\ell}}\,\hat{\mathrm{T}}^{-1} = -\hat{\boldsymbol{\ell}}\,, \qquad \hat{\mathrm{T}}\,\hat{\mathbf{s}}\,\hat{\mathrm{T}}^{-1} = -\hat{\mathbf{s}}\,. \tag{A.4}$$

When the Hamiltonian commutes with the time-reversal operator, degeneracies may be expected; in fact, in the case of a scalar, one-particle wave function the action of the time-reversal operator coincides with the one of the complex conjugation one:

$$\hat{\mathrm{T}}\psi = \hat{K}\psi \quad \Rightarrow \quad \hat{\mathrm{T}}\psi(\mathbf{r}) = \psi^*(\mathbf{r}) \qquad\qquad [\text{scalar}] \tag{A.5}$$

If the one-particle Hamiltonian commutes with $\hat{\mathrm{T}}$, then the eigenstates can be chosen to be real. In the case of a spin-1/2, one-particle wave function one has instead

$$\hat{\mathrm{T}}\psi(\mathbf{r}) = (i\sigma^y)\hat{K}\psi(\mathbf{r})\,, \qquad\qquad [\text{spin-1/2}] \tag{A.6}$$

where the 'i'-phase in front of the Pauli matrix is customary. The major difference between the two cases is that $\hat{\mathrm{T}}^2 = -\mathbb{1}$ in the spin-1/2 case, whereas $\hat{\mathrm{T}}^2 = \mathbb{1}$ in the scalar one. The former scenario always ensures ψ and $\hat{\mathrm{T}}\psi$ to be linearly independent, so that when $\left[\hat{h}, \hat{\mathrm{T}}\right] = 0$ all the states will be at least two-fold degenerate (Kramer's degeneracy), the same cannot be told in the latter case.[1]

[1] We remark that, for the spin-1/2 case, $\hat{\mathrm{T}}^2 = -\mathbb{1}$ holds only for states with an odd-number of particles, whereas with an even number of articles $\hat{\mathrm{T}} = \mathbb{1}$ also in the spin-1/2 case [51].

Bloch States and TRS

The action of $\hat{\mathrm{T}}$ on the Bloch state $\psi_{n\mathbf{k}}$ produces another Bloch state of wave vector $-\mathbf{k}$, due to the complex-conjugation operation. Hence, when TRS holds, $\varepsilon_{n\mathbf{k}} = \varepsilon_{n-\mathbf{k}}$, and the wave functions $\psi_{n\mathbf{k}}$ and $\hat{\mathrm{T}}\psi_{n-\mathbf{k}}$ are related by a unitary transformation acting inside the degenerate subspace.

Spin-Orbit and TRS

Due to the properties (A.1) and (A.4), the spin-orbit term commutes with the time-reversal operator. In particular, the whole pseudopotential term

$$v_{\mathrm{PP}}(r,\theta,\phi,\theta'\phi') = \sum_{lm} \mathrm{Y}_{lm}(\theta,\phi)\left[v_l^{\mathrm{ion}}(r)\sigma^{\circ} + v_l^{\mathrm{SO}}(r)\,\hat{\mathbf{s}}\cdot\hat{\boldsymbol{\ell}}\right]\mathrm{Y}^{*}_{lm}(\theta',\phi')\,, \tag{A.7}$$

satisfies

$$\hat{\mathrm{T}}\,\hat{v}_{\mathrm{PP}}\,\hat{\mathrm{T}}^{-1} = \hat{v}_{\mathrm{PP}}\,. \tag{A.8}$$

APPENDIX

B

THE MAGNETIC LIOUVILLIAN

In Sec. 4.3 the linearized time-dependent Kohn-Sham equations have been written in terms of Bloch functions such as $\Psi^\circ_{\mathbf{k}}(\mathbf{r})$, $\Psi'_{\mathbf{k+q}}(\mathbf{r},\omega)$, $\bar{v}'_{\mathbf{q}}(\mathbf{r},\omega)$, $\bar{\rho}'_{\mathbf{q}}(\mathbf{r},\omega)$, etc. Here we report the same equations in terms of the periodic parts of these functions. The two formulations are equivalent, however in a PW code only the latter is preferred, since the periodic parts are expanded in the reciprocal-lattice $\mathbf{G}$-vectors. We define the periodic parts via

$$\Psi^\circ_{n\mathbf{k}}(\mathbf{r}) = e^{i\mathbf{k}\cdot\mathbf{r}}\, u^\circ_{n\mathbf{k}}(\mathbf{r}) \tag{B.1}$$

$$\tilde{\Psi}'_{n\mathbf{k+q}}(\mathbf{r},\omega) = e^{i(\mathbf{k}+\mathbf{q})\cdot\mathbf{r}}\, \tilde{u}'_{n\mathbf{k+q}}(\mathbf{r},\omega) \tag{B.2}$$

$$\bar{v}'_{\mathbf{q}}(\mathbf{r},\omega) = e^{i\mathbf{q}\cdot\mathbf{r}}\, \tilde{v}'_{\mathbf{q}}(\mathbf{r},\omega) \tag{B.3}$$

$$\bar{\rho}'_{\mathbf{q}}(\mathbf{r},\omega) = e^{i\mathbf{q}\cdot\mathbf{r}}\, \tilde{\rho}'_{\mathbf{q}}(\mathbf{r},\omega)\,, \tag{B.4}$$

where $u^\circ_{n\mathbf{k}}(\mathbf{r}+\mathbf{R}) = u^\circ_{n\mathbf{k}}(\mathbf{r})$ and so on. The definition of $\tilde{n}'_{\mathbf{q}}(\mathbf{r},\omega)$ and $\tilde{\mathbf{m}}'_{\mathbf{q}}(\mathbf{r},\omega)$ follows from the one of $\tilde{\rho}'_{\mathbf{q}}(\mathbf{r},\omega)$.

The Linearized Response Equations

The linearized Kohn-Sham equations in the terms of (B.1)–(B.4) read

$$\begin{aligned}&\left[\hat{h}^\circ_{\mathbf{k+q}} - \varepsilon_{n\mathbf{k}} - (\hbar\omega + i\eta)\right] \tilde{x}_{n\mathbf{k+q}}(\omega) \\ &\qquad + \hat{P}^{\mathbf{k+q}}_{\mathcal{C}(n\mathbf{k})}\, \hat{\tilde{v}}'_{\mathrm{eff},\mathbf{q}}[\tilde{X},\tilde{Y}](\omega)\, u^\circ_{n\mathbf{k}} = -\hat{P}^{\mathbf{k+q}}_{\mathcal{C}(n\mathbf{k})}\, \hat{\tilde{v}}_{\mathrm{ext},\mathbf{q}}(\omega)\, u^\circ_{n\mathbf{k}}\end{aligned} \tag{B.5}$$

$$\begin{aligned}&\left[\hat{h}^{\circ[-\mathbf{b}]}_{\mathbf{k+q}} - \varepsilon_{n-\mathbf{k}} + (\hbar\omega + i\eta)\right] \tilde{y}_{n\mathbf{k+q}}(\omega) \\ &\qquad + \hat{\Pi}^{\mathbf{k+q}}_{\mathcal{C}(n-\mathbf{k})}\, \hat{\tilde{v}}'^{[-\mathbf{b}]}_{\mathrm{eff},\mathbf{q}}[\tilde{X},\tilde{Y}](\omega)\, \hat{\mathrm{T}} u^\circ_{n-\mathbf{k}} = -\hat{\Pi}^{\mathbf{k+q}}_{\mathcal{C}(n-\mathbf{k})}\, \hat{\tilde{v}}^{[-\mathbf{b}]}_{\mathrm{ext},\mathbf{q}}(\omega)\, \hat{\mathrm{T}} u^\circ_{n-\mathbf{k}}\,.\end{aligned} \tag{B.6}$$

where $\hat{h}^\circ_{\mathbf{k+q}}$ is the Hamiltonian defined in (2.73) and the operators $\hat{P}^{\mathbf{k+q}}_{\mathcal{C}(n\mathbf{k})}$, $\hat{\Pi}^{\mathbf{k+q}}_{\mathcal{C}(n-\mathbf{k})}$ have been defined in Eqs. (5.5) and (5.7). The variables $\tilde{x}_{n\mathbf{k+q}}(\omega)$ and $\tilde{y}_{n\mathbf{k+q}}(\omega)$ are

the periodic parts of (4.107) and read

$$\begin{aligned}\tilde{x}_{n\mathbf{k}+\mathbf{q}}(\omega) &\equiv \hat{P}^{\mathbf{k}+\mathbf{q}}_{\mathcal{C}(n\mathbf{k})}\,\tilde{u}'_{n\mathbf{k}+\mathbf{q}}(\omega)\\ \tilde{y}_{n\mathbf{k}+\mathbf{q}}(\omega) &\equiv \hat{\mathrm{T}}\hat{P}^{-\mathbf{k}-\mathbf{q}}_{\mathcal{C}(n-\mathbf{k})}\,\tilde{u}'_{n-\mathbf{k}-\mathbf{q}}(-\omega)\,.\end{aligned} \tag{B.7}$$

The Compact Form

Eqs. (B.6) can be written in the matrix form

$$\begin{aligned}&\left[\begin{pmatrix}\mathcal{D}^X_{\mathbf{q}}+\mathcal{P}^X_{\mathbf{q}}\,\mathcal{K}^{XX}_{\mathbf{q}} & \mathcal{P}^X_{\mathbf{q}}\,\mathcal{K}^{XY}_{\mathbf{q}}\\ -\mathcal{P}^Y_{\mathbf{q}}\,\mathcal{K}^{YX}_{\mathbf{q}} & -\left(\mathcal{D}^Y_{\mathbf{q}}+\mathcal{P}^Y_{\mathbf{q}}\,\mathcal{K}^{YY}_{\mathbf{q}}\right)\end{pmatrix}-(\hbar\omega+i\eta)\right]\begin{pmatrix}\tilde{X}_{\mathbf{q}}\\ \tilde{Y}_{\mathbf{q}}\end{pmatrix}\\ &\qquad=\begin{pmatrix}\left\{-\hat{P}^{\mathbf{k}+\mathbf{q}}_{\mathcal{C}(n\mathbf{k})}\,\hat{\tilde{v}}_{\mathrm{ext},\mathbf{q}}(\omega)\,u^{\circ}_{n\mathbf{k}}\right\}\\ \left\{\hat{\Pi}^{\mathbf{k}+\mathbf{q}}_{\mathcal{C}(n-\mathbf{k})}\,\hat{\tilde{v}}^{[-\mathbf{b}]}_{\mathrm{ext},\mathbf{q}}(\omega)\,\hat{\mathrm{T}}u^{\circ}_{n-\mathbf{k}}\right\}\end{pmatrix},\end{aligned} \tag{B.8}$$

in terms of the batches of the orbitals (B.7). The action of the superoperators is given by

$$\mathcal{D}^X_{\mathbf{q}}\tilde{X}_{\mathbf{q}} \equiv \left\{\left[\hat{h}^{\circ}_{\mathbf{k}+\mathbf{q}}-\varepsilon_{n\mathbf{k}}\right]\tilde{x}_{n\mathbf{k}+\mathbf{q}}\right\} \tag{B.9}$$

$$\mathcal{D}^Y_{\mathbf{q}}\tilde{Y}_{\mathbf{q}} \equiv \left\{\left[\hat{h}^{\circ[-\mathbf{b}]}_{\mathbf{k}+\mathbf{q}}-\varepsilon_{n-\mathbf{k}}\right]\tilde{y}_{n\mathbf{k}+\mathbf{q}}\right\} \tag{B.10}$$

$$\mathcal{K}^{XX}_{\mathbf{q}}\tilde{X}_{\mathbf{q}}+\mathcal{K}^{XY}_{\mathbf{q}}\tilde{Y}_{\mathbf{q}} \equiv \left\{\hat{\tilde{v}}'_{\mathrm{eff},\mathbf{q}}[\tilde{X},\tilde{Y}](\omega)\,u^{\circ}_{n\mathbf{k}}\right\} \tag{B.11}$$

$$\mathcal{K}^{YX}_{\mathbf{q}}\tilde{X}_{\mathbf{q}}+\mathcal{K}^{YY}_{\mathbf{q}}\tilde{Y}_{\mathbf{q}} \equiv \left\{\hat{\tilde{v}}'^{[-\mathbf{b}]}_{\mathrm{eff},\mathbf{q}}[\tilde{X},\tilde{Y}](\omega)\,\hat{\mathrm{T}}u^{\circ}_{n-\mathbf{k}}\right\} \tag{B.12}$$

$$\mathcal{P}^X_{\mathbf{q}}\tilde{X}_{\mathbf{q}} \equiv \left\{\hat{P}^{\mathbf{k}+\mathbf{q}}_{\mathcal{C}(n\mathbf{k})}\,\tilde{x}_{n\mathbf{k}+\mathbf{q}}\right\} \tag{B.13}$$

$$\mathcal{P}^Y_{\mathbf{q}}\tilde{Y}_{\mathbf{q}} \equiv \left\{\hat{\Pi}^{\mathbf{k}+\mathbf{q}}_{\mathcal{C}(n-\mathbf{k})}\,\tilde{y}_{n\mathbf{k}+\mathbf{q}}\right\}\,. \tag{B.14}$$

The Response Potentials

The periodic parts of the response potentials read

$$\begin{aligned}\tilde{v}'_{\mathrm{eff},\mathbf{q}}(\mathbf{r},\omega)=&\sigma^{\circ}\left(\int_{\Omega_0}\mathrm{d}^3r'\,K_{\mathrm{Hxc},\mathbf{q}}(\mathbf{r},\mathbf{r}')\,\tilde{n}'_{\mathbf{q}}(\mathbf{r}',\omega)+\sum_{\alpha}\int_{\Omega_0}\mathrm{d}^3r'\,J^{\alpha}_{\mathrm{xc},\mathbf{q}}(\mathbf{r},\mathbf{r}')\,\tilde{m}'^{\alpha}_{\mathbf{q}}(\mathbf{r}',\omega)\right)\\ &+\sum_{\alpha}\sigma^{\alpha}\left(\int_{\Omega_0}\mathrm{d}^3r'\,J^{\alpha}_{\mathrm{xc},\mathbf{q}}(\mathbf{r},\mathbf{r}')\,\tilde{n}'_{\mathbf{q}}(\mathbf{r}',\omega)+\sum_{\beta}\int_{\Omega_0}\mathrm{d}^3r'\,I^{\alpha\beta}_{\mathrm{xc},\mathbf{q}}(\mathbf{r},\mathbf{r}')\,\tilde{m}'^{\beta}_{\mathbf{q}}(\mathbf{r}',\omega)\right),\\ \tilde{v}'^{[-\mathbf{b}]}_{\mathrm{eff},\mathbf{q}}(\mathbf{r},\omega)=&\sigma^{\circ}\left(\int_{\Omega_0}\mathrm{d}^3r'\,K_{\mathrm{Hxc},\mathbf{q}}(\mathbf{r},\mathbf{r}')\,\tilde{n}'_{\mathbf{q}}(\mathbf{r}',\omega)+\sum_{\alpha}\int_{\Omega_0}\mathrm{d}^3r'\,J^{\alpha}_{\mathrm{xc},\mathbf{q}}(\mathbf{r},\mathbf{r}')\,\tilde{m}'^{\alpha}_{\mathbf{q}}(\mathbf{r}',\omega)\right)\\ &-\sum_{\alpha}\sigma^{\alpha}\left(\int_{\Omega_0}\mathrm{d}^3r'\,J^{\alpha}_{\mathrm{xc},\mathbf{q}}(\mathbf{r},\mathbf{r}')\,\tilde{n}'_{\mathbf{q}}(\mathbf{r}',\omega)+\sum_{\beta}\int_{\Omega_0}\mathrm{d}^3r'\,I^{\alpha\beta}_{\mathrm{xc},\mathbf{q}}(\mathbf{r},\mathbf{r}')\,\tilde{m}'^{\beta}_{\mathbf{q}}(\mathbf{r}',\omega)\right).\end{aligned} \tag{B.15}$$

where

$$K_{\mathrm{Hxc},\mathbf{q}}(\mathbf{r},\mathbf{r}')=e^{i\mathbf{q}\cdot(\mathbf{r}'-\mathbf{r})}K_{\mathrm{Hxc}}(\mathbf{r},\mathbf{r}')=e^{i\mathbf{q}\cdot(\mathbf{r}'-\mathbf{r})}\frac{\delta E_{\mathrm{Hxc}}}{n(\mathbf{r}')n(\mathbf{r})}\,, \tag{B.16}$$

and similarly for $J^{\alpha}_{\mathrm{Hxc},\mathbf{q}}(\mathbf{r},\mathbf{r}')$ and $I^{\alpha\beta}_{\mathrm{Hxc},\mathbf{q}}(\mathbf{r},\mathbf{r}')$. The periodic parts of the density- and magnetization-response are instead given by

$$\tilde{n}'_{\mathbf{q}}(\mathbf{r},\omega) = \sum_{n\mathbf{k}}^{\mathrm{BZ}} \left[u^{\circ\dagger}_{n\mathbf{k}}(\mathbf{r}) \tilde{x}_{n\mathbf{k}+\mathbf{q}}(\mathbf{r},\omega) + \left(\hat{\mathrm{T}} u^{\circ}_{n-\mathbf{k}}(\mathbf{r})\right)^{\dagger} \tilde{y}_{n\mathbf{k}+\mathbf{q}}(\mathbf{r},\omega) \right] \tag{B.17}$$

$$\tilde{m}'^{\alpha}_{\mathbf{q}}(\mathbf{r},\omega) = \mu_B \sum_{n\mathbf{k}}^{\mathrm{BZ}} \left[u^{\circ\dagger}_{n\mathbf{k}}(\mathbf{r}) \sigma^{\alpha}\, \tilde{x}_{n\mathbf{k}+\mathbf{q}}(\mathbf{r},\omega) - \left(\hat{\mathrm{T}} u^{\circ}_{n-\mathbf{k}}(\mathbf{r})\right)^{\dagger} \sigma^{\alpha}\, \tilde{y}_{n\mathbf{k}+\mathbf{q}}(\mathbf{r},\omega) \right] . \tag{B.18}$$

Hermitian Conjugate of the Liouvillian

In order to compute the complex conjugate of the Liouvillian, necessary in Algorithm 1, we first rewrite the self-consistent terms as

$$\begin{aligned} \hat{P}^{\mathbf{k}+\mathbf{q}}_{\mathcal{C}(n\mathbf{k})}\, \hat{\tilde{v}}'_{\mathrm{eff},\mathbf{q}}(\omega) u^{\circ}_{n\mathbf{k}}(\mathbf{r}) = {} & \hat{P}^{\mathbf{k}+\mathbf{q}}_{\mathcal{C}(n\mathbf{k})} \sum_{n'\mathbf{k}'} \hat{K}^{XX}_{n\mathbf{k},n'\mathbf{k}'}\, \tilde{x}_{n'\mathbf{k}'+\mathbf{q}}(\mathbf{r}) \\ & + \hat{P}^{\mathbf{k}+\mathbf{q}}_{\mathcal{C}(\mathbf{nk})} \sum_{n'\mathbf{k}'} \hat{K}^{XY}_{n\mathbf{k},n'\mathbf{k}'}\, \tilde{y}_{n'\mathbf{k}'+\mathbf{q}}(\mathbf{r}) , \end{aligned} \tag{B.19}$$

$$\begin{aligned} \hat{\Pi}^{\mathbf{k}+\mathbf{q}}_{\mathcal{C}(n\mathbf{k})}\, \hat{\tilde{v}}'^{[-\mathbf{b}]}_{\mathrm{eff},\mathbf{q}}(\omega) \hat{\mathrm{T}} u^{\circ}_{n-\mathbf{k}}(\mathbf{r}) = {} & \hat{\Pi}^{\mathbf{k}+\mathbf{q}}_{\mathcal{C}(n\mathbf{k})} \sum_{n'\mathbf{k}'} \hat{K}^{YX}_{n\mathbf{k},n'\mathbf{k}'}\, \tilde{x}_{n'\mathbf{k}'+\mathbf{q}}(\mathbf{r}) \\ & + \hat{P}^{\mathbf{k}+\mathbf{q}}_{\mathcal{C}(\mathbf{nk})} \sum_{n'\mathbf{k}'} \hat{K}^{YY}_{n\mathbf{k},n'\mathbf{k}'}\, \tilde{y}_{n'\mathbf{k}'+\mathbf{q}}(\mathbf{r}) , \end{aligned} \tag{B.20}$$

where $\hat{K}^{XX}_{n\mathbf{k},n'\mathbf{k}'}$, $\hat{K}^{XY}_{n\mathbf{k},n'\mathbf{k}'}$, $\hat{K}^{YX}_{n\mathbf{k},n'\mathbf{k}'}$ and $\hat{K}^{YY}_{n\mathbf{k},n'\mathbf{k}'}$ are operators whose action is given by

$$\begin{aligned} \hat{K}^{XX}_{n\mathbf{k},n'\mathbf{k}'}\, \tilde{x}_{n'\mathbf{k}'+\mathbf{q}}(\mathbf{r}) = \int_{\Omega_0} \mathrm{d}^3 r' \Big[& u_{n\mathbf{k}}(\mathbf{r}) K_{\mathbf{q}}(\mathbf{r},\mathbf{r}') u^{\dagger}_{n'\mathbf{k}'}(\mathbf{r}') + u_{n\mathbf{k}}(\mathbf{r}) J^{\alpha}_{\mathbf{q}}(\mathbf{r},\mathbf{r}') u^{\alpha\dagger}_{n'\mathbf{k}'}(\mathbf{r}') \\ & + u^{\alpha}_{n\mathbf{k}}(\mathbf{r}) J^{\alpha}_{\mathbf{q}}(\mathbf{r},\mathbf{r}') u^{\dagger}_{n'\mathbf{k}'}(\mathbf{r}') + u^{\alpha}_{n\mathbf{k}}(\mathbf{r}) I^{\alpha\beta}_{\mathbf{q}}(\mathbf{r},\mathbf{r}') u^{\beta\dagger}_{n'\mathbf{k}'}(\mathbf{r}') \Big] \tilde{x}_{n'\mathbf{k}'+\mathbf{q}}(\mathbf{r}') \end{aligned} \tag{B.21}$$

$$\begin{aligned} \hat{K}^{XY}_{n\mathbf{k},n'\mathbf{k}'}\, \tilde{y}_{n'\mathbf{k}'+\mathbf{q}}(\mathbf{r}) = \int_{\Omega_0} \mathrm{d}^3 r' \Big[& u_{n\mathbf{k}}(\mathbf{r}) K_{\mathbf{q}}(\mathbf{r},\mathbf{r}') \bar{u}^{\dagger}_{n'\mathbf{k}'}(\mathbf{r}') - u_{n\mathbf{k}}(\mathbf{r}) J^{\alpha}_{\mathbf{q}}(\mathbf{r},\mathbf{r}') \bar{u}^{\alpha\dagger}_{n'\mathbf{k}'}(\mathbf{r}') \\ & + u^{\alpha}_{n\mathbf{k}}(\mathbf{r}) J^{\alpha}_{\mathbf{q}}(\mathbf{r},\mathbf{r}') \bar{u}^{\dagger}_{n'\mathbf{k}'}(\mathbf{r}') - u^{\alpha}_{n\mathbf{k}}(\mathbf{r}) I^{\alpha\beta}_{\mathbf{q}}(\mathbf{r},\mathbf{r}') \bar{u}^{\beta\dagger}_{n'\mathbf{k}'}(\mathbf{r}') \Big] \tilde{y}_{n'\mathbf{k}'+\mathbf{q}}(\mathbf{r}') , \end{aligned} \tag{B.22}$$

$$\begin{aligned} \hat{K}^{YX}_{n\mathbf{k},n'\mathbf{k}'}\, \tilde{x}_{n'\mathbf{k}'+\mathbf{q}}(\mathbf{r}) = \int_{\Omega_0} \mathrm{d}^3 r' \Big[& \bar{u}_{n\mathbf{k}}(\mathbf{r}) K_{\mathbf{q}}(\mathbf{r},\mathbf{r}') u^{\dagger}_{n'\mathbf{k}'}(\mathbf{r}') + \bar{u}_{n\mathbf{k}}(\mathbf{r}) J^{\alpha}_{\mathbf{q}}(\mathbf{r},\mathbf{r}') u^{\alpha\dagger}_{n'\mathbf{k}'}(\mathbf{r}') \\ & - \bar{u}^{\alpha}_{n\mathbf{k}}(\mathbf{r}) J^{\alpha}_{\mathbf{q}}(\mathbf{r},\mathbf{r}') u^{\dagger}_{n'\mathbf{k}'}(\mathbf{r}') - \bar{u}^{\alpha}_{n\mathbf{k}}(\mathbf{r}) I^{\alpha\beta}_{\mathbf{q}}(\mathbf{r},\mathbf{r}') u^{\beta\dagger}_{n'\mathbf{k}'}(\mathbf{r}') \Big] \tilde{x}_{n'\mathbf{k}'+\mathbf{q}}(\mathbf{r}') \end{aligned} \tag{B.23}$$

$$\begin{aligned} \hat{K}^{YY}_{n\mathbf{k},n'\mathbf{k}'}\, \tilde{y}_{n'\mathbf{k}'+\mathbf{q}}(\mathbf{r}) = \int_{\Omega_0} \mathrm{d}^3 r' \Big[& \bar{u}_{n\mathbf{k}}(\mathbf{r}) K_{\mathbf{q}}(\mathbf{r},\mathbf{r}') \bar{u}^{\dagger}_{n'\mathbf{k}'}(\mathbf{r}') - \bar{u}_{n\mathbf{k}}(\mathbf{r}) J^{\alpha}_{\mathbf{q}}(\mathbf{r},\mathbf{r}') \bar{u}^{\alpha\dagger}_{n'\mathbf{k}'}(\mathbf{r}') \\ & - \bar{u}^{\alpha}_{n\mathbf{k}}(\mathbf{r}) J^{\alpha}_{\mathbf{q}}(\mathbf{r},\mathbf{r}') \bar{u}^{\dagger}_{n'\mathbf{k}'}(\mathbf{r}') + \bar{u}^{\alpha}_{n\mathbf{k}}(\mathbf{r}) I^{\alpha\beta}_{\mathbf{q}}(\mathbf{r},\mathbf{r}') \bar{u}^{\beta\dagger}_{n'\mathbf{k}'}(\mathbf{r}') \Big] \tilde{y}_{n'\mathbf{k}'+\mathbf{q}}(\mathbf{r}'). \end{aligned} \tag{B.24}$$

In the last equations, all the $^\circ$ and "xc" have been dropped in order to lighten the notation. Furthermore, summation over the α and β repeated indexes is indended, and we ade use of the shorthands

$$u^{\alpha}_{n\mathbf{k}}(\mathbf{r}) \equiv \sigma^{\alpha} u_{n\mathbf{k}}(\mathbf{r}) \qquad \bar{u}^{\alpha}_{n\mathbf{k}}(\mathbf{r}) \equiv \sigma^{\alpha} \hat{T} u_{n-\mathbf{k}}(\mathbf{r}) \; . \tag{B.25}$$

From Eqs. (B.21)–(B.24) it can be seen that

$$\mathcal{K}^{XX\dagger}_{\mathbf{q}} = \mathcal{K}^{XX\dagger}_{\mathbf{q}} \, , \qquad \mathcal{K}^{YY\dagger}_{\mathbf{q}} = \mathcal{K}^{YY\dagger}_{\mathbf{q}} \, , \qquad \mathcal{K}^{XY\dagger}_{\mathbf{q}} = \mathcal{K}^{YX\dagger}_{\mathbf{q}} \, ; \tag{B.26}$$

moreover, the $\mathcal{D}$- and $\mathcal{P}$-blocks result Hermitian from their definitions, and we can conclude that

$$\begin{aligned} \mathcal{L}_{\mathbf{q}} &\equiv \begin{pmatrix} \mathcal{D}^{XX}_{\mathbf{q}} + \mathcal{P}^{X}_{\mathbf{q}} \, \mathcal{K}^{XX}_{\mathbf{q}} & \mathcal{P}^{X}_{\mathbf{q}} \, \mathcal{K}^{XY}_{\mathbf{q}} \\ -\mathcal{P}^{Y}_{\mathbf{q}} \, \mathcal{K}^{YX}_{\mathbf{q}} & -\mathcal{D}^{Y}_{\mathbf{q}} - \mathcal{P}^{Y}_{\mathbf{q}} \, \mathcal{K}^{YY}_{\mathbf{q}} \end{pmatrix} \\ \mathcal{L}^{\dagger}_{\mathbf{q}} &\equiv \begin{pmatrix} \mathcal{D}^{XX}_{\mathbf{q}} + \mathcal{K}^{XX}_{\mathbf{q}} \, \mathcal{P}^{X}_{\mathbf{q}} & -\mathcal{K}^{XY}_{\mathbf{q}} \, \mathcal{P}^{Y}_{\mathbf{q}} \\ \mathcal{K}^{YX}_{\mathbf{q}} \, \mathcal{P}^{X}_{\mathbf{q}} & -\mathcal{D}^{Y}_{\mathbf{q}} - \mathcal{K}^{YY}_{\mathbf{q}} \, \mathcal{P}^{Y}_{\mathbf{q}} \end{pmatrix} \; . \end{aligned} \tag{B.27}$$

The action of the self-consistent part over a batch can be computed as

$$\mathcal{K}^{XX}_{\mathbf{q}} \mathcal{P}^{X}_{\mathbf{q}} \tilde{X}_{\mathbf{q}} - \mathcal{K}^{XY}_{\mathbf{q}} \, \mathcal{P}^{Y}_{\mathbf{q}} \tilde{Y}_{\mathbf{q}} \equiv \left\{ \hat{\tilde{v}}'_{\mathrm{eff},\mathbf{q}} \Big[\mathcal{P}^{X}_{\mathbf{q}} \tilde{X}, -\mathcal{P}^{Y}_{\mathbf{q}} \tilde{Y} \Big] (\omega) \, u^{\circ}_{n\mathbf{k}} \right\} \tag{B.28}$$

$$\mathcal{K}^{YX}_{\mathbf{q}} \mathcal{P}^{X}_{\mathbf{q}} \tilde{X}_{\mathbf{q}} - \mathcal{K}^{YY}_{\mathbf{q}} \, \mathcal{P}^{Y}_{\mathbf{q}} \tilde{Y}_{\mathbf{q}} \equiv \left\{ \hat{\tilde{v}}'^{[-\mathbf{b}]}_{\mathrm{eff},\mathbf{q}} \Big[\mathcal{P}^{X}_{\mathbf{q}} \tilde{X}, -\mathcal{P}^{Y}_{\mathbf{q}} \tilde{Y} \Big] (\omega) \, \hat{\mathrm{T}} u^{\circ}_{n-\mathbf{k}} \right\} \; , \tag{B.29}$$

due to linearity.

BIBLIOGRAPHY

[1] B. Lenk, H. Ulrichs, F. Garbs, and M. Münzenberg. The building blocks of magnonics. *Phys. Rept.*, 507:107–136, 2011.

[2] A.A. Serga, A.V. Chumak, and B. Hillebrands. Yig magnonics. *J. Phys. D*, 43:264002, 2010.

[3] H.J. Qin, Kh. Zakeri, A. Ernst, L.M. Sandratskii, P. Buczek, A. Marmodoro, T.-H. Chuang, Y. Zhang, and J. Kirschner. Long-living terahertz magnons in ultrathin metallic ferromagnets. *Nat. Commun.*, 27(6):6126, 2015.

[4] Kh. Zakeri, Y. Zhang, J. Prokop, T.-H. Chuang, N. Sakr, W.X. Tang, and J. Kirschner. Asymmetric spin-wave dispersion on fe(110): Direct evidence of the dzyaloshinskii-moriya interaction. *Phys. Rev. Lett.*, 104:137203, 2010.

[5] Kh. Zakeri, Y. Zhang, T.-H. Chuang, and J. Kirschner. Magnon lifetimes on the fe(110) surface: The role of spin-orbit coupling. *Phys. Rev. Lett.*, 108:197205, 2012.

[6] A.T. Costa, R.B. Muniz, T. Lounis, A.B. Klautau, and D.L. Mills. Spin-orbit coupling and spin waves in ultrathin ferromagnets: The spin-wave rashba effect. *Phys. Rev. B*, 82:014428, 2010.

[7] V. Kamberský. Spin-orbital gilbert damping in common magnetic metals. *Phys. Rev. B*, 76:134416, 2007.

[8] T.L. Gilbert. A phenomenological theory of damping in ferromagnetic materials. *IEEE Trans. Magn.*, 40:3443, 2004.

[9] M. dos Santos Dias, B. Schweflinghaus, S. Blügel, and T. Lounis. Relativistic dynamical spin excitations of magnetic adatoms. *Phys. Rev. B*, 91:075405, 2015.

[10] T. Lounis, M. dos Santos Dias, and B. Schweflinghaus. Transverse dynamical magnetic susceptibilities from regular static density functional theory: Evaluation of damping and g shifts of spin excitations. *Phys. Rev. B*, 91:104420, 2015.

[11] N. Nagaosa and Y. Tokura. Topological properties and dynamics of magnetic skyrmions. *Nat. Nanotechnol.*, 8:899, 2013.

[12] C. Pappas, E. Lelièvre-Berna, P. Falus, P.M. Bentley, E. Moskovin, S. Grigoriev, P. Fouquet, and B. Farago. Chiral paramagnetic skyrmion-like phase in mnsi. *Phys. Rev. Lett.*, 102:197202, 2009.

[13] S. Heinze, K. von Bergmann, M. Menzel, J. Brede, A. Kubetzka, R. Wiesendanger, G. Bihlmayer, and S. Blügel. Spontaneous atomic-scale magnetic skyrmion lattice in two dimensions. *Nat. Phys.*, 7:713, 2011.

[14] X.Z. Yu, Y. Onose, N. Kanazawa, J.H. Park, Y. Matsui, N. Nagaosa, and Y. Tokura. Real-space observation of a two-dimensional skyrmion crystal. *Nature*, 465:901, 2010.

[15] D. McKenzie Paul, P.W. Mitchell, H.A. Mook, and U. Steigenberger. Observation of itinerant-electron effects on the magnetic excitations of iron. *Phys. Rev. B*, 38(1):580, 1988.

[16] T.G. Perring, A.T. Boothroyd, D. McK Paul, A.D. Taylor, R. Osborn, R.J. Newport, J.A. Blackman, and H.A. Mook. High-energy spin waves in bcc iron. *J. Appl. Phys.*, 69:6219–6221, 1991.

[17] D. ter Haar. Theory and applications of the density-matrix. *Rep. Prog. Phys.*, 24:304, 1961.

[18] L. Van Hove. Correlations in space and time and born approximation scattering in systems of interacting particles. *Phys. Rev.*, 95(1):249–262, 1954.

[19] M.P Gokhale, A. Ormeci, and D.L. Mills. Inelastic scattering of low-energy electrons by spin excitations on ferromagnets. *Phys. Rev. B*, 46(14):8978–8993, 1992.

[20] D. Venus and J. Kirschner. Momentum dependence of the stoner excitation spectrum of iron using spin-polarized electron-energy-loss spectroscopy. *Phys. Rev. B*, 37(4):2199–2211, 1988.

[21] M. Blume. Polarization effects in the magnetic elastic scattering of slow neutrons*. *Phys. Rev.*, 130:1670, 1963.

[22] R.J. Wojciechowski. Migdal's theorem in heavy fermion systems. *Physica B*, 259:498, 1999.

[23] P. Hohenberg and W. Kohn. Inhomogeneous electron gas. *Phys. Rev.*, 136(3B):B864–B871, 1964.

[24] W. Kohn and J. Sham. Self-consistent equations including exchange and correlation effects. *Phys. Rev.*, 140(4A):A1133–A1138, 1965.

[25] U. von Barth and L. Hedin. A local exchange-correlation potential for the spin polarized case: I. *J. Phys. C*, 5:1629–1642, 1972.

[26] R.M. Martin. *Electronic Structure*. Cambridge University Press, 2004.

[27] J.P. Perdew and Y. Wang. Accurate and simple analytic representation of the electron-gas correlation energy. *Phys. Rev. B*, 45(23):13244–13249, 1992.

[28] G.F. Giuliani and G. Vignale. *Quantum Theory of the Electron Liquid*. Cambridge University Press, 2005.

[29] P. Giannozzi. Metodi numerici in struttura elettronica.

[30] F.G. Eich, S. Pittalis, and G. Vignale. Transverse and longitudinal gradients of the spin magnetization in spin-density-functional theory. *Phys. Rev. B*, 88:245102, 2013.

[31] F.G. Eich and E.K.U. Gross. Transverse spin-gradient functional for noncollinear spin-density-functional theory. *Phys. Rev. Lett.*, 111:156401, 2013.

[32] S. Sharma, J.K. Dewhurst, C. Ambrosch-Draxl, S. Kurth, N. Helbig, S. Pittalis, S. Shallcross, L. Nordström, and E.K.U. Gross. First-principles approach to noncollinear magnetism: Towards spin dynamics. *Phys. Rev. Lett.*, 98:196405, 2007.

[33] J. Kübler, K.-H. Höck, J. Sticht, and A.R. Williams. Density functional theory of non-collinear magnetism. *J. Phys. F*, 18:469–483, 1988.

[34] E. Runge and E.K.U. Gross. Density-functional theory for time-dependent systems. *Phys. Rev. Lett.*, 52:997, 1984.

[35] van Leeuwen. Mapping from densities to potentials in time-dependent density-functional theory. *Phys. Rev. Lett.*, 82:3863, 1999.

[36] D. Rocca, R. Gebauer, Y. Saad, and S. Baroni. Turbo charging time-dependent density-functional theory with lanczos chains. *J. Chem. Phys.*, 128:154105, 2008.

[37] I. Timrov, N. Vast, R. Gebauer, and S. Baroni. Electron energy loss and inelastic x-ray scattering cross sections from time-dependent density-functional perturbation theory. *Phys. Rev. B*, 88:064301, 2013.

[38] S.Y. Savrasov. Linear response calculations of spin fluctuations. *Phys. Rev. Lett.*, 81(12):2570–2573, 1998.

[39] K.L. Liu and S.H. Vosko. A time-dependent spin density functional theory for the dynamical spin susceptibility. *Can. J. Phys.*, 67:1015, 1989.

[40] L. Kleinman. Relativistic norm-conserving pseudopotential. *Phys. Rev. B*, 21(6):2630–2631, 1979.

[41] A. Dal Corso and A. Mosca Conte. Spin-orbit coupling with ultrasoft pseudopotentials: Application to au and pt. *Phys. Rev. B*, 71:115106, 2005.

[42] A. Dal Corso. Projector augmented-wave method: Application to relativistic spin-density functional theory. *Phys. Rev. B*, 82:075116, 2010.

[43] G. Theurich and N.A. Hill. Self-consistent treatment of spin-orbit coupling in solids using relativistic fully separable ab initio pseudopotentials. *Phys. Rev. B*, 64:073106, 2001.

[44] U. von Barth and C.D. Gelatt. Validity of the frozen-core approximation and pseudopotential theory for cohesive energy calculations. *Phys. Rev. B*, 21(6):2222–2227, 1979.

[45] D.R. Hamann, M. Schlüter, and C. Chiang. Norm-conserving pseudopotentials. *Phys. Rev. Lett.*, 43:1494–1497, 1979.

[46] L. Kleinman and D.M. Bylander. Efficacious form for model pseudopotentials. *Phys. Rev. Lett.*, 48(20):1425–1428, 1982.

[47] G.P. Kerker. Non-singular atomic pseudopotentials for solid state applications. *J. Phys. C*, 13:L189–L194, 1980.

[48] N. Troullier and J.S. Martins. Efficient pseudopotentials for plane-wave calculations. *Phys. Rev. B*, 43:1993–2006, 1991.

[49] A.M. Rappe, K.M. Rabe, E. Kaxiras, and J.D. Joannopoulos. Optimized pseudopotentials. *Phys. Rev. B*, 41:1227, 1990.

[50] S.G. Louie, S. Froyen, and M.L. Cohen. Nonlinear ionic pseudopotentials in spin-density-functional calculations. *Phys. Rev. B*, 26(4):1738–1742, 1982.

[51] M. Weissbluth. *Atoms and Molecules*. Academic Press, 1978.

[52] A.K. Rajagopal and J. Callaway. Inhomogeneous electron gas. *Phys. Rev. B*, 7:1912, 1973.

[53] A.H. MacDonald and S.H. Vosko. A relativistic density functional formalism. *J. Phys. C*, 12:2977, 1979.

[54] J. Anton, B. Fricke, and E. Engel. Noncollinear and collinear relativistic density-functional program for electric and magnetic properties of molecules. *Phys. Rev. A*, 69:012505, 2004.

[55] D. Vanderbilt. Soft self-consistent pseudopotentials in a generalized eigenvalue formalism. *Phys. Rev. B*, 41(11):7892–7895, 1990.

[56] Blöchl. Projector augmented-wrave method. *Phys. Rev. B*, 50(24):17953–17979, 1994.

[57] G. Kresse and D. Joubert. From ultrasoft pseudopotentials to the projector augmented-wave method. *Phys. Rev. B*, 59:1758–1775, 1999.

[58] A. Dal Corso. Density-functional perturbation theory with ultrasoft pseudopotentials. *Phys. Rev. B*, 64:235118, 2001.

[59] A. Dal Corso. Density functional perturbation theory within the projector augmented wave method. *Phys. Rev. B*, 81:075123, 2010.

[60] C.-L. Fu and K.-M. Ho. First-principles calculation of the equilibrium ground-state properties of transition metals: Applications to nb and mo. *Phys. Rev. B*, 28:5480, 1983.

[61] M. Methfessel and A.T. Paxton. High-precision sampling for brillouin-zone integration in metals. *Phys. Rev. B*, 40:3616, 1989.

[62] N. Marzari, D. Vanderbilt, A. De Vita, and M.C. Payne. Thermal contraction and disordering of the al(110) surface. *Phys. Rev. Lett.*, 82:3296, 1999.

[63] N. Marzari. *Ab-initio Molecular Dynamics for Metallic Systems*. PhD thesis, Cambridge University, 1996.

[64] S. de Gironcoli. Lattice dynamics of metals from density-functional perturbation theory. *Phys. Rev. B*, 51:6773(R), 1995.

[65] A.L. Fetter and J.D. Walecka. *Quantum Theory of Many-Particle Systems*. McGraw-Hill, 1971.

[66] H.B. Callen and T.A. Welton. Irreversibility and generalized noise. *Phys. Rev.*, 83:34, 1951.

[67] P. Buczek. *Spin dynamics of complex itinerant magnets*. PhD thesis, Martin-Luther-Universität Halle-Wittenberg, 2009.

[68] B. Rousseau, A. Eiguren, and A. Bergara. Efficient computation of magnon dispersions within time-dependent density functional theory using maximally localized wannier functions. *Phys. Rev. B*, 85:054305, 2012.

[69] T. Lounis, A.T. Costa, R.B. Muniz, and D.L. Mills. Theory of local dynamical magnetic susceptibilities from the korringa-kohn-rostoker green function method. *Phys. Rev. B*, 83:035109, 2011.

[70] S. Baroni, S. de Gironcoli, A. Dal Corso, and P. Giannozzi. Phonons and related crystal properties from density-functional perturbation theory. *Rev. Mod. Phys.*, 73:515–562, 2001.

[71] S.V. Halilov, H. Eschrig, A.Y. Perlov, and P.M. Oppeneer. Adiabatic spin dynamics from spin-density-functional theory: Application to fe, co, and ni. *Phys. Rev. B*, 58:293, 1998.

[72] E. Sasioglu, A. Schindlmayr, C. Friedrich, F. Freimuth, and S. Blügel. Wannier-function approach to spin excitations in solids. *Phys. Rev. B*, 81:054434, 2010.

[73] D. Rocca, Y. Ping, R. Gebauer, and G. Galli. Solution of the bethe-salpeter equation without empty electronic states: Application to the absorption spectra of bulk systems. *Phys. Rev. B*, 85:045116, 2012.

[74] O.B. Malcioğlu, R. Gebauer, D. Rocca, and S. Baroni. turbotddft – a code for the simulation of molecular spectra using the liouville–lanczos approach to time-dependent density-functional perturbation theory. *Comput. Phys. Commun.*, 182:1744–1754, 2011.

[75] X. Ge, S.J. Binnie, D. Rocca, R. Gebauer, and S. Baroni. turbotddft 2.0—hybrid functionals and new algorithms within time-dependent density-functional perturbation theory. *Comput. Phys. Commun.*, 185:2080–2089, 2014.

[76] I. Timrov. *Ab initio study of plasmons and electron-phonon coupling in bismuth: from free-carrier absorption towards a new method for electron energy-loss spectroscopy.* PhD thesis, École Polytechnique, 2013.

[77] I. Timrov, N. Vast, R. Gebauer, and S. Baroni. turboeels — a code for the simulation of the electron energy loss and inelastic x-ray scattering spectra using the liouville–lanczos approach to time-dependent density-functional perturbation theory. *Comput. Phys. Commun.*, 196:460, 2015.

[78] E.V. Tsiper. A classical mechanics technique for quantum linear response. *J. Phys. B*, 34:L401–L407, 2001.

[79] S.I. Dorozhkin, F. Lell, and W. Schoepe. Energy relaxation of hot electrons and inelastic collision time in thin metal films at low temperatures. *Solid. State Commun.*, 60:245, 1986.

[80] P. et al. Giannozzi. Quantum espresso: a modular and open-source software project for quantum simulations of materials. *J. Phys. Condens. Matter*, 21:395502, 2009.

[81] R. Gebauer and S. Baroni. Magnons in real materials from density-functional theorey. *Phys. Rev. B*, 61(10):R6459–R6462, 2000.

[82] D. Dragoni, D. Ceresoli, and N. Marzari. Thermoelastic properties of α-iron from first-principles. *Phys. Rev. B*, 91:104105, 2015.

[83] J.J. Adams, D.S. Agosta, R.G. Leisure, and H. Ledbetter. Elastic constants of monocrystal iron from 3 to 500 k. *J. Appl. Phys.*, 100:113530, 2006.

[84] D. Rocca. *Time-Dependent Density Functional Perturbation Theory New algorithms with applications to molecular spectra.* PhD thesis, SISSA, 2007.

[85] C.K. Loong, J.M. Carpenter, J.W. Lynn, R.A. Robinson, and H.A. Mook. Neutron scattering study of the magnetic excitations in ferromagnetic iron at high energy transfers. *J. Appl. Phys.*, 55:1895–1897, 1984.

[86] J.W. Lynn. Temperature dependence of the magnetic excitations in iron. *Phys. Rev. B*, 11(7):2624–2637, 1974.